Dynamics and Fatigue Damage of Wind Turbine Rotors during Steady Operation

Madsen, Peter Hauge; Frandsen, Sten Tronæs; Holley, W. E.;; Hansen, Jens Carsten

Publication date:
1984

Document Version
Publisher's PDF, also known as Version of record

RISØ

Risø-R-512

Dynamics and Fatigue Damage of Wind Turbine Rotors during Steady Operation

Peter Hauge Madsen, Sten Frandsen, William E. Holley and Jens Carsten Hansen

Risø National Laboratory, DK-4000 Roskilde, Denmark
July 1984

RISØ-R-512

DYNAMICS AND FATIGUE DAMAGE OF WIND TURBINE ROTORS DURING STEADY OPERATION

Peter Hauge Madsen, Sten Frandsen, William E. Holley and Jens Carsten Hansen

Abstract. A number of sub-models for use in the evaluation of the load-carrying capacity of a wind turbine rotor with respect to short-term strength and material fatigue are presented. The models constitute the theoretical basis of a computer code ROTORDYN which, in conjunction with an initial finite-element analysis and eigenvalue extraction, performs a dynamic analysis of a wind turbine rotor for lifetime prediction.

The models comprise a structural model which is essentially linear and solves for periodic and stochastic loading in the frequency domain. The model includes the centrifugal stiffening of the blades and a linearization of the aero-elastic effects as well as power regulation by pitch control. The aerodynamic model is based on blade element theory.

(continued on next page)

July 1984
Risø National Laboratory, DK-4000 Roskilde, Denmark

The stationary deterministic loads arising from a spatially non-uniform wind field and gravity as well as loads caused by the rotation are treated as periodic deterministic loads; turbulence loading, on the other hand, is formulated in terms of a stochastic model The turbulence is introduced in terms of power spectra as seen from a point in a rotating frame of reference.

Statistics of the combined deterministic periodic and stochastic response are represented, and an asymptotic theory is derived for the extremes of the responses during typical operation of the wind turbines.

A fatigue model is presented which takes into account the special structure of the stress response. The model avoids computer simulation and succeeding rainflow counting and yields an analytical solution for the expected damage rate at a certain mean wind speed.

The resulting computer program can be used to analyze most Danish types of wind turbines with respect to dynamic response, fatigue damage and extreme loads during steady operation as well as stand-still. The comparisons made up to now between measured and calculated data for wind turbine responses show satisfactory agreement.

EDB Descriptors: AERODYNAMICS; DAMAGE; FATIGUE; FINITE-ELEMENT METHOD; MECHANICAL VIBRATIONS; PEAK LOAD; R CODES; ROTORS; SERVICE LIFE; STRUCTURAL MODELS; TURBULENCE; WIND LOADS; WIND TURBINES.

ISBN 87-550-1046-6
ISSN 0106-2840

Risø Repro 1985

CONTENTS

PREFACE

This report has been made under contract with the Danish Ministry of Energy and marks the termination of the project "Vekselsasters betydning for udmattelse af vindmøllerotorer", which was part of the Ministry of Energy's EFP 84 program (R & D program 4 concerning energy).

The paper is a continuation of a project made for the Research Association of the Danish Electricity Supply Undertakings (DEFU), which was reported in Hauge Madsen et al. "Dynamic analysis of wind turbine rotors for lifetime prediction", Risø 1983.

The present report contains the updated theoretical background corresponding to the report above as well as some new additions, notably the influence of power regulation by pitch control, the aerodynamics and the lifetime models.

Together with the users manual of the developed computer code ROTORDYN and example calculations, which is reported independently, the report constitutes the conclusion of the project.

July 1984

Peter Hauge Madsen
Sten Frandsen
William E. Holley
J.C. Hansen

Wind Engineering Section
Meteorology and Wind Energy Department
RISØ NATIONAL LABORATORY

1. INTRODUCTION

It has become increasingly clear over the last few years that a major problem in the design of wind turbines is the viability to predict the lifetime of various structural components with a sufficient accuracy. A considerable number of failures due to fatique cracks in the load bearing structures have occurred, both on large and small wind turbines. Though many such failures can be attributed to inadequate quality control of materials, weldings and bolt connections, neglect of stress concentrations, etc., it is evident that the capability of overviewing the large complex of load cases and of carrying out realistic computation of response of the structure in each load case is vital.

This has led to the decision of the development of a model and a computer code, which are specifically directed toward the prediction of the lifetime of wind turbine structures. In order to predict lifetime, one must evaluate both the so-called fatigue life and the probability that the structure will fail due to extreme loading.

Since the evaluation process for determining fatigue life necessarily must include all load cases and operational situations, it is important that the analysis of each single case can be executed relatively fast in order to keep the consumption of computer time within acceptable limits. To keep within such reasonable limits it seems necessary to use a probabilistic approach, i.e. describe the response of the structure by means of statistical quantities in contrast to the deterministic approach where the loading is represented by a known time history and the response is calculated time-step by time-step. The latter method is advantageous in the sense that it allows geometrical and material nonlinearities as well as time-varying structural properties, however, the time history of the loading must be specified in full detail. Thus in cases where the load is solely or partly of a stochastic nature, simulation methods must be applied

in order to represent the loading in a form suitable for the time-integration method. To capture the variability in the structural responses many simulated load-realizations must be analyzed, and the method is generally associated with high computational costs

Basically, two approaches can be taken to model the external loads on a structure. Either the loads are modelled as deterministic functions of space and time, or a stochastic model must be used, depending on the uncertainty or nature of the loads. In the latter model the loads are represented by their statistical properties. For a wind turbine, where the total loading is composed of several contributions, both approaches must be applied to model the individual load components. The deterministic loads, which are periodic with a period corresponding to the time of one revolution of the rotor, are due to gravity, tower wake, wind shear etc., while the wind turbulence in generel causes a stochastic load on obstacles in the flow. Until recently, the turbulence had frequently been neglected as an insignificant source to dynamic loading compared to the pure periodic loads. However, preliminary investigations have indicated that the response of the rotor blades, especially in the flapwise direction, may be strongly influenced or even dominated by the random load caused by turbulence, i.e. the variance and the extremes of the response may be a factor of 2 or more larger than what is accounted for by the deterministic loads alone.

This report describes a model that takes into account the problems discussed above. The model is at present restricted to the most common Danish wind turbine type:

> Horizontal axis propeller wind turbines with induction generator connected to main electric grid, active yaw and a relatively stiff tower.

The model aims at the prediction of the lifetime of the structural components of wind turbines and includes the possibility of estimating extreme events during normal operation. The background and goals are described in further detail in the following.

1.1. Background and goals

By now, a number of models including the structure and load-generating mechanisms developed especially for wind turbine design evaluation are available. Most of the models (for example ref. [1], [2], [7] and [11]) have been developed or even derived from general purpose finite element programs and most often the corresponding computer codes are structured for time integration solution, i.e. for each time step the complete set of equations must be solved. As mentioned above time integration will provide correct solutions if the complete load history in time and space is known. While a time series of the fluctuating wind at a fixed point is obtainable, either from measurements or from simulation, it is not straightforward to generate the complete spatial flow field of the wind as seen from a wind turbine. Furthermore, the computational cost tends to be excessive when a large number of load cases is to be treated.

Some researchers (ref. [11]) have included the possibility of producing frequency domain solutions in their models, but they have put little emphasis on modelling the load itself. Since the preparations for the present project were started in 1979, several research groups have initiated investigations on the possibility of carrying out an analysis based purely on frequency domain manipulations (ref. [3], [4], [6] and [11],) which would be the natural line to follow if results are to be presented. Also specific works have been made to clarify the nature of atmospheric turbulence as experienced by a rotating point as is the case with a wind turbine blade (ref. [9], [8] and [5]).

The model presented in this report is intended to be a physically realistic, complete model, which includes all aspects of the complicated problem of predicting the structural lifetime. Thus, the emphasis has been put on the synthesis of a total model rather than the details of each individual sub-model. The specific demands on the model were

- Computational efficiency in order to be able to include all relevant load cases; expected in number to be of the order of 50-100.

- Capability of dealing with the combined stochastic and deterministic loading.
- Sufficient accuracy in the description of the response to each load type and load case.
- Inclusion of a realistic fatigue model.
- Inclusion of a realistic model of the atmospheric turbulence.
- Capability of giving the response statistics of at least the rotor components.

In addition, the special problem of predicting extreme loads and responses was solved in order to complete the model. In order to meet these demands, it has been decided to base the model on the following principles and assumptions:

- The structure is described in a frame of reference, which is fixed relative to the rotor.
- Both the structural and load models are linear.
- Responses due to deterministic loads are in principle given as Fourier series.
- Responses due to stochastic load caused by turbulence are presented by means of spectra.
- Deterministic and stochastic loads (and responses) are independent.
- The rotational speed of the rotor is nearly constant.
- The fatigue model can handle pure deterministic, pure stochastic and combined response cases.
- Structural data are generated by means of a separate finite-element program.
- Other input data includes: atmospheric conditions, aerodynamic data and fatigue data of materials used, and a thorough description of the operational modes of the turbine.

During the work, of course, findings and experiences have altered the plans, but in general it has been possible to follow the overall idea of an efficient, linear and frequency domain based model for prediction of fatigue life.

1.2. Elements in the analysis

In order to reach the previously stated goals a complete model for lifetime prediction must be formulated. As mentioned, such a model comprises several models, which can be roughly classified as belonging to four main groups, namely, load models, aerodynamic models, structural models and models for prediction of extreme responses and lifetime. The elements in the total model are illustrated in Fig. 1.1., and the content of this report is mainly a presentation and discussion of the individual component models.

Following the diagram from the left an important element in the analysis is the load model. A substantial part of the loading is caused by the wind field, and due to the rotation of the rotor a spatial as well as a temporal variation in wind speed gives rise to dynamic loads. The variation due to misalignment of the rotor, wind shear and tower interference can be specified as deterministic functions of time, whereas the temporal variation caused by wind turbulence is introduced in terms of a stochastic process model. In order to quantify the loads caused by the wind field an aerodynamic model is needed. The blade element theory has been chosen due to its relative simplicity, and the theory and the adaption to dynamic loading is treated in section 3. The rest of the loads, centrifugal forces, gyroforces from yawing and gravity forces, which are enhanced by tolerance asymmetry of the rotor, as well as the deterministic variation of the wind field is discussed in section 4. Due to its special nature the turbulence is presented separately in section 5.

The next point is the choice of a structural model. Having decided on a spectral representation of the turbulence, a linear model is imperative, and nonlinear aeroelastic coupling and coupling between displacements and centrifugal forces are thus included in a linearized form. The structural model, in which the dynamic stresses and displacements are found using modal analysis, is the topic of section 2.

A power regulation system, which limits the electric power by changing the blade pitch angle, is incorporated in the structural system equations.

As the deterministic and stochastic load components are assumed independent, the structural model delivers the dynamic responses as a periodic time series plus a stochastic component in terms of a power spectrum. An approach to the calculations of extremes of the responses so given is presented in section 7, and a fatigue model is derived in section 8, which takes into account the special structure of the stress response without use of a simulation procedure. The design of the wind turbine can then be said to b satisfactory if the extreme stresses during the planned lifetime are less than the ultimate material strength and the accumulated fatigue damage does not amount to failure.

The choice of the component models is not unique. However, as the purpose of the project has been an operational and efficient complete model, the emphasis has been put on the synthesis of models of similar accuracy and complexity rather than on derivation of new and refined models, although some original work has been needed. Thus some of the theory presented in the subsequent sections can be found elsewhere. However, due to the scarcity of good reference literature in the field, a uniform level of detail has been pursued throughout the report.

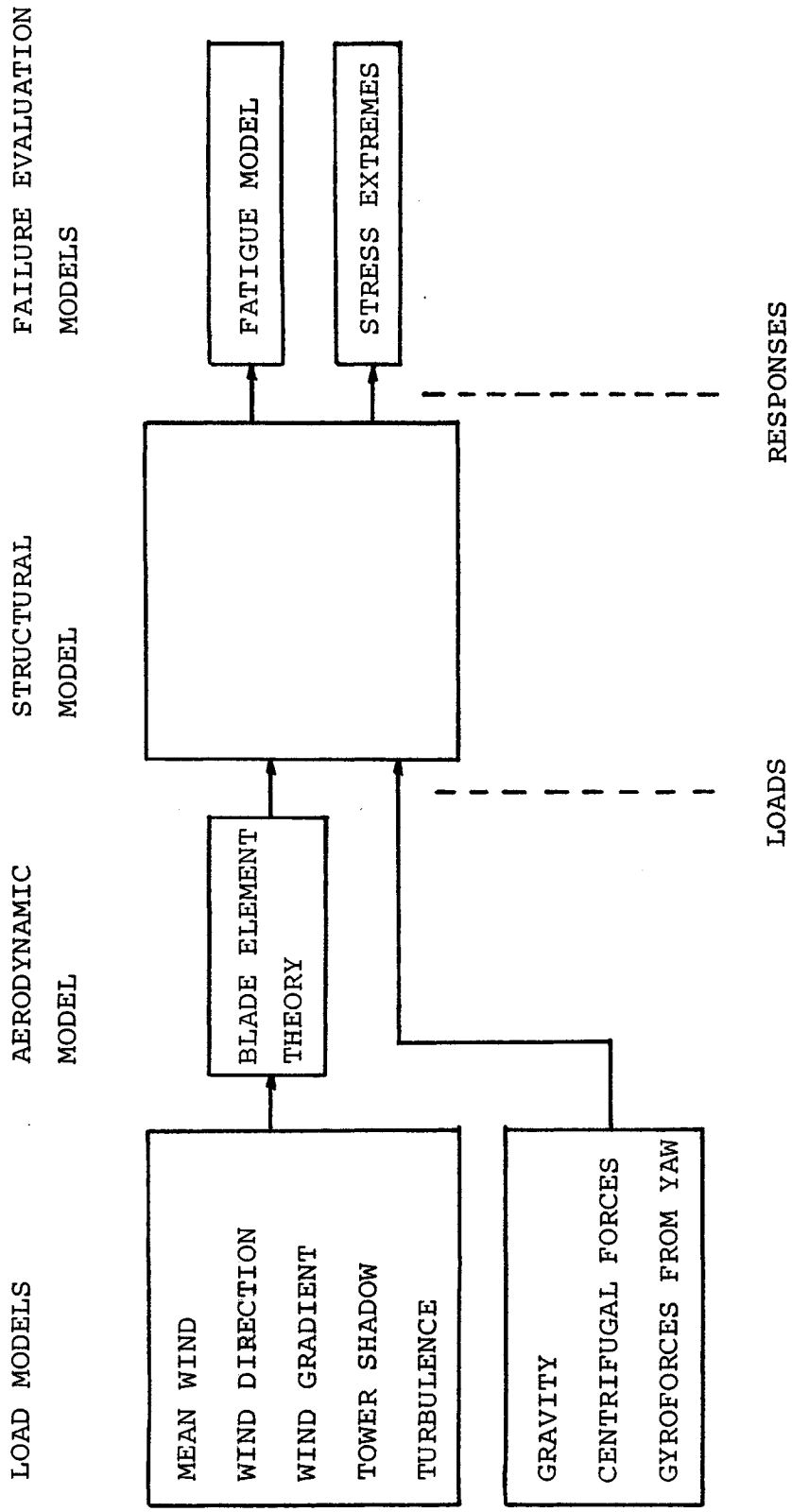

Fig. 1.1. Elements of the model.

REFERENCES

[1] DUGUNDJI, J. and WENDELL, J.H. (1981). General Review of the MOSTAS Computer Code for Wind Turbines, DOE/NASA/3303-1, 79 pp.

[2] FABIAN, O. (1981). A New Method for Aeroelastic Analysis of Wind Turbines", AFM-report 81-06. (DtH, Lyngby, Denmark, 38 pp.

[3] THRESHER, R.W., HOLLEY, W.E. and JAFAREY, N. (1981). Wind Response Characteristics of Horizontal Axis Wind Turbines. In: Second DOE/NASA Wind Turbine Dynamics Workshop held at Cleveland, Ohio, Feb. 24-26, 1981. SERI/CP-635-1238, 87-99.

[4] FRANDSEN, S. and CHRISTENSEN, C.J. (1980). On Wind Turbine Power Measurements. In: Papers presented at the Third International Symposium on Wind Energy Systems held in Copenhagen, August 26-29, 1980. (BHRA Fluid Engineering, Cranfield, Bedford) Paper D4, 207-222.

[5] FROST, W. and TURNER, R.E. (1980). A Discrete Gust Model for Use in the Design of Wind Energy Conversion Systems. Appl. Meteorol. 21, 770-775.

[6] GARRAD, A.D. (1982). An Approximate Method for the Dynamic Analysis of Two Bladed Horizontal Axis Wind Turbine Systems In: Fourth International Symposium on Wind Energy Systems held at Stockholm, September 21-29, 1982. (BHRA Fluid Engineering, Bedford) Paper G3, Vol. 1, 445-461.

[7] KOTTAPALLI, S.B.R. and FRIEDMANN, P.P. (1978). Aeroelastic Stability and Response of Horizontal Wind Turbine Blades. In: Papers presented at the Second International Symposium on Wind Energy Systems held in Amsterdam, October 3-6, 1978. (BHRA Fluid Engineering, Cranfield, Bedford), Vol. 1, paper C4.

[8] KRISTENSEN, L. and FRANDSEN, S. (1982). Model for Power Spectra of the Blade Wind Turbines Measured from the Moving Frame of Reference. J. Wind. Eng. Ind. Aerodyn. 10, 249-262.

9] ROSENBROCK, H.H. (1985). Vibration and Stability Problems in Large Wind Turbines Having Hinged Blades. ERA 75-36 Report C/T 113, 53 pp.

[10] SUNDAR, R.M. and SULLIVAN, J.P. (1981). Performance of Wind Turbines in a Turbulent Atmosphere. In: Second DOE/NASA Wind Turbine Dynamics Workshop held at Cleveland, Ohio, February 29-26, 1981. SERI/CP-635-1238, 79-86.

[11] VOLLAN, A. (1982). Aeroelastic Stability and Dynamic Response Calculations for Wind Energy Converters. In Fourth International Symposium on Wind Energy Systems held at Stockholm, September 21-29, 1982. (BHRA Fluid Engineering, Bedford) Paper G2, Vol. 1, 427-444.

2. THE STRUCTURAL MODEL

An important part of establishing a method for lifetime prediction is the choice of a structural model, which provides the link between the external loading of the windturbine rotor and the material action at a fatique sensitive point of the structure. The choice of method of structural modelling has been influenced by the following factors:

- The model should consider dynamic action of the rotor system.
- The structure will be analyzed for a large number of load cases.
- The model should be suited for stochastic turbulence loading.
- The model should be suited for a spectral representation of loading and response.
- The effect of a pitch-angle control system for regulation of the power output should be included.
- The modelling of inertia and stiffness properties should be simple and rest on a standard finite-element model of the rotor.

These requirements have led to the choice of a linear model in which the number of degrees of freedom to be considered in the dynamic response analysis has been reduced using modal analysis. The response problem is solved in the frequency domain whereby the response is expressed in terms of a Fourier series for the deterministic part and a power spectrum for the stochastic part due to turbulence, respectively. The analysis procedure is separated into an initial standard finite-element analysis of the rotor system in which modal natural frequencies and mode shape vectors are determined, and a following response analysis. The latter is performed in the program ROTORDYN, which generates the static and dynamic loading, corrects natural frequencies and calculates the aerodynamic damping, and finally solves the deterministic and stochastic response problem in order to estimate the fatigue damage or damage rate at the chosen service condition.

This chapter accounts for the structural model and commences with a definition of the frames of reference to which the model is referred in both the finite element analysis and the following response analyses. The method of modal analysis is then briefly presented and the coupling between loading and response and that between blade normal forces and apparent stiffness is introduced in a linearized form. The frequency domain analysis of the response to a stationary deterministic loading is then presented and the effect of a linear pitch-angle control system is included. The approach results in a series solution for the deterministic response and the chapter concludes with the spectral techniques for stochastic response analysis.

2.1. Frames of reference

The rotor system being of main interest makes it convenient to describe the rotor loading as well as the structural response of the rotor in a frame of reference which rotates with the wind turbine rotor such that the undeflected geometry is time invariant. The frame of reference is defined by an ordinary Cartesian X,Y,Z coordinate system which later will be referred to as the global coordinate system. It is assumed that the rotor and hence the global system rotates with the angular velocity vector $\underline{\Omega}$ relative to the nonmoving coordinates X*,Y*,Z*. A limit case is $\Omega = \underline{0}$ corresponding to a fixed rotor. The frames of reference and their relative position at time t=0 are shown on Fig. 2.1.

The axis of rotation and the Y-axis are seen to coincide while at the reference time t=0 the X-axis is horizontal. The angle θ is the angle between the rotorplane (or the XZ-plane) and vertical and specifies together with γ the direction of the mean wind relative to the XY-plane. The rotor blades are assumed to be essentially straight and directed along a radius vector. The location of the blade is thus given by the angle ϕ, defined as positive as shown on the figure.

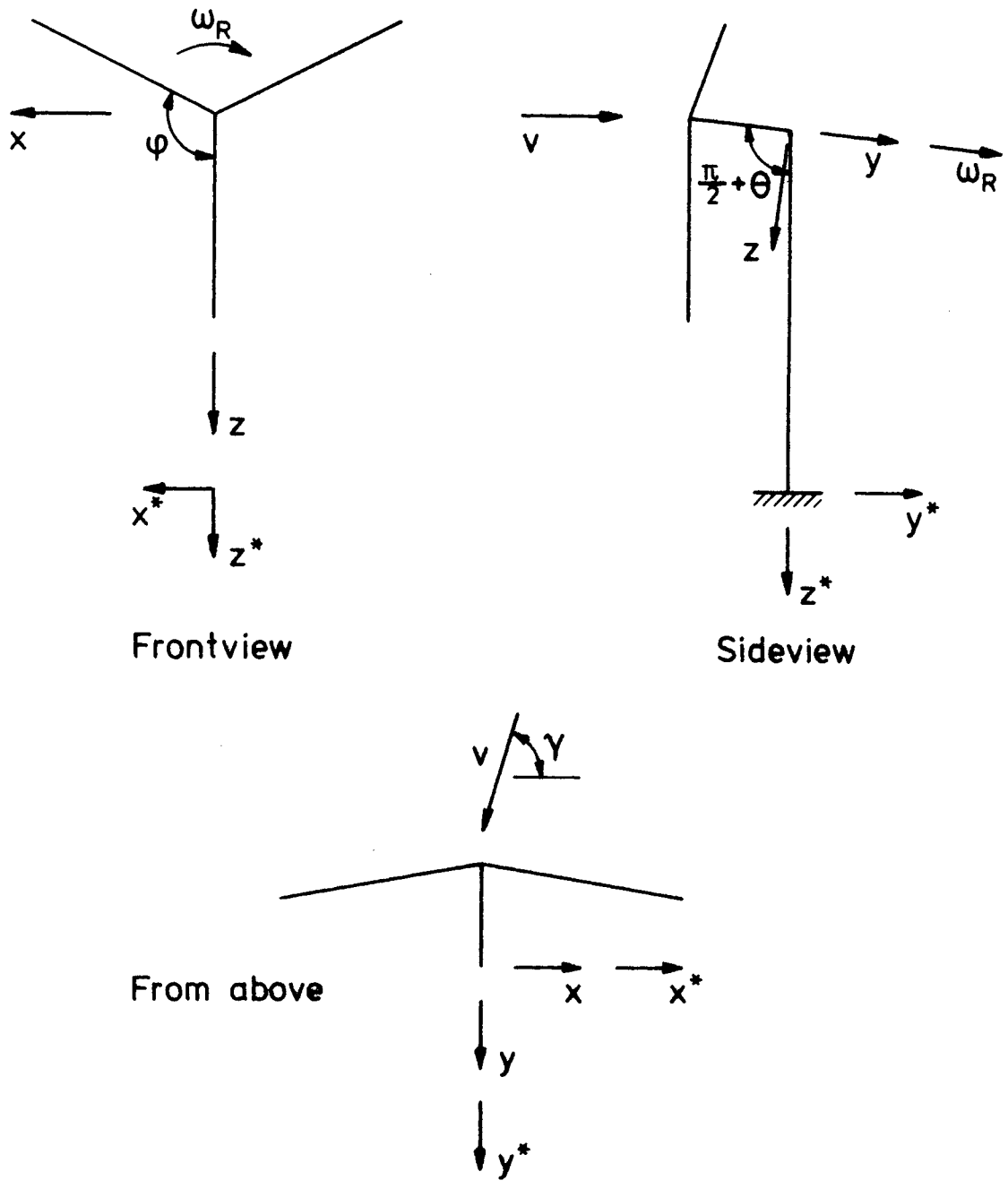

Fig. 2.1. Geometry and Frames of Reference at t=0.

Due to the rotation the equations of motion relative to the rotating coordinates are slightly changed by the introduction of fictive force contributions. When the origin of the X,Y,Z- and the X*Y*Z* system coincides, the equation of motion of a mass m with position vector $\underline{r}$ reads in the global system (Symon [11]).

$$m\frac{d^2\underline{r}}{dt^2} = \underline{F} - 2m\underline{\Omega}\times\frac{d\underline{r}}{dt} - m\underline{\Omega}\times(\underline{\Omega}\times\underline{r}) - m\frac{d\underline{\Omega}}{dt}\times\underline{r} \qquad (2.1)$$

The second and the third term on the right hand side are the Coriolis and the centrifugal forces, respectively. The last term has no special name and appears only for the case of nonuniform rotation. The choice of a rotating frame of reference thus implies that these force terms must explicitly be accounted for.

To be more specific, consider an infinitesimal part of the rotor with mass dm and position vector $\underline{r}$ and assume that the rotor is rotating with angular velocity ω_R while the rotor system is yawing around the Z* axis with angular velocity ω_Y. The rotation vector $\underline{\Omega}$ of the XYZ-system relative to the X*Y*Z*-system is then time dependent and with direction in the latter system

$$\underline{\Omega}^* = \begin{bmatrix} -\omega_R \cos\theta \sin\omega_Y t \\ \omega_R \cos\theta \cos\omega_Y t \\ \omega_R \sin\theta + \omega_Y \end{bmatrix} \qquad (2.2)$$

Hence in the XYZ-system the vector of rotation can be expressed

$$\underline{\Omega} = \begin{bmatrix} -\omega_Y \cos\theta \sin\omega_R t \\ \omega_R + \omega_Y \sin\theta \\ \omega_Y \cos\theta \cos\omega_R t \end{bmatrix} \qquad (2.3)$$

In the XYZ-system the fictive forces $d\underline{F}$ acting on the mass dm thus becomes

$$d\underline{F}_{coriolis} = -2dm\underline{\Omega}\times\frac{d\underline{r}}{dt} \qquad (2.4)$$

which is conveniently expressed as

which is conveniently expressed as

$$d\underline{F}_{coriolis} = 2dm \begin{bmatrix} 0 & \omega_Y\cos\theta\cos\omega_R t & -\omega_R-\omega_Y\sin\theta \\ -\omega_Y\cos\theta\cos\omega_R t & 0 & -\omega_Y\cos\theta\sin\omega_R t \\ \omega_R+\omega_Y\sin\theta & \omega_Y\cos\theta\sin\omega_R t & 0 \end{bmatrix} \begin{bmatrix} \frac{dx}{dt} \\ \frac{dy}{dt} \\ \frac{dz}{dt} \end{bmatrix} \quad (2.5)$$

Similarly for the centrifugal forces

$$d\underline{F}_{cent} = -dm\underline{\Omega}\times(\underline{\Omega}\times\underline{r}) \quad (2.6)$$

$$= dm \begin{bmatrix} \omega_R^2+\omega_Y^2+2\omega_Y\omega_R\sin\theta & \omega_Y\omega_R\cos\theta\sin\omega_R t & \frac{1}{2}\omega_Y^2\cos^2\theta\sin2\omega_R t \\ -\omega_Y^2\cos^2\theta\sin^2\omega_R t & +\frac{1}{2}\omega_Y^2\sin2\theta\sin\omega_R t & \\ \omega_R\omega_Y\cos\theta\sin\omega_R t & \omega_Y^2\cos^2\theta & -\omega_R\omega_Y\cos\theta\cos\omega_R t \\ +\frac{1}{2}\omega_Y^2\sin2\theta\sin\omega_R t & & -\frac{1}{2}\omega_Y^2\sin2\theta\cos\omega_R t \\ \frac{1}{2}\omega_Y^2\cos^2\theta\sin2\omega_R t & -\omega_R\omega_Y\cos\theta\cos\omega_R t & \omega_R^2+\omega_Y^2+2\omega_R\omega\sin\theta \\ & -\frac{1}{2}\omega_Y^2\sin2\theta\cos\omega_R t & -\omega_Y^2\cos^2\theta\cos^2\omega_R t \end{bmatrix} \begin{bmatrix} x \\ y \\ z \end{bmatrix}$$

and finally

$$-dm\frac{d\underline{\Omega}}{dt}\times\underline{r}$$

$$= dm \begin{bmatrix} 0 & -\omega_Y\omega_R\cos\theta\sin\omega_R t & 0 \\ \omega_R\omega_Y\cos\theta\sin\omega_R t & 0 & -\omega_R\omega_Y\cos\theta\cos\omega_R t \\ 0 & \omega_R\omega_Y\cos\theta\cos\omega_R t & 0 \end{bmatrix} \begin{bmatrix} x \\ y \\ z \end{bmatrix} \quad (2.7)$$

In addition to the global coordinates a local coordinate system is introduced in order to facilitate the description of the flow around the blade profile and the interaction between flow and structural response. At a given cross section the origin of the local X',Y',Z' coordinate system is located at the shear center of the profile such that the Y'-axis is parallel to the Y-axis, while the X'Z'-plane is parallel to the XZ-plane and the Z-axis is directed away from the axis of rotation. The location of the local system is illustrated on Fig. 2.2.

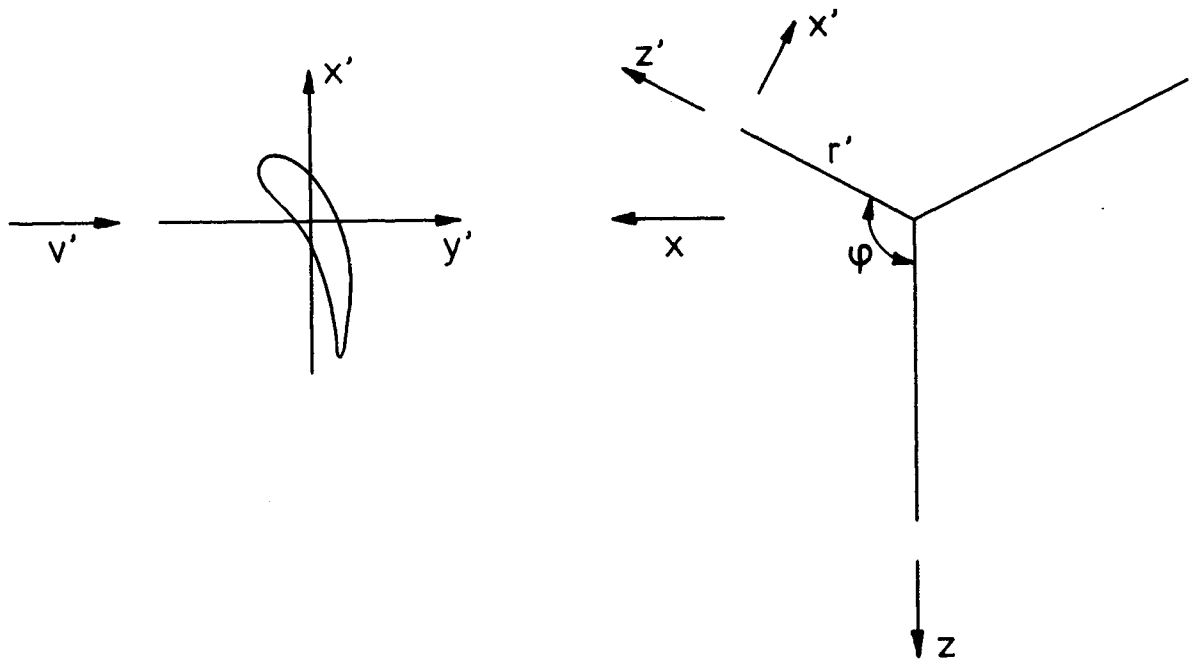

Front view of rotor.

Fig. 2.2. Definition of local coordinates relative to the global system.

The global representation $\underline{F}$ of a vector quantity $\underline{F}'$ in the local system is found by means of the transformation matrix $\underline{\underline{A}}$

$$\underline{F} = \underline{\underline{A}}\underline{F}' \tag{2.8}$$

where $\underline{\underline{A}}$ is defined

$$\underline{\underline{A}} = \begin{bmatrix} \cos\phi & 0 & \sin\phi \\ 0 & 1 & 0 \\ -\sin\phi & 0 & \cos\phi \end{bmatrix} \tag{2.9}$$

The transformation matrix will later be used to transform aerodynamic loads derived in the local system into loads in the global system.

2.2. Dynamics and modal decomposition of a linear MDOF-system

From the basic requirements and assumptions discussed in section 1 it follows that the loaded vibrating wind turbine rotor will be modelled as a linear system with a finite number N of degrees of freedom and time invariant mass, damping and stiffness properties. Consequently the generalized displacement vector $\underline{X}(t)$ is governed by the well known equation of motion

$$\underline{\underline{M}}\,\ddot{\underline{X}} + \underline{\underline{C}}\,\dot{\underline{X}} + \underline{\underline{K}}\,\underline{X} = \underline{P} \qquad (2.10)$$

in terms of a mass matrix $\underline{\underline{M}}$, a damping matrix $\underline{\underline{C}}$, a stiffness matrix $\underline{\underline{K}}$ and a load vector $\underline{P}(t)$.

This fundamental model is obtained using the finite-element technique such that $\underline{X}(t)$ represents the degrees of freedom of selected points of the structure, the nodes. $\underline{X}(t)$ usually contains translations and rotations of the nodes in which case $\underline{P}(t)$ consists of nodal loads in terms of forces and moments.

The matrices $\underline{\underline{M}}$ and $\underline{\underline{K}}$ are basically generated by the chosen finite element program but may be modified due to the linearization procedure as described in next section.

The large number of degrees of freedom generated by ordinary finite-element modelling clearly makes a dynamic analysis quite time consuming. When a large number of load cases should be analyzed it becomes imperative to reduce the number of degrees of freedom. One method is the use of modal analysis. The method is based on the observation that the dynamic response of a linear structure with satisfactory accuracy can be expressed in terms of a few undamped modes of vibration corresponding to the lower frequencies of vibration.

The structure with the equation of motion in (2.10) is said to vibrate in a natural mode when the undamped displacement $\underline{X}$ under no external loading can be separated as

$$\underline{X}(t) = \underline{v}_i \sin(\omega_i t + \phi_i) \tag{2.11}$$

Inserting (2.11) in (2.10) leads to the eigenvalue problem

$$[\underline{\underline{K}} - \omega_i^2 \underline{\underline{M}}]\underline{v}_i = \underline{0} \tag{2.12}$$

to solve for the mode shape vector $\underline{v}_i$ and the natural frequency ω_i of mode i.

For a stable structural system (2.12) results in real and positive values for all ω_i^2 however not necessarily distinct. In any case the mode shape vectors can be selected such that

$$\underline{v}_i^T \underline{\underline{M}} \underline{v}_j = \begin{cases} 0 & i \neq j \\ 1 & i = j \end{cases} \tag{2.13}$$

and

$$\underline{v}_i^T \underline{\underline{K}} \underline{v}_j = \begin{cases} 0 & i \neq j \\ \omega_i^2 & i = j. \end{cases} \tag{2.14}$$

For mode shape vectors with real components this orthogonality condition is not in general valid for the damping matrix.

It can be shown, Caughey (2), that a sufficient condition for

$$\underline{v}_i^T \underline{\underline{C}} \underline{v}_j = \begin{cases} 0 & i \neq j \\ 2\omega_i \zeta_i & i = j \end{cases} \tag{2.15}$$

is that the damping matrix can be expressed in terms of M and K as

= =

$$\underline{\underline{C}} = \underline{\underline{M}} \sum_{i=0}^{N} \alpha_i [\underline{\underline{M}}^{-1} \underline{\underline{K}}]^i \tag{2.16}$$

which includes the case of Rayleigh damping

$$\underline{\underline{C}} = \alpha_o \underline{\underline{M}} + \alpha_1 \underline{\underline{K}} \tag{2.17}$$

In this case the modal damping ratio ζ_i can be expressed by the corresponding modal natural frequency ω_i, and the coefficients α_o, α_1,

$$\zeta_i = \frac{1}{2} \left(\frac{\alpha_o}{\omega_i} + \alpha_1 \omega_i\right) \tag{2.18}$$

Structural damping is often introduced simply either as the coefficients α_i or a_s prescribed modal damping ratios ζ_i due to the little understood mechanism of damping in the structural members.

The reduction of the number of degrees of freedom in the system is based on the assumption that pertinent responses can be expressed in terms of a few mode shape vectors, thus approximating $\underline{X}(t)$ by

$$\underline{X}(t) \approx \sum_{i=1}^{M} \underline{v}_i \, T_i(t) \tag{2.19}$$

in which $\underline{v}_i$ are modeshape vectors corresponding to the M lowest eigenfrequencies and $T_i(t)$ is the modal amplitude function. Arranging the M mode shape vectors as columns in

$$\underline{\underline{v}} = [\underline{v}_1, \underline{v}_2, \ldots \underline{v}_M] \tag{2.20}$$

such that the order corresponds to a non-decreasing sequence of eigenfrequencies, (2.19) is expressed as the product

$$\underline{X}(t) \approx \underline{\underline{v}} \, \underline{T}(t) \tag{2.21}$$

Inserting (2.21) into (2.10) and premultiplying by $\underline{\underline{v}}^T$, (2.13) and (2.14) yields

$$\left[\begin{smallmatrix}1\end{smallmatrix}\right] \ddot{\underline{T}}(t) + \underline{\underline{C}}_m \dot{\underline{T}}(t) + \left[\ \omega_i^2\ \right] \underline{T}(t) = \underline{q}(t) \qquad (2.22)$$

in which the generalized modal load vector $\underline{q}(t)$ is defined as

$$\underline{q}(t) = \underline{\underline{v}}^T \underline{P}(t) \qquad (2.23)$$

and the modal damping matrix $\underline{\underline{C}}_m$ is

$$\underline{\underline{C}}_m = \underline{\underline{v}}^T \underline{\underline{C}}\ \underline{\underline{v}} \qquad (2.24)$$

$\underline{\underline{C}}_m$ is often assumed to be diagonal (2.15) which is strictly true when (2.10) is fulfilled. When the damping gets large however this assumption may lead to erroneous results. The symbol [ ] in (2.22) denotes a diagonal matrix.

The formulation in (2.22) has the advantages that

- the number of simultaneous equations to be solved is greatly reduced
- the structure of the generalized mass and stiffness matrix is simplified, and
- in the case of diagonal damping matrices the dynamic analysis is reduced to solving a number of uncoupled differential equations.

It is, however, important to note that no definite rules exist for selecting the appropriate number of modes to be included. The number needed to give a realistic description of the response depends on the frequency interval of interest and the type of response, i.e. displacements, bending moments or shear forces.

For long slender beams which are often used to model wind turbine blades, displacements and moments are adequately described by rather few modes, 2-4.

A more thorough presentation of the modal analysis may be found in Clough and Penzien [4] or Dyrbye [5].

2.3. The linearized problem

Although a linear structural model is adopted some additional assumptions and considerations must be introduced in order to formulate the response problem as a linear one. The reason is that part of the loading, fictive or nonfictive, is coupled to the response values as is the case for the aerodynamic forces and the fictive Coriolis forces. Furthermore, the centrifugal forces introduce large normal forces in the rotor blades, which, when the changes in geometry during vibration are taken into account, alter the apparent stiffnesses of the structural system.

The forces on the rotor structure can be separated into a static component $\underline{P}_o$, a time-varying component $\underline{P}(t)$, aeroelastic forces $\underline{A}(\underline{X},\dot{\underline{X}},\ddot{\underline{X}})$, which are generated by the blades moving through the air in response to the external loading, and the Coriolis forces $\underline{P}_c(\dot{\underline{X}})$.

Consequently the equation of motion (2.10) can be written

$$\underline{\underline{M}}\,\ddot{\underline{X}} + \underline{\underline{C}}\,\dot{\underline{X}} + \underline{\underline{K}}\,\underline{X} = \underline{P}_o + \underline{P}(t) + \underline{A}(\underline{X},\dot{\underline{X}},\ddot{\underline{X}}) + \underline{P}_c(\dot{\underline{X}}) \qquad (2.25)$$

To obtain linearity the aeroelastic forces are linearized

$$\underline{A}(\underline{X},\dot{\underline{X}},\ddot{\underline{X}}) \approx -\underline{\underline{K}}_{ae}\underline{X} - \underline{\underline{C}}_{ae}\,\dot{\underline{X}} - \underline{\underline{M}}_{ae}\,\ddot{\underline{X}} \qquad (2.26)$$

thus introducing an aerodynamic stiffness, damping and mass. In the following the aerodynamic mass is considered unimportant and

is neglected. The problem of finding $\underline{\underline{K}}_{ae}$ and $\underline{\underline{C}}_{ae}$ is addressed in section 3.3.

The Coriolis forces are obtained from (2.5). Assuming a small yawing angular velocity, i.e. $\omega_y << \omega_R$, the Coriolis vector force on a lumped mass m at (x,y,z) becomes

$$\underline{F}_C = \begin{vmatrix} F_x \\ F_y \\ F_z \end{vmatrix} = \begin{vmatrix} 0 & 0 & -\omega_R \\ 0 & 0 & 0 \\ \omega_R & 0 & 0 \end{vmatrix} \begin{vmatrix} dx/dt \\ dy/dt \\ dz/dt \end{vmatrix} \tag{2.27}$$

Collecting such terms from all nodal masses in the system the total Coriolis load vector can be written

$$\underline{P}_C(\dot{\underline{X}}) = - \underline{\underline{C}}_{co}\, \dot{\underline{X}} \tag{2.28}$$

Moving the Coriolis force term and the aerodynamic force term to the left-hand side of the equation of motion (2.25) the following linear dynamic problem is obtained:

$$\underline{\underline{M}}\, \ddot{\underline{X}} + (\underline{\underline{C}} + \underline{\underline{C}}_{ae} + \underline{\underline{C}}_{co})\dot{\underline{X}} + (\underline{\underline{K}} + \underline{\underline{K}}_{ae})\underline{X} = \underline{P}_o + \underline{P}(t) \tag{2.29}$$

which transformed into modal equations (2.22) yields a modal damping matrix

$$\underline{\underline{C}}_m = \underline{\underline{v}}^T[\underline{\underline{C}} + \underline{\underline{C}}_{ae} + \underline{\underline{C}}_{co}]\underline{\underline{v}} \tag{2.30}$$

which in general is not a diagonal matrix.

Note that $\underline{\underline{C}}_{co}$ is an antisymmetric matrix. Hence the Coriolis contribution to the modal damping matrix is also antisymmetric. Thus if no damping coupling is assumed, the Coriolis force is disregarded. Test calculations indicate that the damping due to the Coriolis force is of no practical importance.

The initial finite-element analysis serves partly to define the structural model and calculate the mass and stiffness matrix $\underline{\underline{M}}$ and $\underline{\underline{K}}$ and partly to solve the eigenvalue problem (2.12) for $\underline{v}_i$ and ω_i for the nonrotating, undamped and nonloaded rotor system. Thus the apparent change in stiffness due to the large blade normal forces from the centrifugal loading and the aerodynamic stiffness contribution are not taken into account in the eigenvalue analysis. Being a fairly extensive numerical procedure the eigenvalue analysis will not be repeated in the subsequent response analysis. Instead an approximative approach is taken to include the influence of the centrifugal field and the aerodynamic stiffness.

The change in stiffness of the blade from the centrifugal forces is mainly due to the induced normal force which for motions in the rotor plane is partially counteracted by the centrifugal forces, as they are always directed away from the center of rotation. This is illustrated in figure 2.3, which considers a segment of a beam with mass m that has a small displacement u perpendicular to the line that connects the origin and the center of the segment.

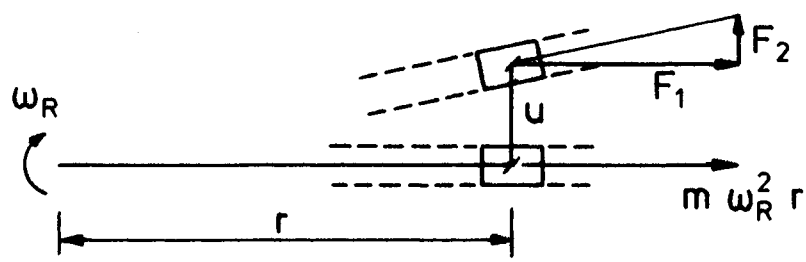

Fig. 2.3. Centrifugal forces for displaced beam element.

For small u and considering only first-order terms the centrifugal force acting on the element with mass m has the two components F_1 and F_2.

$$F_1 = m\omega_R^2 r \tag{2.31}$$

$$F_2 = m\omega_R^2 u \tag{2.32}$$

Thus, the centrifugal forces are divided into constant forces which affects only the stiffness when the equations of equilibrium are formulated in the deformed configuration, and forces which are proportional to the deformation.

The effect of the first-mentioned forces are taken into account by means of a geometric stiffness matrix, Przemiencki [8], which is determined by the induced normal forces in the blade beam elements. Thus, the updated stiffness matrix can be written

$$\underline{\underline{K}}(\omega_R) = \underline{\underline{K}} + \underline{\underline{K}}_{ae} + \omega_R^2(\underline{\underline{K}}_g + \underline{\underline{K}}_2) \tag{2.35}$$

in which $\underline{\underline{K}}_g$ is the geometrical stiffness matrix corresponding to a unit rotation frequency and $\underline{\underline{K}}_2$ follows directly from (2.32). In the program ROTORDYN a linear variation of the displacements throughout the element is assumed, which leads to what is usually referred to as the "string stiffness matrix" for K_g.

Application of a Southwell-type formula

$$\omega^2 = \omega_o^2 + \phi\omega_R^2 \tag{2.34}$$

reported in Putter and Manor [10] for a uniform rotating beam indicates that the change in stiffness is rather small, typically leading to an increase of 5% of the first modal frequency. With this in mind the change in modal frequencies ω_i^2 are estimated by a perturbation method.

Perturbation of the eigenvalue problem has been treated by several authors, e.g. Collins and Thompson [3], the solution, however, becomes especially simple when finding the perturbation in eigenfrequency due to a perturbation of the stiffness matrix. Thus, we represent these terms by

$$\omega^2 = \omega_o^2 + \varepsilon\omega_1^2 \tag{2.35}$$

$$\underline{\underline{K}} = \underline{\underline{K}}_o + \varepsilon\underline{\underline{K}}_1 \tag{2.36}$$

and insert the expansions into the eigenvalue problem

$$[\underline{\underline{K}} - \omega^2\underline{\underline{M}}]\underline{v} = \underline{0} \tag{2.37}$$

Collecting the terms of zero and first order in ε leads to the equations

$$[\underline{\underline{M}} - \omega_o^2\underline{\underline{K}}_o]\underline{v} = \underline{0} \tag{2.38}$$

$$\omega_1^2 = (\underline{v}^T\underline{\underline{K}}_1\underline{v})/(\underline{v}^T\underline{\underline{M}}\underline{v}) \tag{2.39}$$

Both equations should be fulfilled since (2.37) should hold for all values of ε. In the present case (2.38) and (2.39) lead to an updated eigenfrequency given by

$$\omega_i^{*2} = \omega_i^2 + \gamma_i + \omega_R^2\,\phi_i \tag{2.40}$$

where

$$\gamma_i = \underline{v}^T\,\underline{\underline{K}}_{ae}\,\underline{v}_i \tag{2.41}$$

$$\phi_i = \underline{v}_i^T(\underline{\underline{K}}_g + \underline{\underline{K}}_2)\underline{v}_i \tag{2.42}$$

Note that since the normal forces in the beam elements from the static centrifugal loading is used to calculate $\underline{\underline{K}}_g$, the static loadcase must be solved before the dynamic analysis.

In modal coordinates $\underline{T}$ the linearized dynamic problem is given by (2.22) with the modal damping matrix in (2.30) and the modal frequencies of (2.40).

For a rough estimate of the correction of the first flapwise bending mode, which is influenced mostly by the centrifugal forces, a value of $\phi = 1.73$ may be used (Putter and Manor [10]).

2.4 Static response analysis

The loading on a wind turbine during normal operation can be separated into a static part $\underline{P}_o$ and a dynamic part $\underline{P}(t)$. The response to the static load $\underline{P}_o$ will also be static, i.e. independent of time, once the initial conditions have died out, and consequently the acceleration and the velocity term in the equation of motion will vanish. The static response can be expressed in model coordinates $\underline{T}(t)$ using (2.22), however, a representation of the static response in terms of a few low-order modes cannot be recommended. This is due to the need for a combination of many mode shapes to express the static displacement, and often significant static responses like the beam normal forces are associated with modes with high natural mode frequences. Instead of carrying through an eigenfrequency analysis of very high order the static problem is solved using the full structural stiffness matrix $\underline{\underline{K}}$ from the FE-analysis, i.e.

$$\underline{\underline{K}}\ \underline{X} = \underline{P}_o \tag{2.43}$$

From the static displacement $\underline{X}$ the stress responses in the structure are calculated by means of the element stress-displacement matrices. The static beam normal forces are used to define the geometric stiffness matrix such that the modal natural frequencies may be corrected according to (2.40).

2.5 Dynamic response analysis in the frequency domain

In the following the calculation of the dynamic response to the dynamic load $\underline{P}(t)$ will be outlined using a frequency domain formulation.

The equation of motion was stated earlier in (2.22). Taking the Fourier transform on both sides of the equality sign leads to the equation

$$\{-\omega^2[\ 1\ ] + i\omega\ \underline{\underline{C}}_m + [\ \omega_i^2\ ]\}\underline{T}_f(\omega) = \underline{\underline{v}}^T\underline{P}_f(\omega) \tag{2.44}$$

in which $\underline{T}_f(\omega)$ and $\underline{P}_f(\omega)$ are the Fourier transforms.

$$\underline{T}_f(\omega) = \frac{1}{2\pi}\int_{-\infty}^{\infty} \underline{T}(t)e^{-i\omega t}dt \tag{2.45}$$

$$\underline{P}_f(\omega) = \frac{1}{2\pi}\int_{-\infty}^{\infty} \underline{P}(t)e^{-i\omega t}dt \tag{2.46}$$

From (2.46) it follows that $\underline{T}_f(\omega)$ is given by

$$\underline{T}_f(\omega) = \underline{\underline{G}}(\omega)\underline{P}_f(\omega) = \underline{\underline{H}}(\omega)\ \underline{\underline{v}}^T\ \underline{P}_f(\omega) \tag{2.47}$$

where the modal frequency response matrix $H(\omega)$ is

$$\underline{\underline{H}}(\omega) = \{[\ \omega_i^2-\omega^2\ ] + i\omega\underline{\underline{C}}_m\}^{-1} \tag{2.48}$$

When the off-diagonal terms in $\underline{\underline{C}}_m$ are disregarded, i.e.

$$\underline{\underline{C}}_m = \underline{\underline{v}}^T[\underline{\underline{C}} + \underline{\underline{C}}_{ae} + \underline{\underline{C}}_{co}]\ \underline{\underline{v}} \approx [\ 2\omega_i(\zeta_i + \zeta_i^{ae})\ ] \tag{2.49}$$

$\underline{\underline{H}}(\omega)$ is a diagonal matrix with diagonal terms

$$H_i(\omega) = \frac{1}{\omega_i^2 - \omega^2 + 2i\omega\omega_i(\zeta_i + \zeta_i^{ae})} \tag{2.50}$$

When the modes of vibration are coupled through the damping matrix, a complex-valued matrix must be inverted. Separating $\underline{\underline{H}}(\omega)$ in a real and an imaginary part

$$\underline{\underline{H}}(\omega) = \{\underline{\underline{A}} + i\underline{\underline{B}}\}^{-1} \tag{2.51}$$

and noting that $\underline{\underline{A}}$ for certain frequencies is singular the inverse of $\underline{\underline{A}} + i\underline{\underline{B}}$ is, Fröberg [6]

$$[\underline{\underline{A}} + i\underline{\underline{B}}]^{-1} = \underline{\underline{B}}^{-1}\underline{\underline{A}}(\underline{\underline{A}}\underline{\underline{B}}^{-1}\underline{\underline{A}} + \underline{\underline{B}}) - i(\underline{\underline{A}}\underline{\underline{B}}^{-1}\underline{\underline{A}} + \underline{\underline{B}})^{-1} \tag{2.52}$$

Using the inverse Fourier transform the modal displacements in the time-domain are found as

$$\underline{T}(t) = \int_{-\infty}^{\infty} \underline{\underline{H}}(\omega)\underline{\underline{v}}^{T}\underline{P}_{f}(\omega)e^{i\omega t}\, d\omega \tag{2.53}$$

Finally, the displacements can be found from (2.21) and the stress response from the element stress-displacement matrix $\underline{\underline{S}}_I$ and the local-global displacement transformation matrix $\underline{\underline{G}}_I$ as

$$\underline{\sigma}_I(t) = \underline{\underline{S}}_I\, \underline{\underline{G}}_I\, \underline{X}(t) = \underline{\underline{\eta}}^{I}\underline{T}(t) \tag{2.54}$$

The matrices $\underline{\underline{S}}_I$ and $\underline{\underline{G}}_I$ are briefly introduced in Annex 1.

2.6. Periodic loading

As commented upon in the introduction a substantial part of the rotor loading during steady operation depends only on the rotor position $\theta(t)$. The periodicity in θ of this dynamic loading implies that $\underline{P}(\theta)$ can be written as a Fourier series.

$$\underline{P}(\theta) = \mathrm{Re}\left[\sum_{n=1}^{\infty} \underline{p}_n\, e^{in\theta}\right] \tag{2.55}$$

Here a complex notation has been preferred, and Re [ ] denotes the real value.

Most electricity-producing wind turbines employ either an induction or a synchronous generator, which keeps the rate of revolution either nearly or completely constant. The rotor position can therefore in most cases be expressed as

$$\theta(t) \simeq \omega_R t + \phi \tag{2.56}$$

where ϕ is the initial phase angle, and the period of rotation is $T_o = 2\pi/\omega_R$. Hence, this part of the loading can be assumed periodic in time with the Fourier expansion

$$\underline{P}(t) = \mathrm{Re}\left[\sum_{n=1}^{\infty} \underline{\alpha}_n \, e^{in\omega_R t}\right] \tag{2.57}$$

in which the complex amplitude vector $\underline{\alpha}_n$ is defined as

$$\underline{\alpha}_n = \frac{\omega_R}{2\pi} \int_{-\pi/\omega_R}^{\pi/\omega_R} \underline{P}(t) \, e^{-in\omega_R t} \, dt \tag{2.58}$$

The Fourier transform (2.44) of $\underline{P}(t)$ is expressed in terms of Dirac's delta function $\delta(x)$ as

$$\underline{P}_f(\omega) = \sum_{n=1}^{\infty} \alpha n \; \delta(\omega - n\omega_R) \tag{2.59}$$

Inserting in (2.53) and carrying out the integration yields the solution for the periodic modal response

$$\underline{T}(t) = \mathrm{Re}\left[\sum_{n=1}^{\infty} \underline{\underline{H}}(n\omega_R)\underline{\underline{v}}^T \underline{\alpha}_n \, e^{in\omega_R t}\right] \tag{2.60}$$

In reality, the summation in (2.57) and (2.60) will be truncated after a limited number of terms, e.g. 20.

2.7. Stochastic loading

In addition to the static and the periodic loading a wind turbine rotor will experience a random fluctuating load due to turbulence in the wind. This part of the loading may conveniently be modelled as a stochastic vector process $\underline{P}(t)$ with zero mean

$$E\{\underline{P}(t)\} = \underline{\mu}^P = \underline{0} \tag{2.61}$$

and a covariance matrix

$$\underline{\underline{R}}^P(t_1,t_2) = \underline{\underline{R}}^P(\tau) = E\{(\underline{P}(t_1) - \underline{\mu}P)(\underline{P}(t_2) - \underline{\mu}P)T\} \tag{2.62}$$

Stationarity has been assumed here for the first two moment functions which leads to a time-independent mean vector and a covariance matrix, which depends only on time differences $\tau = t_1 - t_2$.

A traditional and convenient representation of the covariance matrix is in terms of a power spectral density matrix $\underline{\underline{S}}^P(\omega)$ which is related to $\underline{\underline{R}}(\tau)$ by

$$\underline{\underline{R}}^P(\tau) = \int_{-\infty}^{\infty} \underline{\underline{S}}^P(\omega) e^{i\omega\tau} \, d\omega \tag{2.63}$$

i.e., $\underline{\underline{S}}^P(\omega)$ is the Fourier transform of $\underline{\underline{R}}^P(\tau)$. The diagonal elements in $\underline{\underline{R}}^P(\tau)$) are usually denoted the autocovariance function of the elements of $\underline{P}(t)$ which for zero timelag τ is equal to the variance. The off-diagonal elements are the cross-covariance functions of the load components which in contrast to the autocovariance functions are in general not symmetric in τ. From the definition (2.62) is seen that

$$\underline{\underline{R}}^P(\tau) = \underline{\underline{R}}^P(-\tau)^T \tag{2.64}$$

which implies that $S^P(\omega)$ is Hermitian. The systematic time delay, which is reflected in the non-symmetry of the cross-covariance, is contained in the imaginary part of the cross-spectral density functions. Since the response of structures of a certain size due to turbulent wind loading strongly depends on the spatial structure of the turbulence, cross-spectral densities are important when using a discretized wind load model.

From the theory of linear random vibration, e.g. Madsen [7], it follows that the power spectral density matrix $\underline{\underline{S}}(\omega)$ for a linear system with the frequency response matrix $\underline{\underline{G}}(\omega)$ is

$$\underline{\underline{S}}(\omega) = \underline{\underline{G}}(\omega) \, \underline{\underline{S}}^P(\omega) \, \overline{\underline{\underline{G}}(\omega)}^T \tag{2.65}$$

where an overbar denotes the complex conjugate and $[\ ]^T$ the transposed matrix. Hence, using (2.47) the power spectral density matrix $\underline{\underline{S}}^T(\omega)$ for the modal displacements $\underline{T}(t)$ can be written

$$\underline{\underline{S}}^T(\omega) = \underline{\underline{H}}(\omega)\ \underline{\underline{v}}^T\ \underline{\underline{S}}^P(\omega)\ \underline{\underline{v}}\ \overline{\underline{\underline{H}}(\omega)}^T \tag{2.66}$$

where $\underline{\underline{H}}(\omega)$ is given in (2.48).

The covariance matrix of the modal displacements $\underline{T}(t)$ is obtained by Fourier transforming (2.66) as in (2.63).

From $\underline{\underline{S}}^T(\omega)$ power spectral density functions for displacements $X_j(t)$ and element stresses $\sigma_{Ij}(t)$ can be calculated using

$$X_j(t) = \sum_{k=1}^{N} v_{jk} T_k(t) \tag{2.67}$$

from (2.23) and

$$\sigma_{Ij}(t) = \sum_{k=1}^{N} \eta^I_{jk} T_k(t) \tag{2.68}$$

from (2.54). Hence

$$S^{Xj}(\omega) = \sum_k \sum_\ell \left[v_{jk} v_{j\ell} S^T_{k\ell}(\omega) \right] \tag{2.69}$$

and

$$S^{\sigma Ij}(\omega) = \sum_k \sum_\ell \left[\eta^I_{jk}\ \eta^I_{j\ell}\ S^T_{k\ell}\ (\omega) \right] \tag{2.70}$$

As (2.69) and (2.70) are quadratic forms, only the real part of $S^T_{k\ell}\ (\omega)$ need be considered such that

$$S^{Xj}(\omega) = \sum_k \sum_\ell \left[v_{jk} v_{j\ell}\ \mathrm{Re}\left[S^T_{k\ell}(\omega) \right] \right] \tag{2.71}$$

$$S^{\sigma Ij}(\omega) = \sum_k \sum_\ell \left[\eta^I_{jk}\ \eta^I_{j\ell}\ \mathrm{Re}\left[S^T_{k\ell}(\omega) \right] \right] \tag{2.72}$$

An incomplete, but for certain purposes sufficient discription of the covariance structure of a stationary random process is in terms of the spectral moment λ_n, Vanmarcke [12]. The spectral moments are defined

$$\lambda_n = 2 \int_0^\infty \omega^n S(\omega) d\omega, \quad n = 0,1,2..N \tag{2.73}$$

Note from the definition (2.65) that λ_0 is the variance of the process itself, λ_2 is the variance of the process derivative, λ_4 of the double derivative and henceforth.

From (2.73) and (2.74) it follows that λ_k for both stress or displacement response can be written in terms of the real modal response moment, e.g.

$$\lambda_k^{Xj} = \sum_k \sum_\ell [v_{jk} \, v_{j\ell} \, \lambda_n^{k\ell}] \tag{2.74}$$

in which

$$\lambda_n^{k\ell} = 2 \int_0^\infty \omega^k \, \mathrm{Re}[S_{k\ell}^T(\omega)] d\omega \tag{2.75}$$

Since $\lambda_n^{k\ell}$ is symmetric in k and ℓ, (2.74) can be written

$$\lambda_n^{Xj} = \sum_{k=1}^N v_{jk}^2 \, \lambda_n^{kk} + 2 \sum_{k=1}^N \sum_{\ell=k+1}^N v_{jk} \, v_{j\ell} \, \lambda_n^{k\ell} \tag{2.76}$$

Usually only the four spectral moments λ_0, λ_1, λ_2, λ_4 are of interest. Note that the higher order of λ_n, the greater the emphasis put on the high-frequency tail of the spectrum. Due to limited resolution in measuring systems this part of the spectra of real physical processes is poorly known. Thus formulations should be avoided which use high-order spectral moments.

From the numerical calculation of modal load and response spectra as described in ch. 5, a truncated spectrum is obtained

$$S_{k\ell}^{T*}(\omega) = \begin{cases} S_{k\ell}^T(\omega) & |\omega| \leq \omega_c \\ 0 & |\omega| > \omega_c \end{cases} \tag{2.77}$$

Thus spectral moment corresponding to a truncated spectrum can be calculated. An additional correction term, however, is proposed

based on the observation that for large ω, $S^T_{k\ell}(\omega)$ decays as $\omega^{-4}\omega^{-5/3}$. The first power is due to the system response and the second to the von Karman spectrum of turbulent wind fluctuations.

Assuming that for $\omega > \omega_c$

$$\mathrm{Re}[S^T_{k\ell}(\omega)] \approx \mathrm{Re}[S^T_{k\ell}(\omega_c)]\ \omega_c^{17/3}\ \omega^{-17/3} \tag{2.80}$$

$\lambda_n^{k\ell}$ can be written

$$\lambda_n^{k\ell} = 2 \int_0^{\omega_c} \omega^k\ \mathrm{Re}[S^T_{k\ell}(\omega)]d\omega$$

$$+ \frac{6}{14-3n}\ \mathrm{Re}[S^T_{k\ell}(\omega_c)]\omega_c^{n+1} \tag{2.81}$$

The integral in (2.79) is calculated numerically, using an extended Simpson rule (Abramowitz and Stegun [1]).

2.8. Power regulation by pitch control

An essential part of a wind energy conversion system is the method by which the power output is controlled. As mentioned above, most wind turbines operate at a constant frequency of rotation using either stall- or pitch-regulation. Stall-regulation implies nothing more than a fixed rotor geometry where the pitch angle is adjusted such that stall occurs at the rated power, thus reducing the lift on the blades and consequently the power output. For larger wind turbines pitch-regulation is usually preferred, and in this section the inclusion of a simple pitch-regulation system in the structural system equations is outlined.

The principle of pitch-regulation is that by actively changing the pitch angle and thus the angle of attack $\theta(t)$ at the blades the lift forces and the power can be controlled. $\theta(t)$ is forced by the structural response through a regulation algoritm and a feedback loop. Often the electrical power which can be assumed linearly related to the torsional moment in the rotor axle, is

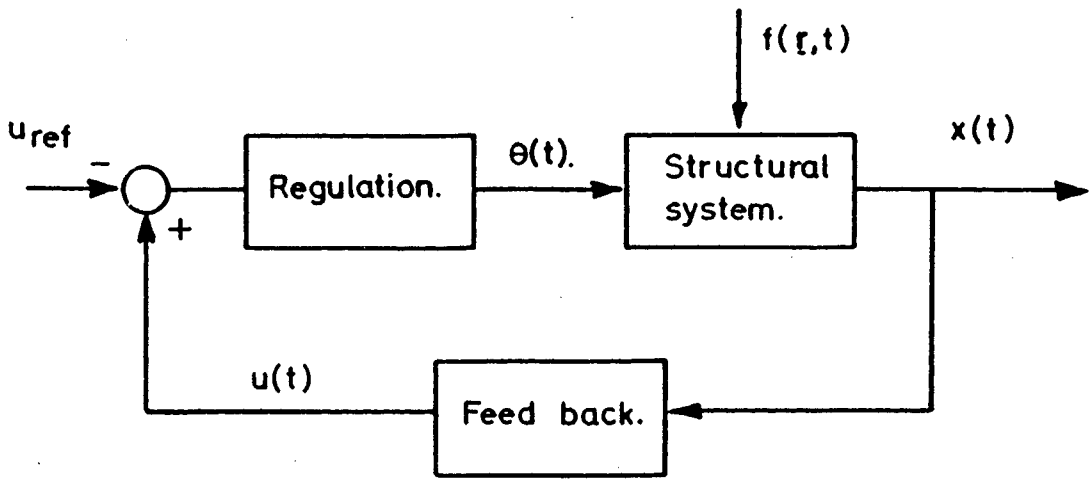

Fig. 2.4. Elements of a pitch angle controlled wind energy conversion system.

used as forcing term in the regulation algorithm. A diagram of the total system is shown in Fig. 2.4.

The regulation algoritm is assumed to be of the form

$$\alpha\dot{\theta} + \beta\dot{\theta} = c(u(t)-u_{ref}) \tag{2.80}$$

When the influence of the pitch angle is linearized, the structural system equation reads

$$\underline{\underline{M}}\ddot{\underline{X}} + \underline{\underline{C}}\ddot{\underline{X}} + \underline{\underline{K}}\underline{X} = P_o + P(t) - \underline{F}_\theta\,(\theta-\theta_o) \tag{2.81}$$

in which θ_o is the reference pitch angle. Expressed in the modal coordinates and excluding the static load $\underline{P}_o$, (2.83) becomes

$$\begin{bmatrix} 1 \end{bmatrix}\ddot{\underline{T}} + \underline{\underline{C}}_m\dot{\underline{T}} + \begin{bmatrix} \omega_i^2 \end{bmatrix}\underline{T} = \underline{q}(t) - \underline{\underline{v}}^T\,\underline{F}_\theta(\theta-\theta_o) \tag{2.82}$$

Finally, the feedback signal u(t) is related to the system variables by

$$u(t) - u_{ref} = \underline{A}^T\underline{X} = \underline{A}^T\underline{\underline{v}}\underline{T} \tag{2.83}$$

Substituting (2.83) into (2.80) and taking the Fourier transform yields

$$\theta_f = H_1(\omega)\ \underline{A}^T\underline{\underline{v}}\underline{T}_f \tag{2.84}$$

where

$$H_1(\omega) = \frac{1}{i\beta\omega - \alpha\omega^2} \tag{2.85}$$

Finally, inserting (2.84) into the Fourier transform of (2.80) leads to the relation

$$\underline{T}_f = \underline{\underline{H}}(\omega)\ \underline{q}_f \tag{2.86}$$

in which

$$\underline{\underline{H}}(\omega) = \{[\ \omega_i^2 - \omega^2\ ] + i\underline{\underline{C}}_m\omega + H_1(\omega)\underline{\underline{v}}^T\underline{F}_\theta\ \underline{A}^T\underline{\underline{v}}\}^{-1} \tag{2.87}$$

(2.87) should be compared to (2.48) for the unregulated system. Note that the total system now acts as a band-pass filter, thus excluding very low and very high load frequencies. Note also that the pitch angle control couples the modes.

In (2.81) the mass, damping and stiffness matrices are assumed independent of the pitch angle. This is not strictly true, however, the variation of θ is usually very slow and small $\sigma_\theta \approx 1.5^o$ and the assumption therefore seems justified.

REFERENCES

[1] ABRAMOVITZ, M. and STEGUN, I.A. (eds) (1965). Handbook of Mathematical Functions (Dover, New York), 1046 pp.

[2] CAUGHEY, T.K. (1960). Classical Normal Modes in Damped Linear Dynamic Systems, 27, 269-271.

[3] COLLINS, J.D. and THOMPSON, W.T. (1969). The Eigenvalue Problem for Structural Systems with Statistical Properties, AIAA, 7, 642-648.

[4] CLOUGH, R.W. and PENZIEN, J. (1975). Dynamics of Structures, (McGraw-Hill, New York), 634 pp.

[5] DYRBYE, C. (1977). Bygningsdynamik, Vol. 2 (Den private Ingeniørfond, Lyngby), 214 pp.

[6] FRÖBERG, C.E. (1965). Introduction to Numerical Analysis. (Addison-Wesley, Reading, Mass.), 350 pp.

[7] MADSEN, P.H. (1983). Stochastic response analysis and first-passage probabilities, Risø-R-485, 171 pp.

[8] PAPOULIS, A. (1962). The Fourier Integral and its applications (McGraw-Hill, New York), 318 pp.

[9] PRZEMIENCKI, J.S. (1968). Theory of Matrix Structural Analysis (McGraw-Hill, New York), 468 pp.

[10] PUTTER, S. and MANOR, H. (1978). Natural Frequencies of Radial Rotating Beams", J. Sound Vib., 56, 175-185.

[11] SYMON, K.R. (1960). Mechanics. 2nd ed. (Addison-Wesley Reading Mass.), 557 pp.

[12] VANMARCKE, E.H. (1972). Properties of Spectral Moments with Applications to Random Vibration. J. Eng. Mech. Div., ASCE, 98, EM2, 425-446.

3. THE AERODYNAMIC MODEL

In order to quantify the aerodynamic loads on the blades of a wind turbine due to the airflow, an aerodynamic model is necessary to relate the wind pressure to the direction and the magnitude of the relative wind speed. Several theories are available for the aerodynamic loads on horizontal-axis propeller-type wind turbines, De Vries [4], among which the blade element theory is noticed for its relative simplicity.

The basic assumption is that the flow is laminar and homogeneous, which is not representative of the flow experienced under atmospheric conditions. Nevertheless, with respect to the static loads on wind turbine blades good results have been obtained with the blade element theory. The method, which is described in detail in Andersen et al. [2], assumes that the wind speed is constant over the entire rotor, and that the wind velocity vector is perpendicular to the rotorplane. In most cases this is not strictly true. However, when the static mean load is considered, the deviations from the assumptions are small enough to be neglected in this context. Although the basic assumptions to some degree are violated, the load derivatives with respect to fluctuations in wind speed as predicted by the blade element theory will be used for the dynamic wind loading.

The chapter commences with a brief review of the principles and the fundamental equations of the blade element theory. In its ordinary form the method is used to predict the static rotor loads.

The fluctuating loads are determined under the assumption that the blade element theory holds for all rates of changes of the wind velocity. A linearization of the relation between wind pressure and the relative airspeed and angle of attack is described, and the resulting aerodynamic influence coefficients are presented.

Finally, the aerodynamic damping and stiffness are derived following the considerations in section 2.3.

3.1. Blade element theory

The blade element theory relates the forces on the blades of a wind turbine or a propeller to the motion relative to the air. Basically the propeller is divided into a number of annular elements characterized by the radius r and the width dr. It is assumed that each element can be considered independently and that the axial and tangential flow is uniform across the annular element. The blade elements are further assumed to act as two-dimensional aerofoils such that for an angle of attack α and a relative air velocity W, the lift and drag forces on one blade of the element are

$$dL = \rho W^2 c\, C_L(\alpha) dr \qquad (3.1)$$

$$dD = \rho W^2 c\, C_D(\alpha) dr \qquad (3.2)$$

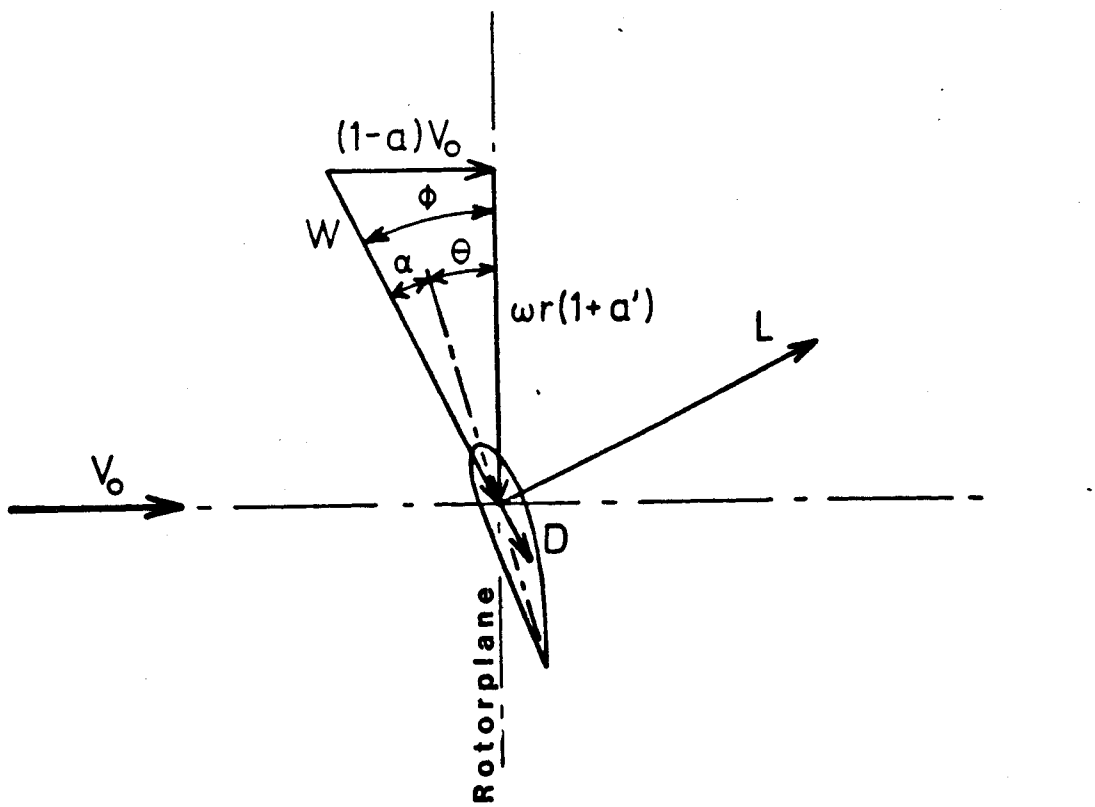

Fig. 3.1. Illustration of loads on a profile of the blade element.

as is illustrated in Fig. 3.1. In (3.1) and (3.2) ρ is the density of the air (ρ = 1.29 kg/m^3, dry air at 0°C, 760 mm), c is the profile chord and C_L, C_D are the lift and drag curves of the profile.

The thrust and torque on an annular rotor element dr can then be written

$$dT = \tfrac{1}{2} \rho W^2 c B C_Y dr \tag{3.3}$$

$$dQ = \tfrac{1}{2} \rho W^2 c B C_X r dr \tag{3.4}$$

in which B is the number of blades and dT, dQ are the thrust and torque, respectively.

The force coefficients are given by

$$C_Y = C_L(\alpha)\cos\phi + C_D(\alpha)\sin\phi \tag{3.5}$$

$$C_X = C_L(\alpha)\sin\phi - C_D(\alpha)\cos\phi \tag{3.6}$$

and

$$\phi = \alpha + \theta \tag{3.7}$$

where θ is the pitch angle as shown in Fig. 3.1.

To proceed further the induced axial and tangential air speed described in terms of the interference factors a,a'. Fig. 3.1., must be determined. According to the sign and magnitude of the axial interference factor a the operation of the wind turbine is divided into the propeller, windmill, turbulent wake and vortex ring states, among which the windmill state is the normal one. The propeller and turbulent wake states may be encountered during braking and high tip speed ratios, respectively. The states are illustrated in Fig. 3.2 from Yamane et al. [9]. In the case of $a < 1/2$ the momentum theory of Betz, Glauert [5] holds the necessary relations to determine the rotor loads.

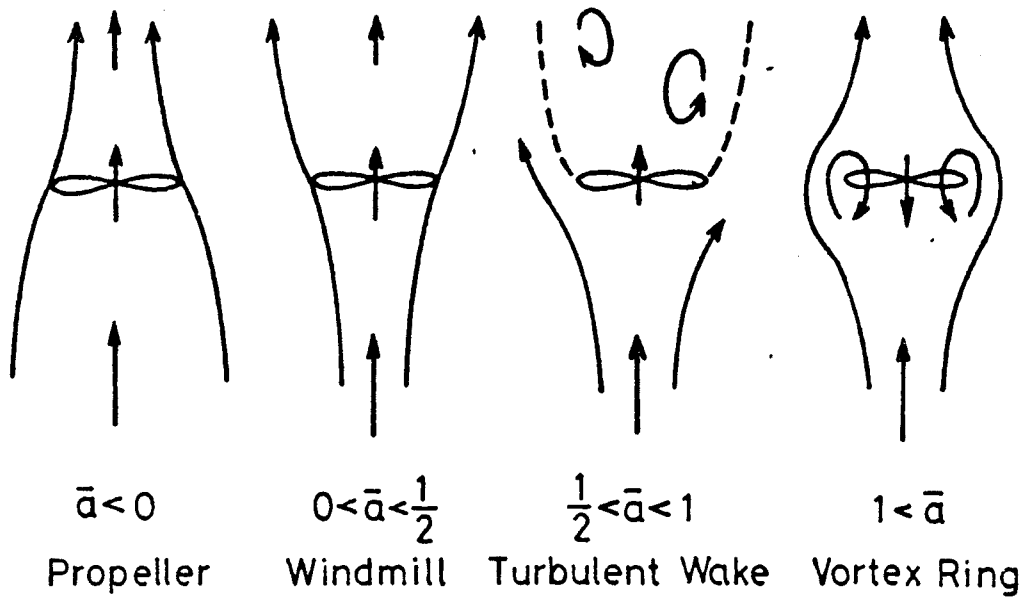

Fig. 3.2. Operation states of a wind turbine, from [9].

Thus, for an annular element the momentum theory predicts the following thrust and torque on the annular element.

$$dT = 4\pi r \rho V_o^2 a(1-a)dr \tag{3.8}$$

$$dQ = 4\pi r^3 \rho V_o \omega_R \, a'(1-a)dr \tag{3.9}$$

By equating (3.8) and (3.9) to (3.3) and (3.4) a,a' and dT,dQ can be determined by an iterative procedure. In deriving (3.8) it has been assumed that the rotational velocities are small and can be disregarded in the momentum equations for the axial flow.

The assumption of uniform flow across the annular element is correct only for an infinite number of blades. Due to the flow around the edges leading to vortex sheets being shed from the trailing edges of the blades at the boundary of the wake, the flow through the annular element is periodic, which must be taken into account in the momentum equation. The usual method (Glauert [5]) is to introduce a tip loss correction based on the assump-

tion that the maximum changes of the axial and tangential velocities, $2aV_o$ and $2a\,\omega_R r$, in the slipstream occur only on the vortex sheets, and the average change is only a fraction F of this change.

Based on simplified assumptions on the periodic flowfield Prandtl has suggested the solution (Glauert [5]),

$$F = \frac{2}{\pi} \arccos(e^{-f}) \tag{3.10}$$

and

$$f = \frac{B}{2} \frac{R-r}{\sin\phi} \tag{3.11}$$

in which R is the length of the blade and r the considered radius.

Multiplying the thrust and torque from the momentum considerations, (3.8) and (3.9), with F the induction factors a,a' can be written

$$a = 1/\left(\frac{4\sin^2\phi F}{\sigma C_Y} + 1\right) \tag{3.12}$$

$$a' = 1/\left(\frac{4\sin\phi\cos\phi F}{\sigma C_X} - 1\right) \tag{3.13}$$

in which the solidity σ is given by

$$\sigma = \frac{cB}{2\pi r} \tag{3.14}$$

The determination of a and a' from (3.12) and (3.13) is an iterative process, since ϕ and C_X,C_Y are functions of a,a'. Once the induction factors have been determined the elemental thrust and torque can be calculated from (3.3) and (3.4).

From the simple axial momentum theory a velocity of $V_o(1-2a)$ in the far slipstream is predicted. It is therefore clear that the blade element theory in the form above is valid only for a = 1/2, i.e. in the windmill and the propeller state. Several attempts have been made to extend blade element theory to the case where no ordinary slipstream exists (see e.g. Rosenbrock [7], Yamane et al. [9] and Anderson et al. [3]). In this work the proposed extension by Anderson et al.[3] will be used due to the good agreement with experimental result. Thus, the axial momentum equation (3.8) for the thrust on an annular element is replaced for a > 0.326 by

$$dT = F(1.39a + 0.425)\ \rho V_o^2\ 2\pi r\ dr;\ a > 0.326 \qquad (3.15)$$

in which the tip loss correction has been included without much theoretical justification. Apart from a modification of (3.12) the calculations proceed as before.

For practical calculations, the blades are divided into a suitable number of elements N, and for each element i, a_i and a_i' are calculated, assuming the element to be independent of the neighbouring ones. The force elements dT_i and dQ_i act at the distance

$$r_i = \left(\frac{i-\frac{1}{2}}{N}\right)R \qquad (3.16)$$

from the rotor centre and should be distributed equally on all blades. Once dT_i and dQ_i have been determined, any cross section forces due to air loads are easily calculated by adding the contributions from each blade element. Up to this point the airloads on the blade in terms of the lift and the drag forces shown in Fig. 3.1 have been referred to the aerodynamic centre of the blade profile. The aerodynamic center is defined as the point at which the moment from the airloads on a two-dimensional blade profile vanishes. Referring the loads to the aerodynamic center, however, has two disadvantages. Firstly, the location of the aerodynamic center is not constant but depends on the angle of attack α. This problem can be circumvented by referring the loads to a fixed point, the front quarterpoint of the profile

chord and introducing the pitching moment (Abbott et al. [11]) as

$$dM_{c/4} = \tfrac{1}{2}\rho w^2 c^2 C_M(\alpha)\, dr \tag{3.17}$$

in which $C_M(\alpha)$ is the pitch-moment coefficient. An example of the lift, drag and moment coefficients as functions of the angle of attack is shown in Fig. 3.3 from Abbott et al. [1] for the NACA 4415 wing profile.

The second problem arises where the aerodynamic loads are used in the subsequent structural analysis. Using ordinary three-dimensional beam elements, as is assumed in the present context the loads should be given with respect to the shear center of the beam element.

In Fig. 3.4 a cross-section of a blade at radius r is shown. The point 0 is the shear center while the other point is the chord quarterpoint. In the local blade coordinates the load vector for the blade element at the $c/4$-point is

$$\begin{vmatrix} df_x^* \\ df_y^* \\ dM_{c/4} \end{vmatrix} = \begin{vmatrix} dQ/(rB) \\ dT/B \\ dM_{c/4} \end{vmatrix} \tag{3.18}$$

Hence, at the shear center 0 the load vector is

$$d\underline{F}' = \begin{vmatrix} df_x' \\ df_y' \\ dM' \end{vmatrix} = \begin{vmatrix} df_x^* \\ df_y^* \\ dM_{c/4} - df_x^* Y' + df_y^* X' \end{vmatrix} \tag{3.19}$$

Here, X',Y' are the coordinates of the c/4 point in the local blade coordinates and can be expressed by

$$X' = X_0 \cos\theta + Y_0 \sin\theta \tag{3.20}$$

$$Y' = -X_0 \sin\theta + Y_0 \cos\theta \tag{3.21}$$

X_0, Y_0 are the coordinates for zero pitch angle, and θ is the pitch angle.

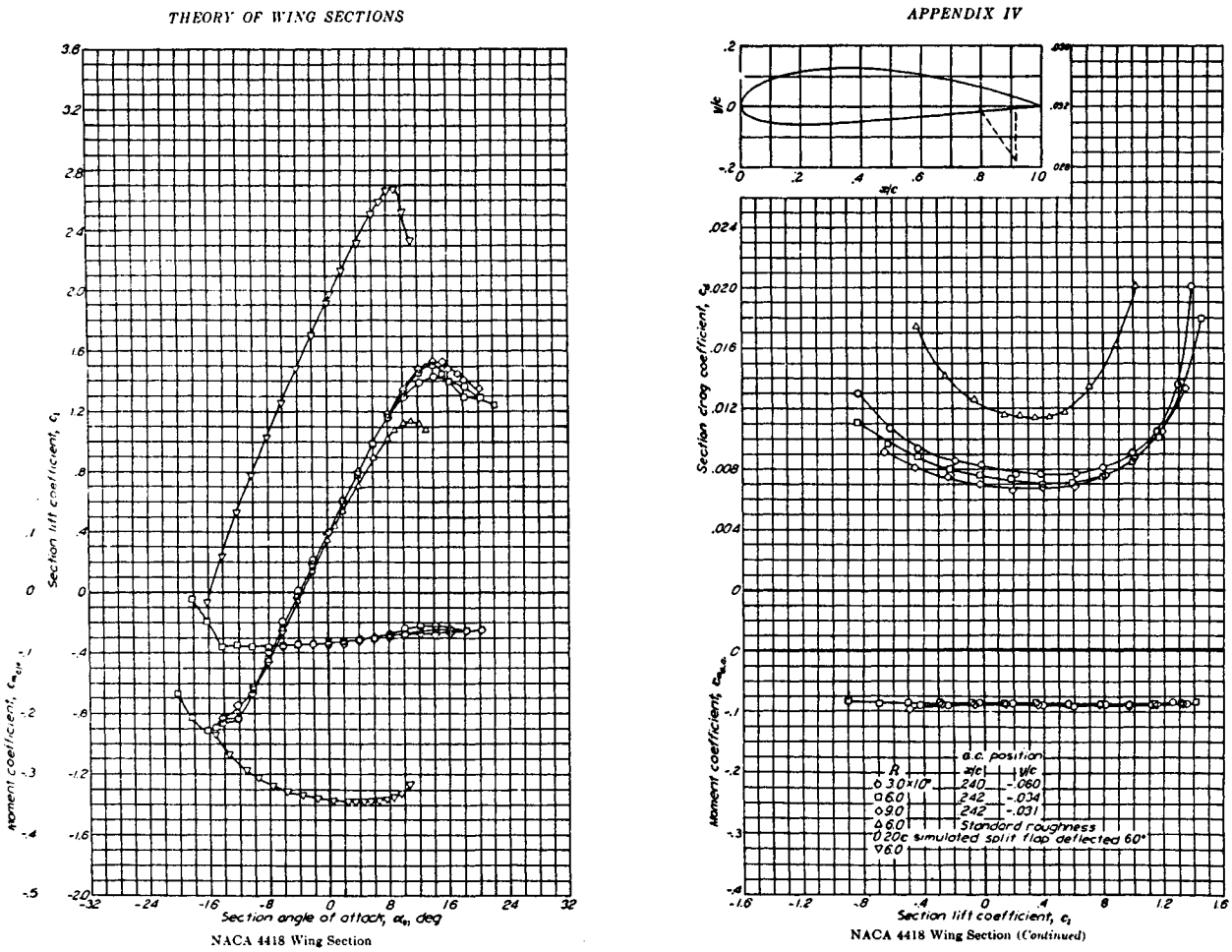

Fig. 3.3. Lift, drag and moment curves for the NACA 4415 profile, [1].

Using the relations in (2.8) and (2.9) the blade element loads are expressed in the global coordinate system as

$$d\underline{F} = \begin{vmatrix} dP_x \\ dP_y \\ dP_z \\ dM_x \\ dM_y \\ dM_z \end{vmatrix} = \underline{\underline{T}}_2 \underline{\underline{T}}_1 d\underline{F}' = \begin{vmatrix} df'_x \cos\theta \\ df'_r \\ -df'_x \sin\theta \\ dM' \sin\theta \\ 0 \\ dM' \cos\theta \end{vmatrix} \qquad (3.22)$$

$\underline{\underline{T}}_1$ and $\underline{\underline{T}}_2$ are transformation matrices which transform from the local two-dimensional frame of reference to the corresponding

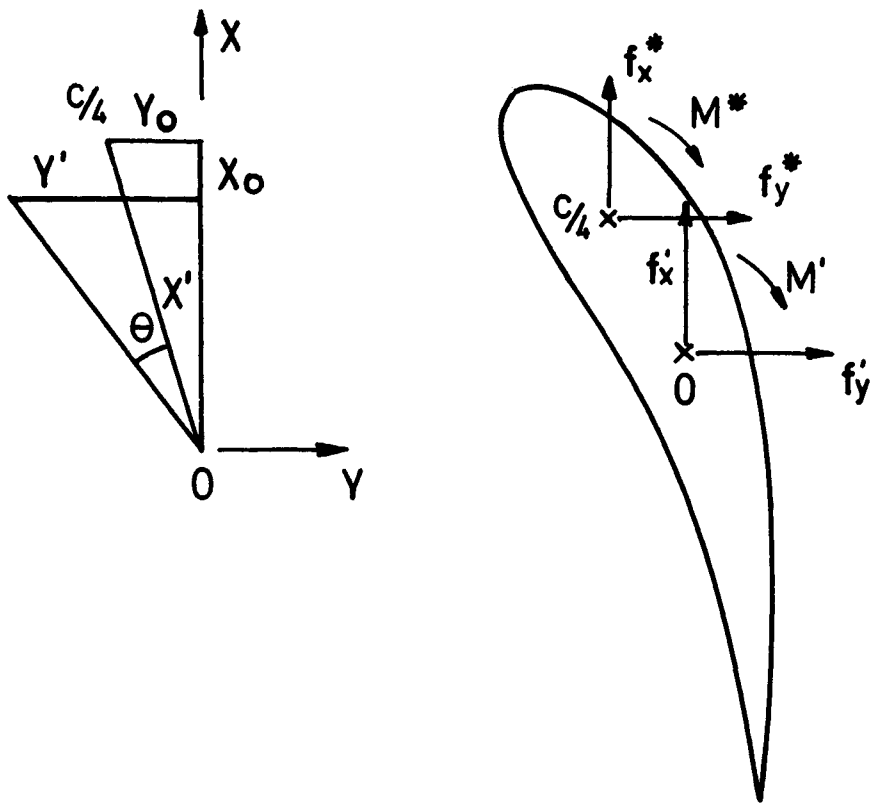

Fig. 3.4. Blade profile geometry.

three-dimensional one and from there to the global coordinate system.

$$\underline{\underline{T}}_1 = \begin{vmatrix} 1 & 0 & 0 \\ 0 & 1 & 0 \\ 0 & 0 & 0 \\ 0 & 0 & 0 \\ 0 & 0 & 0 \\ 0 & 0 & 1 \end{vmatrix} \qquad (3.23)$$

$$\underline{\underline{T}}_2 = \begin{vmatrix} \underline{\underline{A}} & \underline{\underline{0}} \\ \underline{\underline{0}} & \underline{\underline{A}} \end{vmatrix} \qquad (3.24)$$

in which the matrix $\underline{\underline{A}}$ follows from (2.9).

3.2. Aerodynamic influence coefficient

The blade element theory as presented in the previous section predicts the windforcing on the rotor arising from a uniform windfield constant in time. Although the basic assumptions will be violated, the blade element theory will, in addition, be used for calculating the dynamic loads from a nonsteady windfield due to the lack of a simple model for unsteady windturbine aerodynamics. Hence, the relation between the windspeed and steady aerodynamic loads will be assumed to apply in the dynamic case. It follows from the presentation of the theory that the relation is nonlinear which is contrary to the linearity requirements put forward in section 2.3. A linearization of the relation between on the one hand the fluctuation of windspeed and the angle of attack and on the other the load fluctuations around the mean value predicted by the blade element theory in its original form will be pursued.

In short the task is to find the aerodynamic influence coefficients, such that the forces on a blade element in the local blade X'Y'-coordinate system, Fig. 2.2, for a fluctuating windspeed

$$\underline{V} = \frac{v}{V_o+u} \tag{3.25}$$

and a fluctuation in pitch angle $\Delta\theta$, are given approximately by

$$d\underline{F} = \begin{vmatrix} df'_x \\ df'_y \\ dM' \end{vmatrix} + \begin{vmatrix} c_{11} & c_{12} & c_{13} \\ c_{21} & c_{22} & c_{23} \\ c_{31} & c_{32} & c_{33} \end{vmatrix} \begin{vmatrix} u \\ v \\ \Delta\theta \end{vmatrix} \tag{3.26}$$

in which the first terms follows from (3.19).

By use of (2.9) the aerodynamic loads can be expressed in the global coordinates. For a lightly loaded rotor with a high tip-speed ratio, i.e. a, a' $\sim$ 0 and $\omega_R r_{tip} >> V_o$, the relative windspeed W and the angle of attack near the tips are approximated well by

$$W^2 = (V_o + u)^2 + (\omega_R r + v)^2 \simeq \omega_R^2 r^2 \tag{3.27}$$

$$\alpha = \arctan\left(\frac{V_o+u}{\omega_R r+v}\right) - (\theta + \Delta\theta) \simeq \frac{V_o+u}{\omega_R r} - (\theta + \Delta\theta) \tag{3.28}$$

for small windspeed fluctuations v,u in the X,Y direction of the local blade coordinates (Fig. 2.2). The main effect is thus the change of angle of attack and within this approximation only the fluctuating component perpendicular to the rotorplane is of interest. A similar consideration was used in Jensen and Frandsen [6] for taking into account only the along-wind component of wind turbulence.

Using (3.27) and (3.28) a simple set of influence coefficients is easily obtained as the coefficients of the linear term in a Taylor expansion of (3.3) and (3.4).

The assumptions leading to (3.27) and (3.28) are unacceptable in the present context where a large number of various operating conditions must be analyzed among which low tip speed ratios are likely to occur. Preserving the concept of influence coefficients as the coefficients of the linear term in a Taylor expansion of the relation between load and windspeed predicted by the blade element theory, two possibilities exist. Either the coefficients are derived assuming constant induction factors, the 'frozen wake' approach, or that the induced velocities have the steady state values for the instantaneous wind speed, the 'equilibrium wake' approach (Tresher et al. [8]).

The latter approach is adopted here, and the dynamic windspeed/load relation is thus approximated by the tangents to the curves of the steady state loads as functions of windspeed or rotational speed. An example of the load curves as functions of windspeed is shown in Fig. 3.5, showing the load per unit length at radius r = 10 m and r = 19 m for the Nibe-A turbine. This turbine is stall regulated with an induction generator, and stall occurs at windspeeds larger than ca. 12 m/s. The pitch angles are changed at V = 10 m/s which causes the discontinuity in the curves.

The local slopes of the curves can be determined analytically; the expressions, however, are complicated. Instead the influence coefficients are determined numerically, calculating the loads by the blade element theory at windspeeds, $v_o - \frac{\Delta V}{2}$, V_o, $V_o + \frac{\Delta V}{2}$ at rotational speeds $\omega_R - \frac{\Delta\omega}{2}$, ω_R, $\omega_R + \frac{\Delta\omega}{2}$ and at pitch angles $\theta - \Delta\theta/2$, θ, $\theta + \Delta\theta/2$.

3.3. Aerodynamic damping

The velocity fluctuations v,u at a point of the blade are in general caused both by fluctuations in the natural wind v',u' and the vibrational velocities of the blade at the point in question. Thus

$$\begin{vmatrix} v \\ u \end{vmatrix} = \begin{vmatrix} v' \\ u' \end{vmatrix} + \begin{vmatrix} \dot{x}' \\ \dot{y}' \end{vmatrix} \tag{3.29}$$

The Z-component is of no interest due to the assumption of two-dimensional aerodynamics. It follows that the aerodynamic damping matrix derived in section 2.3 can be expressed in terms of the influence coefficients, however, the linearized relationship should be expressed in the global XYZ-coordinate system instead of in the local blade X',Y',Z' coordinates.

Consider therefore a node in the structural model which in the local two-dimensional frame of reference has the generalized velocity $\underline{\dot{u}} = [\dot{X},\dot{Y},\dot{\theta}]^T$. It follows from the aerodynamic model that a nonzero time derivative of the pitch angle in itself does not induce load changes. Thus, the aerodynamic damping matrix for the node in question can be written

$$\underline{\underline{C}}_{ac} = - \underline{\underline{T}}_2 \underline{\underline{T}}_1 \, \underline{\underline{C}}^* \underline{\underline{T}}_1^T \underline{\underline{T}}_2^T \tag{3.30}$$

in which $\underline{\underline{T}}_1$ and $\underline{\underline{T}}_2$ are the transformation matrices in (3.23) and (3.24), and $\underline{\underline{C}}^*$ is given in (3.26), however, with the third column substituted by zeros. The aerodynamic influence co-efficients

corresponding to the nodes of the structural model are determined by adding together the contributions from the adjoining elements assuming a linear displacement field. Carrying out the multiplication yields the following expression for the aerodynamic damping

$$\underline{\underline{C}}_{ac} = [\underline{\underline{C}} \quad \underline{\underline{0}}] \tag{3.31}$$

where

$$\underline{\underline{C}} = - \begin{vmatrix} C_{11}\cos^2\phi & C_{12}\cos\phi & -C_{11}\cos\phi\sin\phi \\ C_{21}\cos\phi & C_{22} & -C_{21}\sin\phi \\ -C_{11}\sin\phi\cos\phi & -C_{12}\sin\phi & C_{11}\sin^2\phi \\ C_{31}\sin\phi\cos\phi & C_{32}\sin\phi & C_{31}\sin^2\phi \\ 0 & 0 & 0 \\ C_{31}\cos^2\phi & C_{32}\cos\phi & C_{31}\cos\phi\sin\phi \end{vmatrix} \tag{3.32}$$

The damping matrix in (3.31) thus corresponds to both the translational and the rotational degrees of freedom of the node at the position r,ϕ in polar coordinates.

3.4. Aerodynamic stiffness

As pointed out earlier, a deflection thath changes the pitch angle will also induce changes in the loading. Thus, if a node has the instantaneous displacement $\underline{u}^* = [X,Y,\Delta\theta]^T$, the rotation component $\Delta\theta$ will result in an aerodynamic load. The aerodynamic stiffness matrix for the node can then be written as

$$\underline{\underline{K}}_{ac} = - \underline{\underline{T}}_2\underline{\underline{T}}_1 \, \underline{\underline{K}}^* \, \underline{\underline{T}}_1^T\underline{\underline{T}}_2^T \tag{3.33}$$

in terms of the transformation matrices in (3.23) and (3.24), and $\underline{\underline{K}}^*$, which contains the third column from $\underline{\underline{C}}$ in (3.26). The elements in $\underline{\underline{K}}_{ac}$ follow from

$$\underline{\underline{K}}_{ac} = [0 \quad \underline{\underline{K}}] \tag{3.34}$$

where

$$\underline{\underline{K}}_{ac} = - \begin{vmatrix} k_{13} \cos\phi \sin\phi & 0 & k_{13} \cos^2\phi \\ k_{23} \sin\phi & 0 & k_{23} \cos\phi \\ -k_{13} \sin^2\phi & 0 & -k_{13} \cos\phi \sin\phi \\ k_{33} \sin^2\phi & 0 & k_{33} \sin\phi \cos\phi \\ 0 & 0 & 0 \\ k_{33} \cos\phi \sin\phi & 0 & k_{33} \cos^2\phi \end{vmatrix} \qquad (3.35)$$

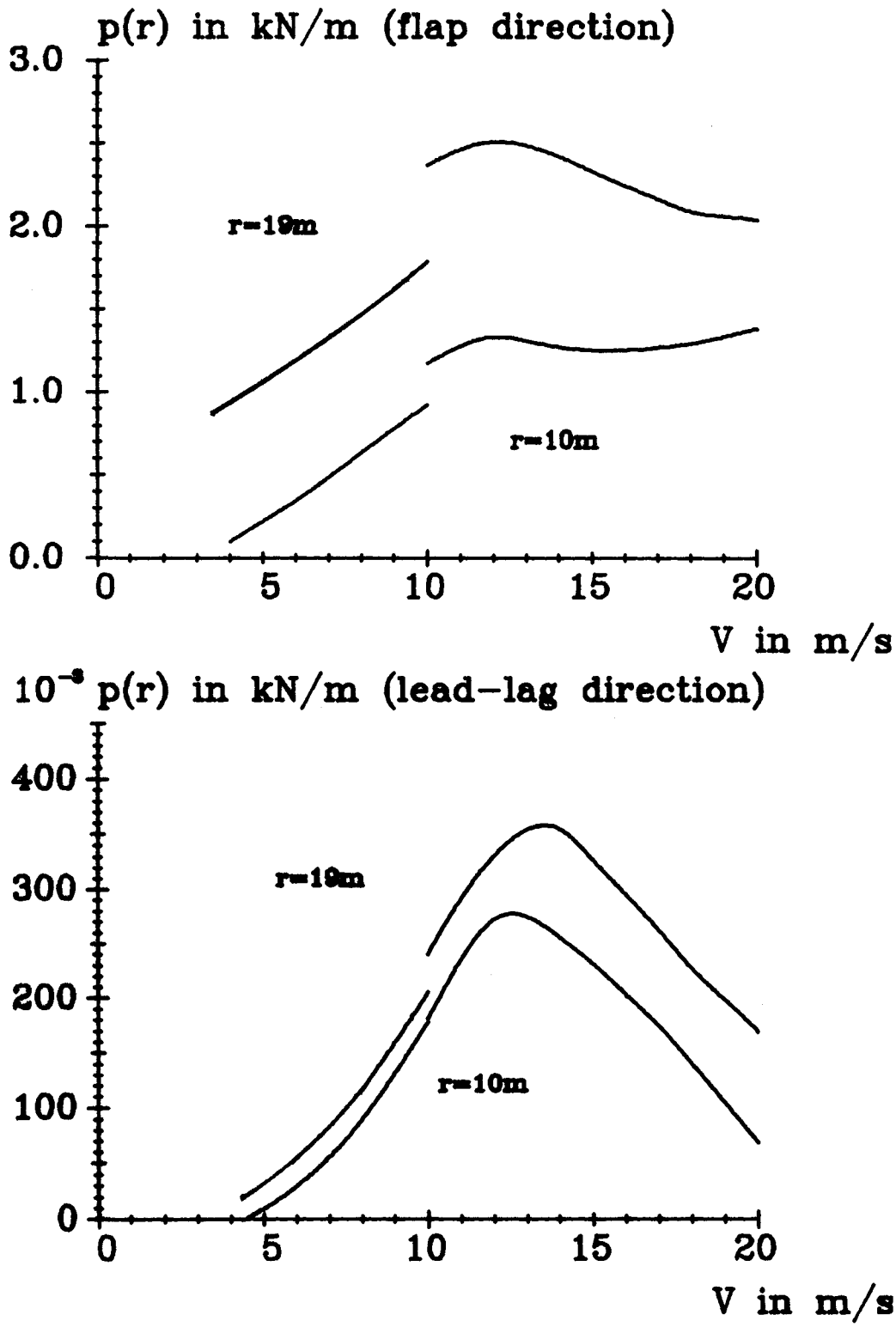

Fig. 3.5. Windloads at r = 10 m and r = 19 m as function of windspeed in the flap- and the lead-lag directions.

REFERENCES:

[1] ABBOTT, I.H. and VON DORENHOFF, A.E. (1959). Theory of Wing Sections. (Dover, New York), 693 pp.

[2] ANDERSEN, P.S., KRABBE, U., LUNDSAGER, P. and PETERSEN, H. (1980). Basismateriale for Beregning af Propelvindmøller, Risø-M-2153, 146 pp.

[3] ANDERSON, M.B., MILBORROW, D.J. and ROSS, J.W. (1982). Performance and Wake Measurements on a 3 m Diameter Horizontal Axis Wind Turbine. Comparison of Theory, Wind Tunnel and Field Test Data. In: Fourth International Symposium on Wind Energy Systems held at Stockholm, September 21-24, 1982 (BHRA Fluid Engineering, Bedford) Paper J5, 113-135.

[4] DE VRIES, O. (1982). On the Theory of the Horizontal-Axis Wind Turbine. Ann. Rev. Fluid Mech., 15, 77-96.

[5] GLAUERT H. (1935). Airplane Propellers. In: Aerodynamic Theory. Ed. by Durand, W.F. (Springer, Berlin), 169-269.

[6] JENSEN, N.O. and FRANDSEN, S. (1978). Atmospheric Turbulence Structure in Relation to Wind Generator Design. In: Papers presented at the Second International Symposium on Wind Energy Systems held in Amsterdam, October 3-6, 1978. Vol. 1, Paper C1.

[7] ROSENBROCK H.H. (1951). An Extension of the Momentum Theory of Wind Turbines, ERA 75-76, Report C/T 105, 12 pp.

[8] THRESHER, R.W., HOLLEY, W.E. and JAFAREY, N. (1981). Wind Response Characteristics of Horizontal Axis Wind Turbines, Proc. Second DOE/NASA Wind Turbine Dynamics Workshop, Cleveland, Ohio, 87-98.

[9] YAMANE, T., TSUTSUI, Y. and ORITA, T. (1982) The Aerodynamic Performance of a Horizontal-Axis Turbine in Large Induced-Velocity States. In: Fourth International Symposium on Wind Energy Systems held at Stockholm , September 21-24, 1982. (BHRA Fluid Engineering, Bedford) Paper J3, Vol. 2, 85-100.

4. STATIONARY DETERMINISTIC LOADS

A substantial part of the loading on a wind turbine rotor during normal operation can be explicitly expressed as functions of time. with good accuracy. When an induction generator is used in the wind turbine, the rotation angular velocity is nearly constant. Thus loads which depend on the location of the rotor become periodic, while the wind turbine rotates.

These deterministic loads can be divided into windflow-induced loads, gravity loads and loads due to the rotation such as centrifugal forces and gyroforces, and the chapter is sectioned accordingly.

A convenient way to represent a periodic function is by a Fourier series. As shown in section 2.4 this formulation is very suitable for a frequency domain response analysis for a linear system with modal decomposition. Consequently, the deterministic forces during normal operation are expressed in terms of a truncated Fourier series.

The loading being in principle distributed along the rotor structure is transformed into nodal forces by means of relation (9) in annex 1. A consistent modal load is defined by integrating the displacement interpolation function times the distributed load over the element in question. In order to preserve the independence from the particular finite-element program used, the actual displacement-interpolation polynomials are not applied. Instead a linear variation is assumed.

4.1. Wind forces

The aerodynamic loads are calculated by means of the blade element theory, which provides both the mean load due to the mean wind and the influence factor. The influence factors used as proportionality coefficients assume linear relationship between dynamic wind loads and the fluctuations in wind speed. The fluctuating

The fluctuating wind speeds as felt by a moving point on a rotor blade are assumed in this chapter to be the result of the points moving in a spatial nonuniform but time-invariant wind field. Due to the assumption that the wind field is almost constant but with small perturbations, the changes in wind speed from the various phenomena are treated separately. The contributions are finally combined additively. Hence the wind speed at a point on the blade can be written

$$\underline{U}(x,y,z,t) = \underline{U}_o(x,y,z) + \sum_i \underline{u}_i(x,y,z,t) \qquad (4.1)$$

in which $\underline{U}_o$ is the mean wind speed while $\underline{u}_i$ are the time-dependent perturbations. Once $\underline{U}_o$ is found the mean load is determined from blade element theory, while the dynamic loads due to $\underline{u}_i$ appear as the influence factors times $\underline{u}_i$.

Thus the loads on the blade elements arising from a wind fluctuation $\underline{u}$ in the local two-dimensional coordinate system are found from

$$d\underline{F} = \begin{vmatrix} dfx \\ dfy \\ dM \end{vmatrix} = \begin{vmatrix} C_{11} & C_{12} \\ C_{21} & C_{22} \\ C_{31} & C_{32} \end{vmatrix} \begin{vmatrix} u_x \\ u_y \end{vmatrix} \qquad (4.2)$$

As the loading from strong winds U_o > 8-10 m/s is of primary interest, it will be assumed that the flow is neutrally stratified.

4.1.1. Wind shear

Due to the friction between the ground surface and the moving air a wind profile with the mean windspeed increasing with altitude is generated by the shear in the wind. Due to the rotation of the rotor, a given point on a rotor blade will experience a time varying wind velocity. This phenomenon results in a dynamic loading of the rotor which will be quantified below in accordance with the principal assumption of the total model. The mean velocity profile in the boundary layer is assumed to follow the logar-

ithmic law. When z denotes the height above the ground, the wind speed U(Z) is given in terms of the friction velocity u_*, the roughness length z_o and the von Karmann constant κ as (Simiu and Scanlan [2]) p.45,

$$U(z) = \frac{u_*}{\kappa} \ln(z/z_o) \tag{4.3}$$

In the interval of interest (4.3) can be substituted by a few terms of the Taylor series with good approximation, and expanded around the hub height h. Thus

$$U(h + \Delta z) = \frac{u_*}{\kappa} \{\ln(h/z_o) + \frac{\Delta z}{h} - \frac{\Delta z^2}{2h^2}\} \tag{4.4}$$

Consider now a point P on a rotor blade. At t=0 the point is located as shown on the Fig. 4.1

The distance from the ground to the point P is then

$$h + \Delta z = h - r \cos\theta\cos(\omega_R t + \phi) \tag{4.5}$$

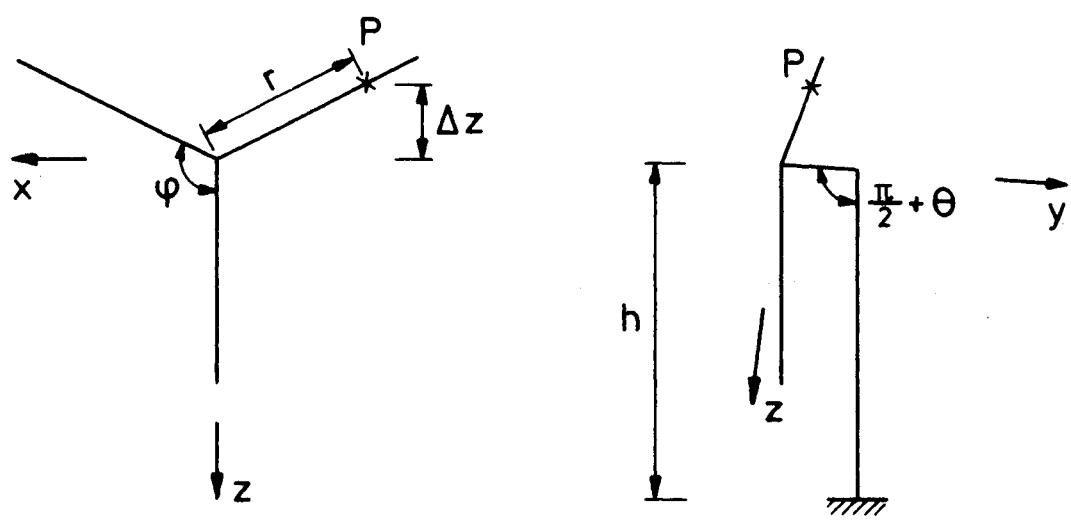

Fig. 4.1. Initial geometry, t=0.

where ω_R is the rotation frequency. Inserting (4.5) in (4.4) the experienced wind speed will be

$$U_p(t) = \frac{u_*}{\kappa} \{\ln(\frac{h}{z_o}) - \frac{1}{4h^2} r^2\cos^2\theta$$

$$- \frac{1}{h} r \cos\theta\cos(\omega_R t + \phi) \qquad (4.6)$$

$$- \frac{1}{4h^2} r^2\cos^2\theta\cos(2\omega_R t + 2\theta)\}$$

Let now the wind velocity in hub height perpendicular to the rotorplane be denoted by V

$$V = \frac{u_*}{\kappa} \ln(\frac{h}{z_o}) \qquad (4.7)$$

In terms of V, $U_p(t)$ becomes

$$U_p(t) = V - \frac{V}{4h^2\ln(\frac{h}{z_o})} r^2\cos^2\phi)]$$

$$- \frac{V}{h\ln(\frac{h}{z_o})} r\cos\theta\cos(\omega_R t + \phi) \qquad (4.8)$$

$$- \frac{V}{4h^2\ln(\frac{h}{z_o})} r^2\cos^2\theta\cos(2\omega_R t + 2\phi)$$

In order to facilitate the computation of the mean wind load, the constant term is assumed independent of the radius. Instead, the constant value $r^* = 2/3\ r_{tip}$ is inserted into (4.7). Hence

$$U_p(t) = V - \frac{V}{4h^2 \ln(\frac{h}{z_o})} \frac{4}{9} r_{tip}^2 \cos^2\theta$$

$$- \frac{V}{h \ln(\frac{h}{z_o})} r\cos\theta\cos(\omega_R t + \phi) \qquad (4.9)$$

$$- \frac{V}{4h^2 \ln(\frac{h}{z_o})} r^2\cos^2\theta\cos(2\omega_R t + 2\phi)$$

The time-varying wind speed as experienced by a point on a rotating blade is shown in Fig. 4.2. The figure also illustrates the effect of including the quadratic term in (4.3).

The influence of the quadratic term is seen to be moderate. However, as the dynamic amplification at the frequencies ω_R and $2\omega_R$ may be quite different, the relative importance of the quadratic term may be greater for the rotor response.

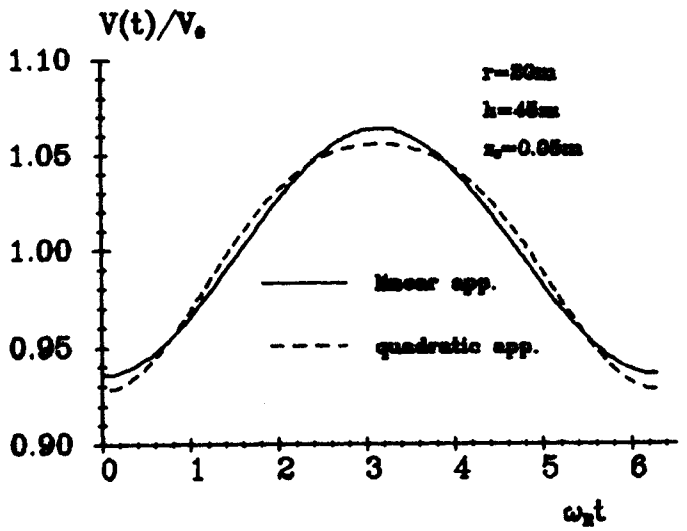

Fig. 4.2. Wind speed fluctuations as experienced at a point on a rotating blade due to wind shear.

4.1.2. Skew wind

When the rotorplane is inclined such that the wind direction is not perpendicular to the rotor plane, the relative air speed felt for the rotor blade is nonuniform during the revolution. This variation introduces a dynamic load.

Consider first a rotor with a tilt angle θ, as defined in Fig. 2.1. For a point rotating with frequency ω_R and initially located at the position (r,ϕ) the wind variation in the rotor plane becomes

$$\Delta V_{rp} = - V \sin\theta\sin(\omega_R t + \phi) \tag{4.10}$$

In the case of skew wind in the horizontal plane, i.e. $\gamma \neq \pi/2$ in Fig. 2.1,

$$\Delta V_{rp} = V \cos\gamma\cos(\omega_R t + \phi) \tag{4.11}$$

Thus the total wind speed variation in the rotor plane becomes

$$\Delta V_{rp}(t) = V(\cos\gamma\cos(\omega_R t + \phi) - \sin\theta\sin(\omega_R t + \phi)) \tag{4.12}$$

The wind speed at hub height is constant

$$U_o = V \cos\theta\sin\gamma \tag{4.13}$$

The resulting dynamic forces on the blades follow from (4.2), noting that skew wind results in airspeed fluctuations in the local X-direction.

4.1.3 Tower interference

The presence of the wind turbine tower is responsible for a change in flow pattern close to the tower. The disturbance upstream of the tower, Fig. 4.3., is moderate and can be modelled with good approximation, assuming a potential flow field. The wake behind the tower is of larger magnitude and turbulent and can be separated into a velocity deficiency and an unsteady part which consists of an increased turbulence and a periodic motion.

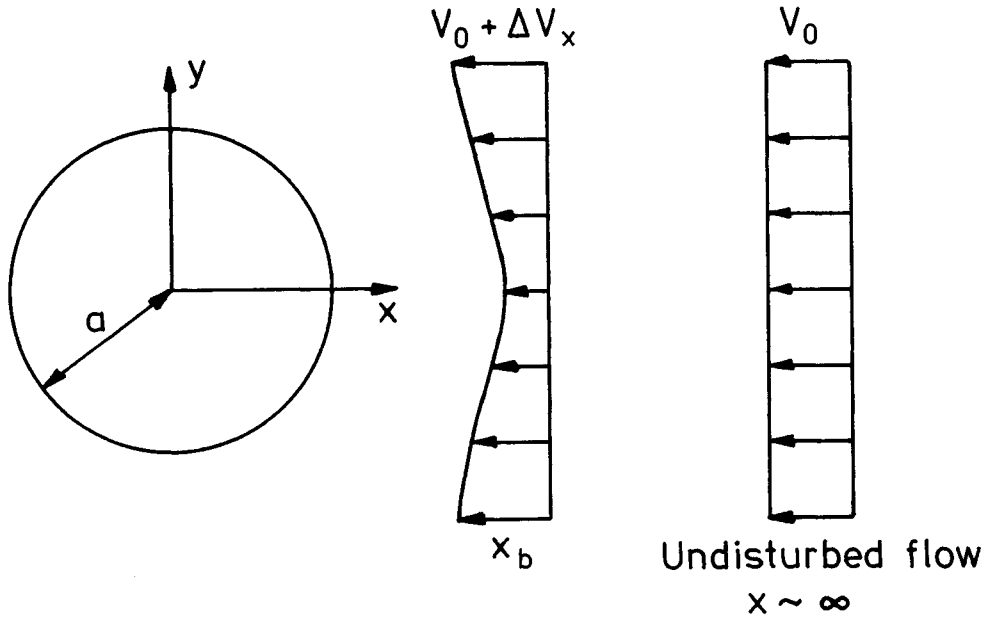

Fig. 4.3. Disturbance upstream of a circular cylinder, assuming potential flow field.

The present model of the tower interference will be limited to the change in the mean velocity in the direction of the undisturbed mean wind flow. The flow around the tower is assumed to be two-dimensional, and two shapes of the disturbance will be considered. The shapes are illustrated in Fig. 4.4 and have the analytical forms

$$U_I(y) = U_o(1-\alpha(H(y+\delta/2) - H(y-\delta/2))) \tag{4.14}$$

$$U_I(g) = U_o(1-\alpha\cos(\frac{\pi y}{\delta}(H(y+\delta/2) - H(y-\delta/2))) \tag{4.15}$$

where H( ) is the Heaviside step function.

A point of a rotating blade at a distance r from the center will experience a periodic fluctuation in wind speed. Assuming r >> a, where 2a is the tower diameter

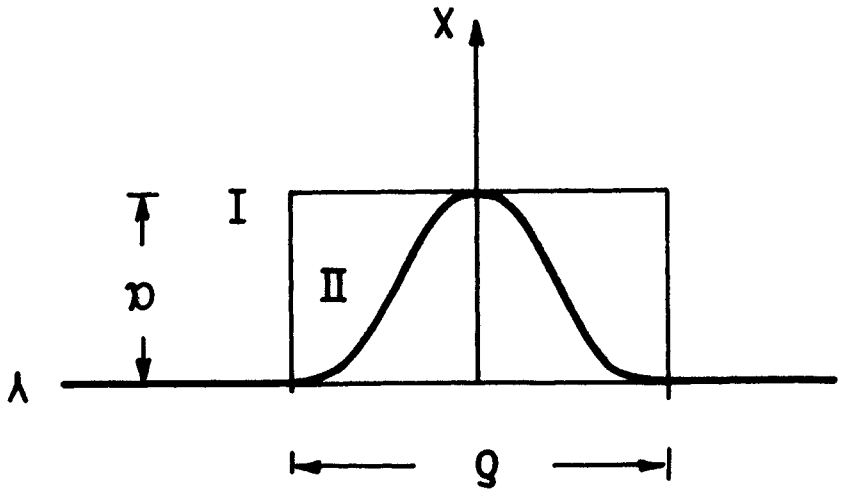

Fig. 4.4. Shapes of flow disturbances from the wind turbine towers.

$$y = [(\omega_R\, t + \phi) \bmod 2\pi]\, r \tag{4.16}$$

The disturbance $\Delta V = U_o - U(t)$ is shown schematically in Fig. 4.5.

Following the principle in chapter 2 the disturbances given by 4.14-16 are expressed as a Fourier series, i.e.

$$\Delta V = U_o - U(t) = \mathrm{Re}\left\{ \sum_{n=0}^{\infty} c_n\, e^{in\omega_R t} \right\} \tag{4.17}$$

The Fourier coefficients for a rectangular disturbance are given by

$$c_n = \frac{1}{T} \int_{-T/2}^{T/2} \Delta V(t) e^{-in\omega_R t}\, dt$$

$$= e^{in\phi}\ \alpha\ U_o\ np\ \frac{\sin(\pi np)}{\pi np} \tag{4.18}$$

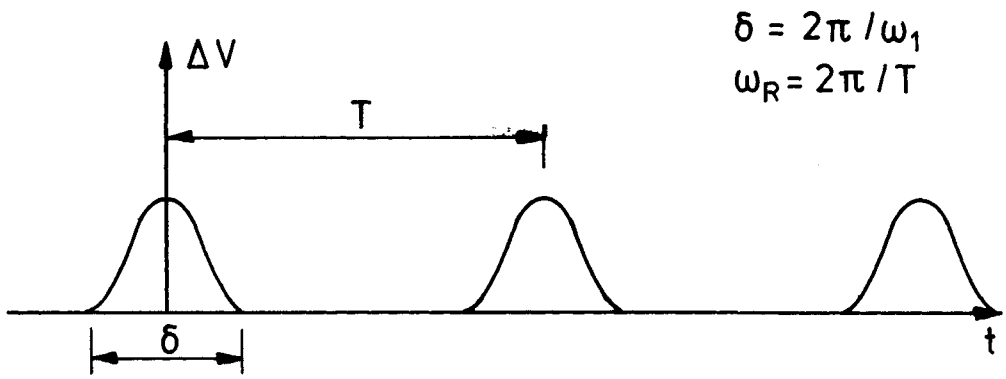

Fig. 4.5. Schematic image of the disturbance from the tower as experienced from a rotating blade element.

In (4.18) the period is $T = 2\pi/\omega_R$ and

$$p = \frac{\delta}{2\pi r} \tag{4.19}$$

Similarly for a cosine-shaped disturbance

$$c_n = e^{in\phi} \quad \alpha \; U_o \; p \quad \frac{\sin(\pi np)}{\pi np} \quad \frac{1}{1-(pn)^2} \tag{4.20}$$

In the case when the rotor is upstream of the tower the disturbance can be modelled using potential flow theory. Consider therefore the situation in Fig. 4.3. For the wind speed at hub height U_o the disturbance in the undisturbed flow direction is, Engelund [1],

$$\Delta V = U_o \; a^2 \; \frac{x^2-y^2}{(x^2+y^2)^2} \tag{4.21}$$

x and y are the coordinates of the point considered. Each blade will pass the tower along the line $x = x_o$ and at the time t, the blade will be in position $y = \omega_R t$, ω_R being the rotational frequency. Obviously, there will also be a flow velocity component

v_y along the y-axis close to the tower. However, when the distance from the outer surface of the tower to the blade (in the closest position) is not too small, this component is small enough to be disregarded.

In order to simplify the expansion into a Fourier series, the "potential flow disturbance" due to tower interference is modelled by a cosine profile of the type as shown in Fig. 4.6.

The cosine disturbance is chosen to coincide with (4.21) for $y = 0$, and $y = a$ which yields

$$\alpha = a^2/x_o^2 \tag{4.22}$$

$$\delta = \pi a/\arccos\left(\frac{x_o^4 - a^2x_o^2}{(x_o^2 + a^2)^2}\right) \tag{4.23}$$

On Figs. 4.7 and 4.8 are shown the maximal velocity deficiency and the width of the disturbance. As can be seen the disturbance of the flow in front of the tower dies out very quickly.

4.1.4 Mean wind

From the preceeding pages it is noted that the mean wind speed perpendicular to the rotor plane U_o depends on whether wind shear, tower interference or skew wind is present. Since U_o both determines the mean aerodynamic load from use of the blade element method and the linearization point, all contributions must be included.

For a mean wind speed U_o at hub height the mean wind speed U perpendicular to the rotor plane is from (4.9), (4.13) and (4.20)

$$U \simeq U_o\cos\theta \sin\gamma \left(1 - \frac{r_{tip}^2 \cos^2\theta}{9h^2\ln(h/z_o)} - \frac{\alpha\delta}{2\pi r}\right) \tag{4.24}$$

which is used in the analysis.

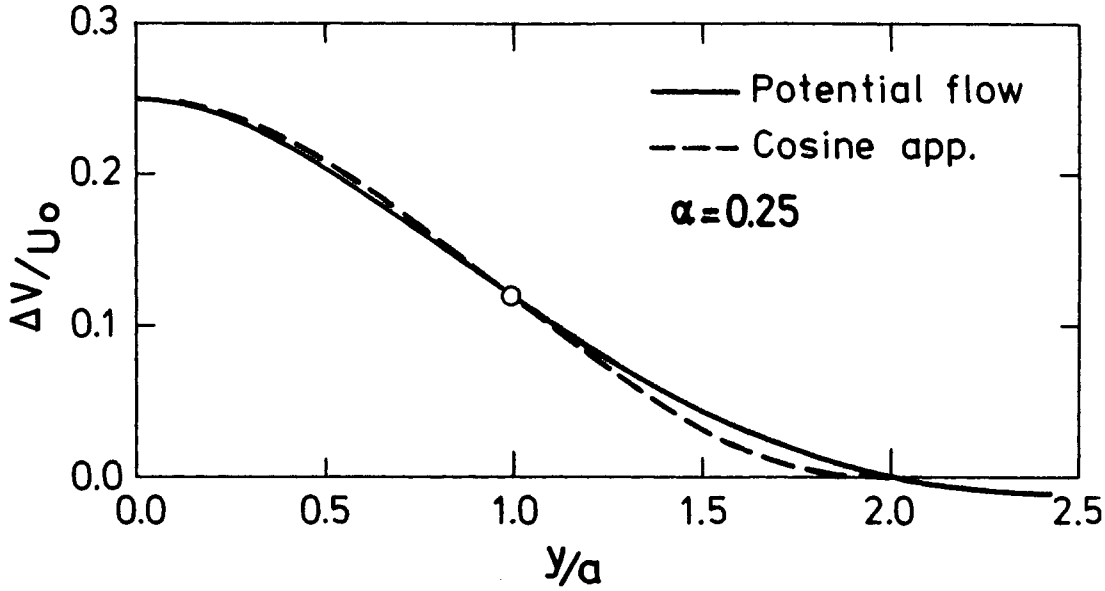

Fig. 4.6. Comparison of the flow disturbance from the tower, assuming potential flow.

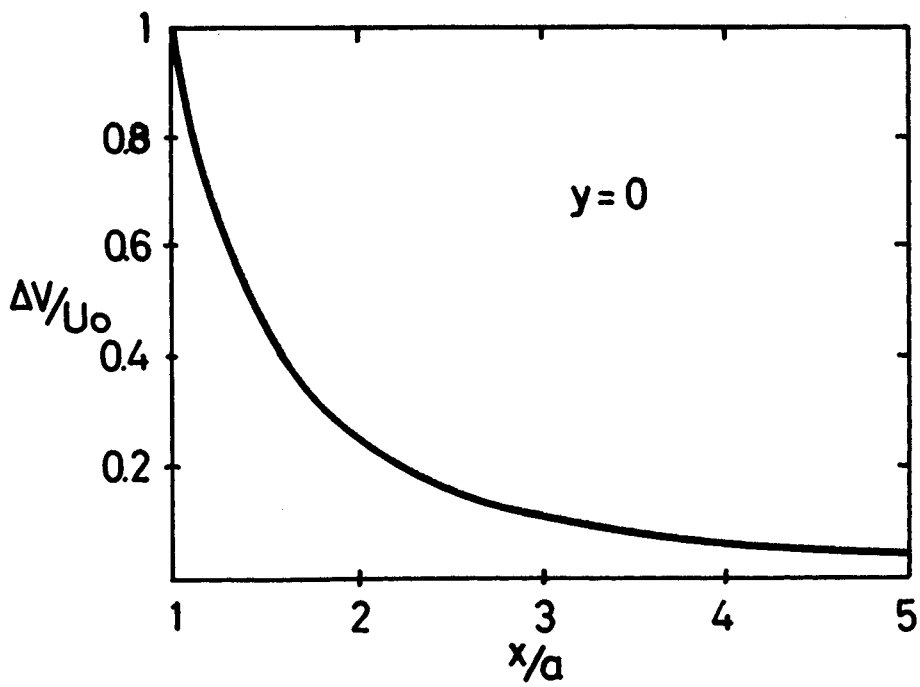

Fig. 4.7. Velocity deficiency in front of the tower at y = 0.

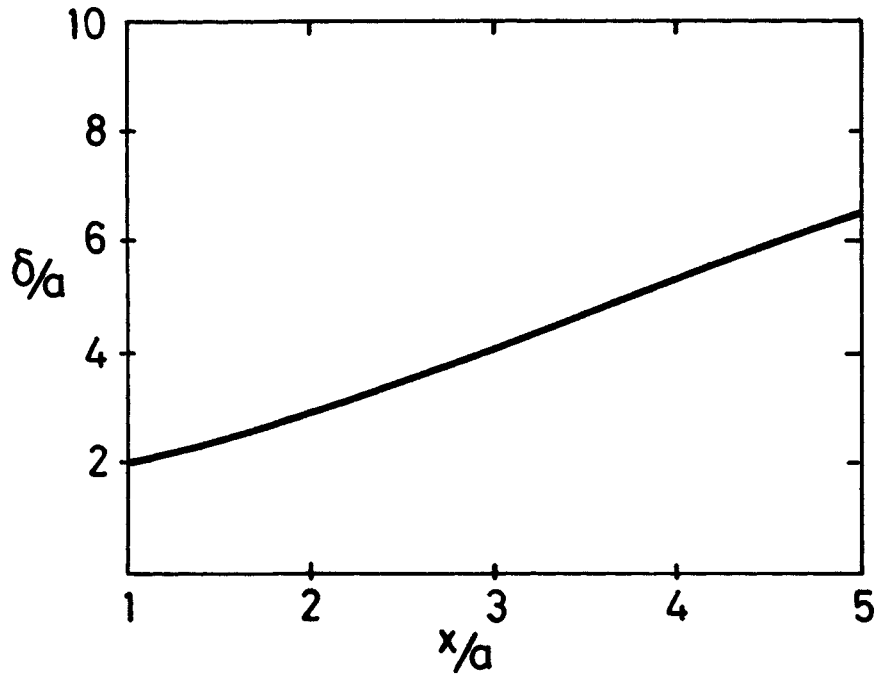

Fig. 4.8. Width of the disturbance in front of the tower.

4.2. Gravity loading

A major load on the wind turbine rotor is due to gravity. Using a lumped mass formulation in the FE-model, by a number of force vectors the load is equivalent to the lumped mass multiplied by the acceleration of gravity.

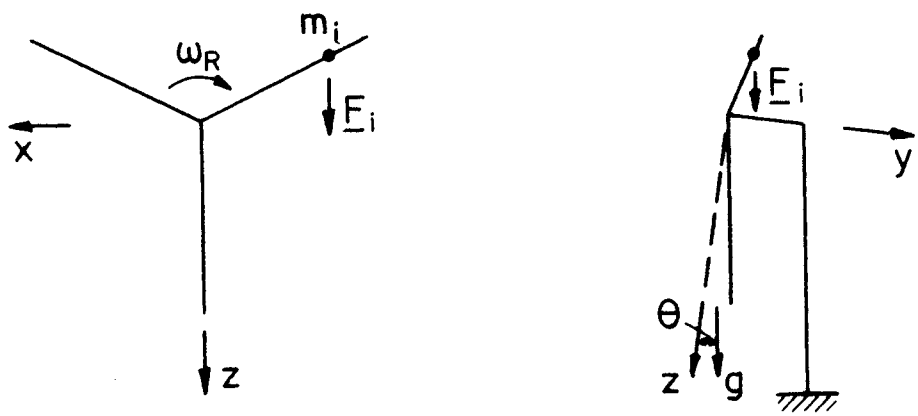

Fig. 4.9. Notation.

At time t=0 the gravity acceleration vector is located in the Y,Z plane of the global system as shown in Fig. 4.9. The force $\underline{F}_i$ on the lumped mass m_i has the components

$$\underline{F}_i = m_i g \begin{vmatrix} 0 \\ \sin\theta \\ \cos\theta \end{vmatrix} \tag{4.25}$$

Now on letting the coordinate system, X,Y,Z, rotate with the angular velocity $\underline{\omega}_R$, relative to $\underline{g}$, we introduce the time dependent gravity forces

$$\underline{F}_i(t) = m_i g \begin{vmatrix} -\cos\theta & \sin\omega_R t \\ \sin\theta & \\ \cos\theta & \cos\omega_R t \end{vmatrix} \tag{4.26}$$

4.3. Centrifugal forces

The fictive forces which must be introduced using rotating coordinates were briefly discussed in section 2.1. Of these the Coriolis forces are seen to be proportional to the time derivatives of the coordinates in question and may thus be perceived as an additional linear damping. The rest of the forces are dependent on the location in space relative to the axis of rotation. In general, the angular velocity ω_y of the yawing motion is very small compared to the rotation frequency ω_R of the rotor. With adequate accuracy the forces may be separated into centrifugal forces F_{cent} and forces due to the yawing motion F_{yaw}.

Again assuming a lumped mass formulation in the FE-model the centrifugal forces are introduced as a set of force vectors, each perpendicular to the rotation axis and acting on nodal point i with the lumped mass m_i as shown in Fig. 4.10.

Since the axis of rotation is identical to the Y-axis, the distance from the center of rotation to mass m_i is

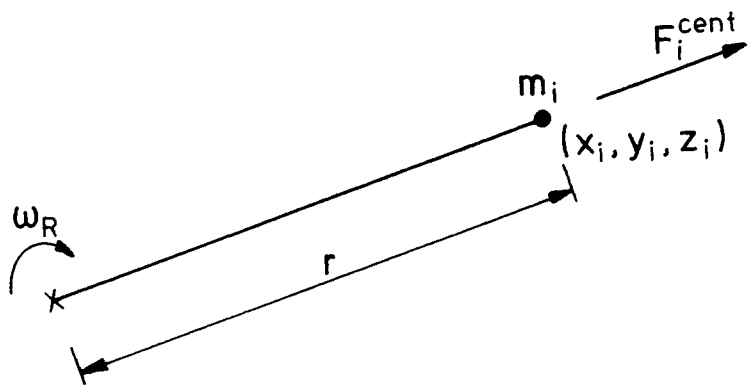

Fig. 4.10. Direction of the centrifugal forces.

$$r_i = \sqrt{x_i^2+z_i^2} \tag{4.27}$$

in which x_i, z_i are coordinates of point no i with the lumped mass m_i.

The magnitude of the force is

$$F_i^{cent} = m_i \omega_R^2 r_i \tag{4.28}$$

Thus the constant force vector due to the centrifugal forces at point no i becomes

$$\underline{F}_i^{cent} = m_i \omega_R^2 \begin{vmatrix} x_i \\ 0 \\ z_i \end{vmatrix} \tag{4.29}$$

4.4. Gyroforces due to yawing

For most wind turbines with active yaw control the yaw rate ω_y is kept rather low to avoid large loadings on the rotor. For the Nibe turbines the number is $\omega_y = 0.4^o/s$ [3], while yawing is first initiated, when the misalignment exceeds a certain number, e.g.,

five degrees. Compared to the time scales of the rotation and the structural vibrations the yawing is of long duration. The yaw-induced loads on the rotating rotor can thus with good approximation be treated as stationary and periodic.

For $\omega_y << \omega_R$ the gyroforces at a nodal point i with the lumped mass m_i are approximately

$$\underline{F}_{yaw}(x,y,z,t) \simeq \left| \begin{matrix} 0 \\ 2m_i\omega_R\omega_y\cos\theta(x\,\sin(\omega_R t) - z\,\cos(\omega_R t)) \\ 0 \end{matrix} \right| \quad (4.30)$$

for the point located at (x,y,z) in the rotating frame of reference.

Consider now a periodic time-varying yawing angular velocity ω_y with the fundamental period $T_o = 2\pi/\omega_R$. Expanding ω_y in a Fourier series

$$\omega_y(t) = \mathrm{Re}\{\sum_{n=0}^{\infty} c_n\, e^{in\omega_R t}\} \quad (4.31)$$

and inserting (4.31) into (4.30) and adding the term corresponding to the last term in (2.1) the resulting forces on the mass m can be written

$$\underline{F}_{Yaw}(x,y,z,t) = m_i\omega_R\cos\theta \;\; \mathrm{Re}\left[\sum_{n=0}^{\infty} c_n e^{in\omega_R t}\right] \left| \begin{matrix} in(y\cos\omega_R t - z\tan\theta) \\ x(2\sin\omega_R t - in\cos\omega_R t) - z(2\cos\omega_R t + in\sin\omega_R t) \\ in(x\tan\theta + y\sin\omega_R t) \end{matrix} \right| \quad (4.32)$$

In most cases a few terms in the summation will be sufficient. It should be noted that the fluctuations in the yawing velocity usually are a consequence of an unbalanced rotor or fluctuations in the wind pressure across the rotor disk. Applying a time dependent yawing angular velocity in the manner described here can be only a crude approximation to the actual problem.

REFERENCES

[1] ENGELUND, F.A. (1968). Hydrodynamik. Newtonske væskers mekanik. (Den private Ingeniørfond), 322 pp.

[2] SIMIU, E. and SCANLAN R.H. (1978). Wind Effects on Structures. Introduction to wind engineering. (Wiley, New York), 458 pp.

[3] Energiministeriets og Elværkernes Vindkraftprogram (1981). Teknisk beskrivelse af Nibe møllerne, EEV 81-02.

5. STOCHASTIC LOADING AND RESPONSE FROM TURBULENCE

The velocity of the wind acting on a wind turbine may be viewed as consisting of three parts, a constant mean velocity $\underline{U}$, a deterministically varying part $\underline{u}(t)$ and a randomly fluctuating contribution due to the wind turbulence $\underline{v}(t)$. Arranging a Cartesian coordinate system such that the mean wind speed is directed along the Y-axis, the components of the wind speed can be written:

$$\begin{aligned} U_1(t) &= u_1(t) + v_1(t) \\ U_2(t) &= U + u_2(t) + v_2(t) \\ U_3(t) &= u_3(t) + v_3(t) \end{aligned} \tag{5.1}$$

Although all three turbulence components v_i contribute to the loading on a body suspended in the windflow only the longitudinal component, here $v_2(t)$, is considered to be important for wind-turbine loading (Jensen and Frandsen [5]). Their conclusion agrees with the observation in section 3.2 that the influence factor for along-wind fluctuations is much larger than for fluctuations perpendicular to the wind direction. Assuming that the second axis is perpendicular to the rotorplane the local forces on a turbine blade in the local blade coordinates of Fig. 2.2 due to turbulence becomes

$$\underline{F} = \begin{vmatrix} f_x \\ f_y \\ M \end{vmatrix} = \begin{vmatrix} C_{12}(r) \\ C_{22}(r) \\ C_{32}(r) \end{vmatrix} v_2(r,\phi,t) \tag{5.2}$$

in terms of the influence coefficients derived in section 3.2.

Undoubtedly, the action of wind turbulence on wind turbines is important when extreme stresses and fatigue lifetime are considered. However, there exists discussion on which way to represent the wind fluctuations for calculations, namely either by a discreet gust model having a gust shape, duration and amplitude or by a stochastic process model. The latter is adopted here,

thus representing the wind fluctuations as a zero-mean Gaussian stationary process with a frequency content characterized by a power spectrum.

In the following the turbulence will be modelled as being homogeneous and isotropic. In a fixed frame of reference relative to the ground the von Karman spectrum is used to model the correlation structure of the turbulence. The model and the evaluation of parameters is the subject of section 5.1.

Due to the rotation of the wind turbine rotor in the turbulent wind field, the turbulence seen from a point on a moving blade is altered. The change in apparent correlation and spectra is treated in section 5.2.

A corresponding discrete load model in terms of load spectra is finally described in section 5.3. The model is well suited to the response methods outlined in section 2.7.

5.1. Stochastic Turbulence Model

Basically the turbulence model is rather simple: The turbulence is assumed to be homogeneous and isotropic, and only the along-wind component is considered. The turbulent wind fluctuations are assumed to be Gaussian distributed, i.e. the joint probability density function of the wind fluctuations at point with a mutual position vector $\underline{r}$ can be written

$$f_{VV}(x,y) = \frac{1}{2\pi\sigma_V^2\sqrt{1-\rho^2}} \exp\left\{\frac{-1}{2\sigma_V^2(1-\rho^2)} \left[x^2-2\rho xy+y^2\right]\right\} \qquad (5.1)$$

in which the standard deviation σ_V and the coefficient of correlation ρ are obtained from the covariance function

$$\sigma_v^2 = R(o) \tag{5.2}$$

$$\rho = R(\underline{r})/\sigma_v^2 \tag{5.3}$$

It thus follows that the turbulence is fully described once the covariance as function of space and time of the along-wind component is determined.

The correlation structure as seen from the rotating blades of a wind turbine will be introduced in the next section, whereas in this section parameters and the correlation of the along-wind fluctuations as seen by an observer fixed in space will be presented. Using the von Karman energy spectrum to describe the turbulence, the longitudinal correlation function becomes (Hinze [4])

$$R_L(r) = \frac{2\sigma_o^2}{\Gamma(1/3)} \left(\frac{r}{2L}\right)^{1/3} K_{1/3}(r/L) \tag{5.4}$$

Using the Taylor hypothesis, i.e. $r = U\tau$ the corresponding power spectrum can be evaluated as

$$S_L(\omega) = \frac{1}{2\pi} \int_{-\infty}^{\infty} R_L(\tau) e^{-i\omega\tau}\, dt$$

$$= \frac{\Gamma(5/6)}{\Gamma(1/3)} \frac{\sigma_o^2}{\sqrt{\pi}} \frac{(L/U)}{(1+(\frac{\omega L}{U})^2)^{5/6}} \tag{5.5}$$

In (5.4) and (5.5) $\Gamma(\ )$ is the Gamma function and $K_{1/3}$ is a modified Bessel function of the second kind and order 1/3. U is the mean wind speed at the hub height, and the remaining parameters to be determined are the variance σ_o^2 and the length scale L.

The variance σ_o^2 is known to increase with windspeed and roughness of the terrain. A simple expression from Lumley and Panofsky [7] is

$$\sigma_o = \frac{U}{\ln(\frac{z}{z_o})} \tag{5.6}$$

in which z is the height above the ground and z_o is the roughness length. For the four terrain classes defined in the Danish Wind-atlas (Petersen et al. [8]) the roughness length is

$$z_o = \begin{cases} 0.001 \text{ m}; & \text{terrain class } 0 \\ 0.01 \text{ m}; & \text{" } 1 \\ 0.05 \text{ m}; & \text{" } 2 \\ 0.30 \text{ m}; & \text{" } 3 \end{cases} \tag{5.7}$$

The length scale L is determined by the relation

$$L = 6.5\ z \tag{5.8}$$

which ensures that the maximum of $\omega S_L(\omega)$ occurs at the frequency $f_m = \omega z/(2\pi U) = 0.03$ (Simiu and Scanlan [10]). It should be noted that L is not what is usually denoted the integral length scale L_i, however; in this case they are related as

$$L_i = \frac{1}{\sigma_o^2} \int_0^\infty R_L(r)\, dr$$

$$= \frac{\Gamma(5/6)}{\Gamma(1/3)} \sqrt{\pi}\ L \cong 0.7474\ L \tag{5.9}$$

5.2. Cross-correlation of wind fluctuations at points on rotating wind turbine blades

The main frame of reference in which loads and structural responses of the wind turbine rotor are described rotates with a constant angular velocity relative to the ground. For further calculations it is desirable to describe the wind turbulence in a rotating frame of this kind, thereby describing the turbulence as felt at the blade of a rotating wind turbine.

Such a model was developed by Kristensen and Frandsen [6] using the von Karman energy spectrum and based on earlier work by Rosenbrock [9]. Their model is applied here and is therefore briefly reviewed.

In an isotropic turbulent windfield the correlation tensor of windfluctuations in different directions can be written in terms of two scalar functions of the spatial distance $r = |\underline{r}|$. Thus, Engelund [2],

$$R_{ij}(\underline{r}) = R_T(r)\ \delta_{ij} + (R_L(r) - R_T(r))r_i r_j/r^2 \qquad (5.10)$$

in which δ_{ij} is the Kroeneckers delta and R_L, R_T are the longitudinal and the transversal correlations, respectively. In an incompressible flow, which will be assumed, the two are related as

$$R_T(r) = R_L(r) + (r/2)\ \frac{dR_L(r)}{dr} \qquad (5.11)$$

Thus, the correlation for the along-wind component, the Y-axis being the mean wind direction, can be written

$$R(\underline{r}) = R_L(r) - \frac{r}{2}\frac{dR_L(r)}{dr}\quad (1 - \frac{r^{*2}}{r^2}) \qquad (5.12)$$

where r^* is the distance in the wind direction. Inserting the expression (5.4) for the von Karman longitudinal correlation in (5.12) yields

$$R(\underline{r}) = \frac{2\sigma_o^2}{\Gamma(\frac{1}{3})}(\frac{r}{2L})^{1/3}\ \{K_{1/3}(\frac{r}{L}) - \frac{r^2-r^{*2}}{r^2}\frac{r}{2L}\ K_{2/3}\ (\frac{r}{L})\} \qquad (5.13)$$

With the Taylor hypothesis of frozen turbulence assumed valid, $R(\underline{r})$ can be expressed using timelag instead of spatial separation. Thus, for two points rotating with the angular velocity ω_R and mutual location given by the radia a,b and the angle $\underline{\phi}$, the disttance r as a function of time can be written

$$r = (r^{*2} + r_p^{\,2})^{1/2} \qquad (5.14)$$

in which the distance in the wind direction is

$$r^* = U\tau \qquad (5.15)$$

and the distance in the rotorplane is given by

$$r_p^2 = a^2 + b^2 - 2ab \cos(\omega_R \tau + \phi) \tag{5.16}$$

as is illustrated in Fig. 5.1.

From the correlation function $R(\tau)$, auto- and cross spectra of the wind fluctuations at points on the rotor can be calculated by

$$S(\omega) = \int_{-\infty}^{\infty} R(\tau) e^{i\omega\tau} \, d\tau \tag{5.17}$$

As no analytical solution has been found for the integral in (5.17) the problem is solved numerically over a limited interval $[-T/2, T/2]$ using a digital Fourier transform. To avoid numerical instability with a reasonable amount of integration points, e.g. 2^9, the calculated spectra are smoothed by multiplying the correlation function $R(\tau)$ with a Tukey window which has the form (George [3]),

$$D(\tau) = \begin{cases} \frac{1}{2}[1 + \cos(2\pi\tau/T)] & |\tau| < \frac{T}{2} \\ 0 & |\tau| > \frac{T}{2} \end{cases} \tag{5.18}$$

In Fig. 5.2 the auto- and cross spectra for two points on a rotating blade are shown.

5.3. Load spectra

From the wind speed fluctuations due to turbulence the load density component α on blade β (out of M blades) can be calculated as

$$p^{\alpha\beta}(r) = C^{\alpha\beta}(r) \, v_2^{\beta}(r,t) \tag{5.19}$$

The load density has six components, three force densities and

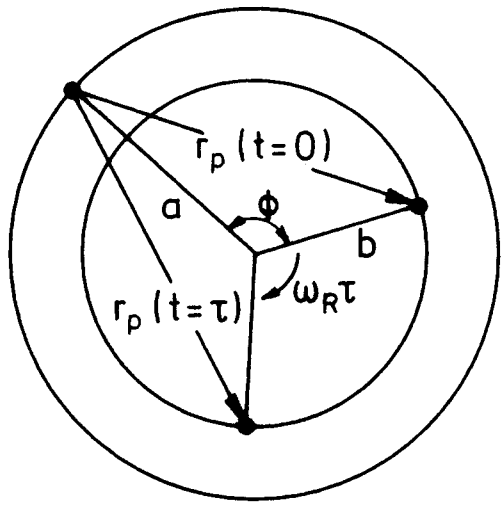

Fig. 5.1. Distance between points in the rotorplane as function of time τ.

The load density has six components, three force densities and three moment densities, and in the global coordinates the influence coefficients are

$$C^{\alpha\beta}(r) = \underline{\underline{T}}_2 \; \underline{\underline{T}}_1 \begin{vmatrix} C_{12} \\ C_{22} \\ C_{32} \end{vmatrix} \tag{5.20}$$

in terms of the transformation matrices in (3.23) and (3.24). Assuming identical straight blades the angle with the Z-axis is

$$\phi^{\beta} = \frac{2\pi}{M}(\beta-1) \tag{5.21}$$

In the global rotating frame of reference the appropriate wind fluctuations can be put

$$v_2^{\beta}(\underline{r},t) = v_2(r, \tfrac{2\pi}{M}(\beta-1), t) \tag{5.22}$$

using the polar coordinates defined in Fig. 2.1.

In order to carry through the analysis the generalized or modal loads must be determined in terms of auto- and crossspectra. In

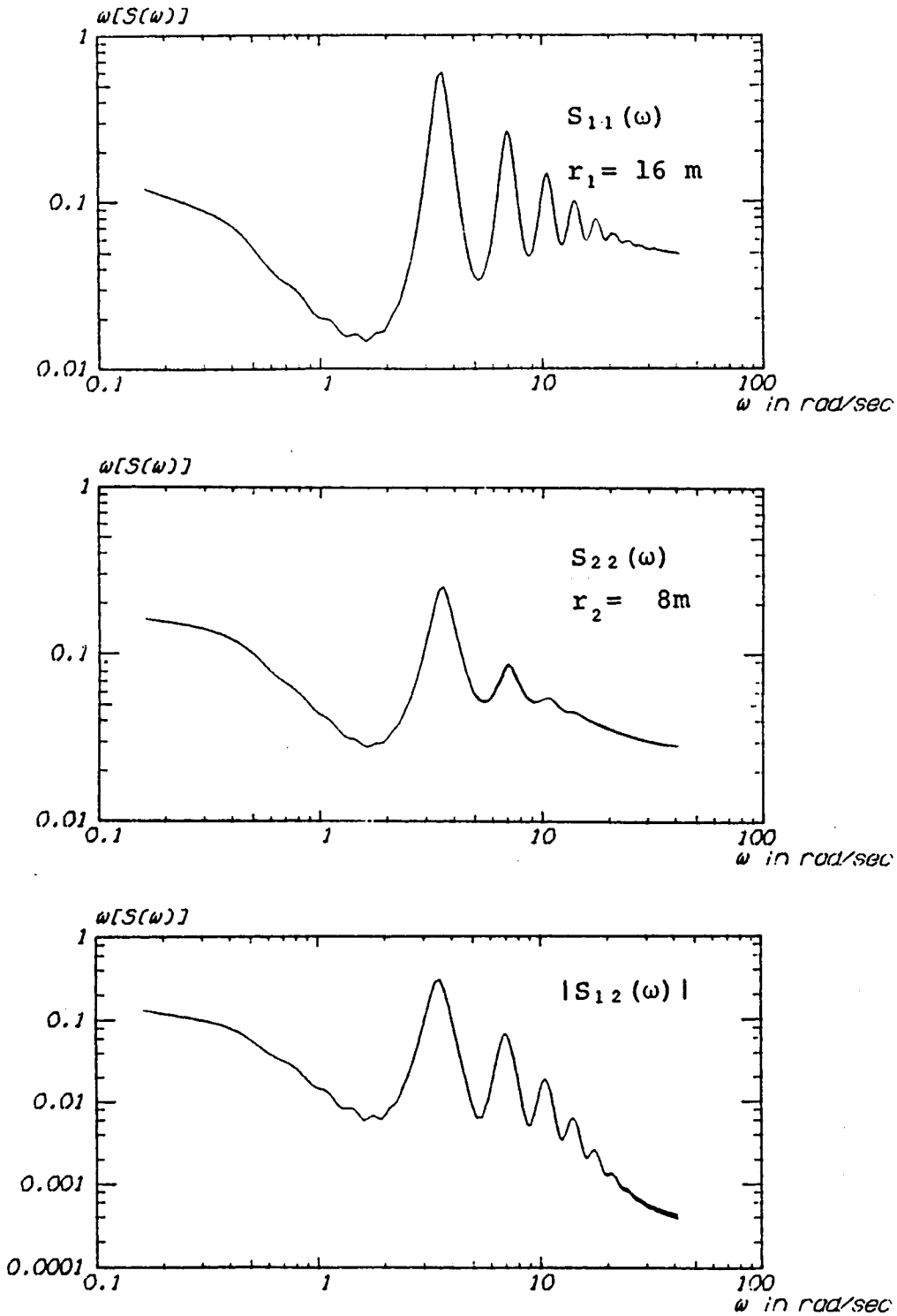

Fig. 5.2. Auto- and cross spectra at two points on a rotating wind tubine blade.

(2.23) the generalized load of mode i is written as the vector product of the eigenvector $\underline{v}_i$ and a loadvector $\underline{P}(t)$

$$q_i(t) = \underline{v}_i^T \underline{P}(t) \tag{5.23}$$

where $\underline{P}(t)$ represents the distributed loading collected in the nodes of the structure by means of (9) in annex 1. Thus (5.23) is a discrete approximation to the integral

$$q_i(t) = \int_R v_i^{\alpha\beta}(r)\ p^{\alpha\beta}(r)dr \tag{5.24}$$

in which $v_i^{\alpha\beta}$ is the i'th eigenfunction on blade β in direction α, $\alpha = 1,2,3$ in the corresponding continuous structural model. Since the discrete finite element model is chosen primarily to obtain an accurate representation of the stiffness properties of the rotor, it is by no means evident that this level of detail is appropriate for describing the turbulence loading. Instead, an alternative numerical way of solving the integral (5.24) is chosen.

From Fig. 5.3 which shows the wind load density along a wind turbine blade for two windspeeds, it can be deduced that the influence factor C(r) varies linearly with the radius, especially in the flap direction. It is therefore natural to calculate (5.24) using Gaussian quadrature with a linear weight function, i.e. using

$$\int_0^1 x^k f(x)dx \cong \sum_{i=1}^{n} w_i\ f(x_i) \tag{5.25}$$

with k equal to one and the weights w_i and integration points x_i taken from Table 5.1 from Abramovitz and Stegun [1]. Hence

$$\begin{aligned} q_i(r) &= \int_R v_i^{\alpha\beta}(r)\ C^{\alpha\beta}(r)\ v_2^{\beta}(r)dr \\ &\cong \sum_n \frac{w_n}{x_n}(R-r_o)\ v_i^{\alpha\beta}(r_n)C^{\alpha\beta}(r_n)v_2^{\beta}(r_n) \\ &= \sum_n \Gamma_i^{n\beta}\ v_2^{\beta}(r_n) \end{aligned} \tag{5.26}$$

ABSCISSAS AND WEIGHT FACTORS FOR GAUSSIAN INTEGRATION OF MOMENTS

Table 25.8

$$\int_0^1 x^k f(x)dx \approx \sum_{i=1}^{n} w_i f(x_i)$$

Abscissas $= x_i$ Weight Factors $= w_i$

	$k=0$		$k=1$		$k=2$	
n	x_i	w_i	x_i	w_i	x_i	w_i
1	0.50000 00000	1.00000 00000	0.66666 66667	0.50000 00000	0.75000 00000	0.33333 33333
2	0.21132 48654	0.50000 00000	0.35505 10257	0.18195 86183	0.45584 81560	0.10078 58821
	0.78867 51346	0.50000 00000	0.84494 89743	0.31804 13817	0.87748 51773	0.23254 74513
3	0.11270 16654	0.27777 77778	0.21234 05382	0.06982 69799	0.29499 77901	0.02995 07030
	0.50000 00000	0.44444 44444	0.59053 31356	0.22924 11064	0.65299 62340	0.14624 62693
	0.88729 83346	0.27777 77778	0.91141 20405	0.20093 19137	0.92700 59759	0.15713 63611
4	0.06943 18442	0.17392 74226	0.13975 98643	0.03118 09710	0.20414 85821	0.01035 22408
	0.33000 94782	0.32607 25774	0.41640 95676	0.12984 75476	0.48295 27049	0.06863 38872
	0.66999 05218	0.32607 25774	0.72315 69864	0.20346 45680	0.76139 92624	0.14345 87898
	0.93056 81558	0.17392 74226	0.94289 58039	0.13550 69134	0.95149 94506	0.11088 84156
5	0.04691 00770	0.11846 34425	0.09853 50858	0.01574 79145	0.14894 57871	0.00411 38252
	0.23076 53449	0.23931 43352	0.30453 57266	0.07390 88701	0.36566 65274	0.03205 56007
	0.50000 00000	0.28444 44444	0.56202 51898	0.14638 69871	0.61011 36129	0.08920 01612
	0.76923 46551	0.23931 43352	0.80198 65821	0.16717 46381	0.82651 96792	0.12619 89619
	0.95308 99230	0.11846 34425	0.96019 01429	0.09678 15902	0.96542 10601	0.08176 47043
6	0.03376 52429	0.08566 22462	0.07305 43287	0.00873 83018	0.11319 43838	0.00183 10758
	0.16939 53068	0.18038 07865	0.23076 61380	0.04395 51656	0.28431 88727	0.01572 02972
	0.38069 04070	0.23395 69673	0.44132 84812	0.09866 11509	0.49096 35868	0.05128 95711
	0.61930 95930	0.23395 69673	0.66301 53097	0.14079 25538	0.69756 30820	0.09457 71867
	0.83060 46932	0.18038 07865	0.85192 14003	0.13554 24972	0.86843 60583	0.10737 64997
	0.96623 47571	0.08566 22462	0.97068 35728	0.07231 03307	0.97409 54449	0.06253 87027
7	0.02544 60438	0.06474 24831	0.05626 25605	0.00521 43622	0.08881 68334	0.00089 26880
	0.12923 44072	0.13985 26957	0.18024 06917	0.02740 83567	0.22648 27534	0.00816 29256
	0.29707 74243	0.19091 50253	0.35262 47171	0.06638 46965	0.39997 84867	0.02942 22113
	0.50000 00000	0.20897 95918	0.54715 36263	0.10712 50657	0.58599 78554	0.06314 63787
	0.70292 25757	0.19091 50253	0.73421 01772	0.12739 08973	0.75944 58740	0.09173 38033
	0.87076 55928	0.13985 26957	0.88532 09468	0.11050 92582	0.89691 09709	0.09069 88246
	0.97455 39562	0.06474 24831	0.97752 06136	0.05596 73634	0.97986 72262	0.04927 65018
8	0.01985 50718	0.05061 42681	0.04463 39553	0.00329 51914	0.07149 10350	0.00046 85178
	0.10166 67613	0.11119 05172	0.14436 62570	0.01784 29027	0.18422 82964	0.00447 45217
	0.23723 37950	0.15685 33229	0.28682 47571	0.04543 93195	0.33044 77282	0.01724 68638
	0.40828 26788	0.18134 18917	0.45481 33152	0.07919 95995	0.49440 29218	0.04081 44264
	0.59171 73212	0.18134 18917	0.62806 78354	0.10604 73594	0.65834 80085	0.06844 71834
	0.76276 62050	0.15685 33229	0.78569 15206	0.11250 57995	0.80452 48315	0.08528 47692
	0.89833 32387	0.11119 05172	0.90867 63921	0.09111 90236	0.91709 93825	0.07681 80933
	0.98014 49282	0.05061 42681	0.98222 00849	0.04455 08044	0.98390 22404	0.03977 89578

Compiled from H. Fishman, Numerical integration constants, Math. Tables Aids Comp. 11, 1-9, 1957 (with permission).

Table 5.1. Abscissa and weight values for Gaussian quadrature, from [1].

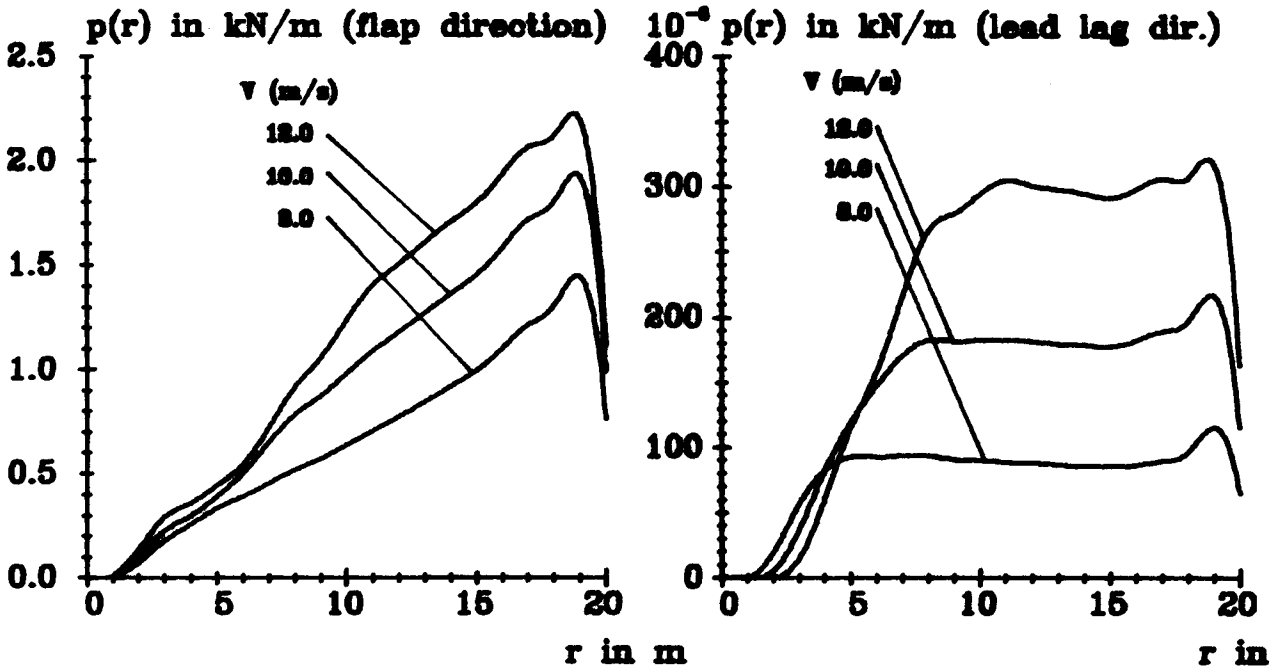

Fig. 5.3. Wind pressure distribution on a blade of the Nibe-B type in and out of the rotorplane.

with

$$r_n = X_n R + (1 - X_n) r_o \tag{5.27}$$

In (5.26) and (5.27) R and r_o are the outer radius of the blade and the radius at which the blade begins, respectively.

In this notation the crossvariance of the modal loads can be written

$$R^q_{ij}(\tau) = E\{q_i(t+\tau) q_j(\tau)\}$$

$$= \sum_n \sum_m \Gamma_i^{n\beta} \Gamma_j^{m\gamma} R_{v_2}^{\beta\gamma} \quad (r_n, r_m, \tau) \tag{5.28}$$

By comparison with (5.13) and (5.18) it follows that

$$a = r_n$$
$$b = r_m \qquad (5.29)$$
$$\phi = \frac{2\pi}{M}(n-m)$$

and that $R^{\beta\gamma}$ has the symmetry properties

$$\begin{aligned} R_{v_2}^{\beta\gamma}(r_n,r_m,\tau) &= R_{v_2}^{\beta\gamma}(r_m,r_n,\tau) \\ &= R_{v_2}^{\gamma\beta}(r_n,r_m,-\tau) \\ &= R_{v_2}^{\gamma\beta}(r_m,r_n,-\tau) \end{aligned} \qquad (5.30)$$

Consequently the spectra calculated from (5.17) have the symmetries

$$\begin{aligned} S^{\beta\gamma}(r_n,r_m,\omega) &= S^{\beta\gamma}(r_m,r_n,\omega) \\ &= \overline{S^{\gamma\beta}}(r_n,r_m,\omega) \\ &= S^{\gamma\beta}(r_n,r_m,-\omega) \end{aligned} \qquad (5.31)$$

which facilitates the calculation of the desired modal loadspectra

$$S_{ij}^{q}(\omega) = \sum_n \sum_m \Gamma_i^{n\beta}\, \Gamma_j^{m\gamma}\, S^{\beta\gamma}(r_n,r_m,\omega) \qquad (5.32)$$

$S_q^{ij}(\omega)$ from (5.32) is then inserted into (2.68) and the spectra of the responses can be determined as described in Chapter 2.

REFERENCES

[1] ABRAMOVITZ, H. and STEGUN, I.A. (eds) (1968). Handbook of Mathematical Functions (Dover, New York), 1046 pp.

[2] ENGELUND, F. (1968). Hydrodynamik. Newtonske væskers mekanik. (Den private Ingeniørfond), 322 pp.

[3] GEORGE, W.K. (1979). Processing of random signals. In: Proceedings of the Dynamic Flow Conference 1978 on Dynamic Measurements in Unsteady Flows held in Marseille, September 1978. (Sijthoff & Noordhoff, Rockville, MD), 757-800.

[4] HINZE, J.O. (1959). Turbulence. An introduction to its mechanism and theory. (McGraw-Hill, New York), 586 pp.

[5] JENSEN, N.O. and FRANDSEN, S. (1978). Atmospheric Turbulence Structure in Relation to Wind Generator Design. In: Papers presented at the Second International Symposium on Wind Energy Systems held in Amsterdam, October 3-6, 1978. Vol. 1, Paper C1.

[6] KRISTENSEN, L. and FRANDSEN, S. (1982). Model for Power Spectra of the blade of a Wind Turbine. Measured from the Moving Frame of Reference. J. Wind Eng. Ind. Aerodyn., 10, 249-262.

[7] LUMLEY, J.L. and PANOFSKY, H.A. (1964). The Structure of Atmospheric Turbulence. (Wiley, New York), 239 pp.

[8] PETERSEN, E.L. et al. (1981). Windatlas for Denmark. A rational method of wind energy siting. (Risø National Laboratory, Roskilde, Denmark), 229 pp.

[9] ROSENBROCK, H.H. (1985). Vibration and Stability Problems in Large Wind Turbines Having Hinged Blades. ERA 75-36 Report C/T 113, 53 pp.

[10] SIMIU, E. and SCANLAN, R.H. (1978). Wind Effects on Structures, an Introduction to Wind Engineering. (Wiley, New York, 458 pp.

6. RESPONSE STATISTICS DURING NORMAL OPERATION

During normal operation the response analysis is performed according to the principles outlined in Chs. 2-5. Any selected rotor response quantity is thus expressed in two parts, a deterministic periodic component and a zero mean stochastic component which is assumed to be Gaussian distributed. The deterministic part is formulated in terms of a truncated Fourier series, while the correlation structure of the stochastic part is expressed in terms of a power spectral density function. For a non-rotating wind turbine the deterministic component is constant.

Although the combined response becomes a stochastic process, it may be viewed in several ways. Thus it can be characterized as a nonstationary Gaussian process with a periodic mean function and a covariance function which depend on the time difference only. Since the location in time of the periodic part is uncertain it may also be interpreted as a stationary non-Gaussian process.

While the description of the response in terms of a Fourier series and power spectrum is complete, it is not particularly well suited to engineering decisions concerning the adequacy of the strength or fatigue lifetime of the rotor structure. It is therefore desirable to develop a set of parameters which is sufficient for the evaluation of extreme responses and damage accumulation.

In the following the stochastic part as well as the combined response will be characterized in terms of a few statistical parameters such as mean value, standard deviation and expected number of crossings and local extremes. These quantities will thus be used to define a characteristic extreme response during a given time period of operation and under a specified set of service conditions. The problem of lifetime evaluation is addressed in Chapter 7.

6.1. Response statistics

For a given stationary service condition, i.e. normal operation at a certain mean wind speed and no yawing, the response analysis yields a stress or displacement response in the form

$$Y(t) = Z(t) + X(t) \tag{6.1}$$

in which $Z(t)$ is a periodic function with the period T_o given by the angular velocity of the rotor ω_R

$$T_o = 2\pi/\omega_R \tag{6.2}$$

$Z(t)$ is expressed in terms of a truncated Fourier series as

$$Z(t) = \mathrm{Re}\left[\sum_{n=0}^{N} \alpha_n \, e^{in(\omega_R t+\theta)} \right] \tag{6.3}$$

where θ is uniformly distributed in the interval $[0,2\pi]$. $X(t)$ is a stationary Gaussian stochastic process with zero mean and an auto covariance function $R(\tau)$, expressed in terms of the power spectrum as

$$R_X(\tau) = E\{X(t+\tau)X(t)\} = \int_{-\infty}^{\infty} S_X(\omega) e^{i\omega\tau} \, d\omega \tag{6.4}$$

$E\{\ \}$ denotes the expected value of the quantity inside the bracket. $X(t)$ and $Z(t)$ are assumed to be stochastically independent.

Before the problem of characterizing the combined signal $Y(t)$ in (6.1) by a few parameters is addressed, some concepts for a purely stationary Gaussian stochastic process will be presented. Consider for that reason the process $X(t)$ and assume that the process has a finite variance of the double derivative. The variance of $X(t)$ is defined as

$$\sigma_X^2 = R_X(o) = \int_{-\infty}^{\infty} S_X(\omega)d\omega = \lambda_o \tag{6.5}$$

in which λ_o, the spectral moment of order zero, was previously defined in Chapter 2.

A characteristic frequency of the process can be defined as the average number of process upcrossings per unit time of the mean value, which here is chosen as zero. The frequency is found from Rice's formula [6],

$$\nu_o = \int_o^{\infty} \dot{x}\, f_{X\dot{X}}(o,\dot{x})d\dot{x} \tag{6.6}$$

in which $f_{X\dot{X}}(x,\dot{x})$ is the joint density function of X(t) and $\dot{X}(t)$. Since X(t) is Gaussian and differentiation is a linear operation, $\dot{X}(t)$ is also Gaussian. Stationarity implies that X(t) and $\dot{X}(t)$ are uncorrelated and that $\dot{X}(t)$ has the variance (Papoulis [5])

$$\sigma^2_{\dot{X}} = -\frac{\partial^2}{\partial\tau^2} R_X(\tau)\Big|_{\tau=0} = \int_{-\infty}^{\infty} \omega^2 S_X(\omega)d\omega = \lambda_2 \tag{6.7}$$

Hence, the joint density function can be written as

$$f_{X\dot{X}}(x,\dot{x}) = \frac{1}{2\pi\,\sigma_X\sigma_{\dot{X}}} \exp\{-\frac{1}{2}\left[(\frac{x}{\sigma_X})^2 + (\frac{\dot{x}}{\sigma_{\dot{X}}})^2\right] \tag{6.8}$$

Inserting (6.8) in (6.6) yields

$$\nu_o = \frac{1}{2\pi}\,\frac{\sigma_{\dot{X}}}{\sigma_X} = \frac{1}{2\pi}\,\sqrt{\lambda_2/\lambda_o} \tag{6.9}$$

Another characteristic frequency of the process is the average number of peaks per unit time. A peak is characterized by $\dot{X}(t)$ changing its sign from positive to negative. The peak frequency ν_m is therefore equal to the frequency of zero-downcrossings by $\dot{X}(t)$. Applying Rice's formula

$$\nu_m = \int_{-\infty}^{0} \ddot{x}\, f_{X\dot{X}\ddot{X}}(0,\ddot{x})d\ddot{x} \qquad (6.10)$$

$\ddot{X}(t)$ is also Gaussian and uncorrelated with $\dot{X}(t)$ and has the variance

$$\sigma_{\ddot{x}}^2 = \frac{\partial^4}{\partial\tau^4} R_x(\tau)\Big|_{\tau=0} = \int_{-\infty}^{\infty} \omega^4 S_x(\omega)d\omega = \lambda_4 \qquad (6.11)$$

Using the variances from (6.11) and (6.7), (6.10) then yields

$$\nu_m = \frac{1}{2\pi}\frac{\sigma_{\ddot{x}}}{\sigma_{\dot{x}}} = \frac{1}{2\pi}\sqrt{\lambda_4/\lambda_2} \qquad (6.12)$$

For a narrow-band process, i.e. a process with realizations that resemble sinusoids with slowly varying amplitudes, $\nu_o \approx \nu_m$. A band-width parameter α can then be defined as

$$\alpha = \frac{\nu_o}{\nu_m} = \lambda_2/\sqrt{\lambda_o\lambda_4} \qquad (6.13)$$

For a narrow-band process $\alpha \approx 1$, while $\alpha << 1$ implies a wide-band process with very irregular realizations.

Another parameter that also characterizes the bandwidth of the random problem is δ. In terms of the spectral moments δ is defined by

$$\delta = \lambda_1/\sqrt{\lambda_o\lambda_2} \qquad (6.14)$$

In a similar way to α, δ gives a measure of the frequency content of the process, being close to one for a narrow-band process. The value of δ, however, is less sensitive to the high frequency part of the spectrum; this is advantageous as this part is often poorly known for physical processes.

In contrast to α the δ-parameter has no simple physical interpretation, being the correlation coefficient between $-X(t)$ and the Hilbert-transformed $\hat{X}(t)$ of the process (Krenk et al. [4]).

In connection with extremes of the process the frequency of up-crossing of thresholds $\xi(t)$ other than the mean value of the process are of interest. Allowing the threshold to be time dependent, Rice's formula yields (Krenk and Madsen [4])

$$\nu(\xi(t)) = \int_{\xi}^{\infty} (\dot{x}-\dot{\xi})\, f_{X\dot{X}}(\xi,\dot{x})d\dot{x}$$

$$= 2\pi\nu_o\, \phi(\xi/\sigma_x)\, \Psi(\dot{\xi}/(2\pi\nu_o\sigma_x)) \qquad (6.15)$$

where $\phi(\ )$ is the standard normal probability density function, with distribution function $\Phi(\ )$. The function $\Psi(\ )$ is defined by

$$\Psi(x) = \int_{x}^{\infty} (z-x)\, \phi(z)dz = \phi(x) - x\, \Phi(-x) \qquad (6.16)$$

and shown in Fig. 6.1.

For a constant threshold, $\dot{\xi} = 0$, and (6.15) reduces to

$$\nu(\xi) = \int_{o}^{\infty} \dot{x}\, f_{X\dot{X}}(\xi,\dot{x})d\dot{x} = \nu_o \exp\{-\tfrac{1}{2}(\tfrac{\xi}{\sigma_x})^2\} \qquad (6.17)$$

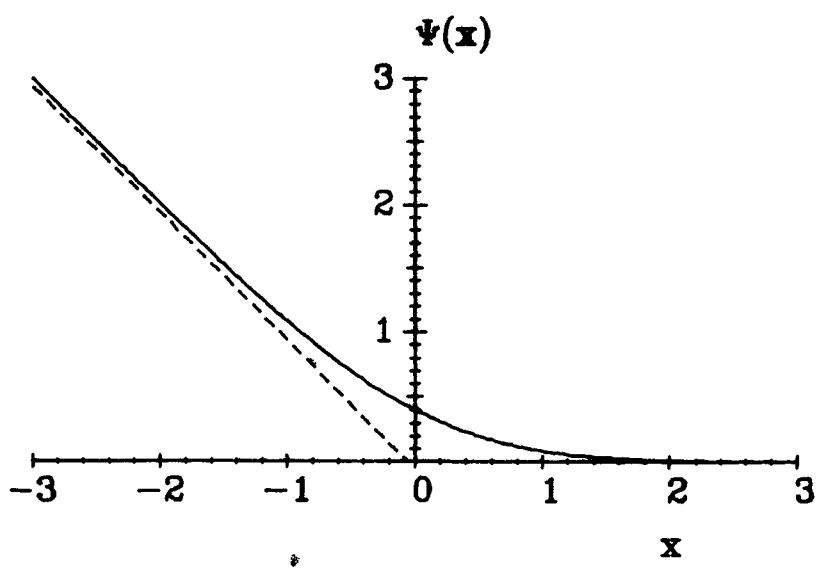

Fig. 6.1. The function $\Psi(x)$.

The mean value, variance, and characteristic frequencies defined here in connection with a Gaussian process also provide a rough description of the combined signal Y(t). The actual calculation of the parameter values however, get somewhat more complicated as will be seen.

Initially, consider the mean and the variance of Y(t). Since Z(t) and X(t) are assumed to be stochastically independent

$$\mu_Y = E\{Y(t)\} = \frac{1}{T_o}\int_o^{T_o} Z(t)dt = \alpha_o \tag{6.18}$$

where α_o is assumed to be real, and

$$\sigma_Y^2 = R_x(o) + \frac{1}{T_o}\int_o^{T_o}(Z(t)-\alpha_o)^2 dt$$

$$= \lambda_o + \frac{1}{2}\sum_{n=1}^{N}|\alpha_n|^2 \tag{6.19}$$

using the spectral moments λ_k to characterize X(t).

The average number of crossings will be calculated in two steps. First the crossing frequencies of Y(t) are determined on $\theta = \theta_o$. Secondly, θ_o is integrated out to yield the unconditional crossing frequency.

Consider now the upcrossing by Y(t) of the mean μ_Y, on $\theta = \theta_o$. The event is identical to an upcrossing of the time dependent level

$$\gamma(t,\theta_o) = \mu_Y - z(t,\theta_o)$$

$$= -\mathrm{Re}\left[\sum_{n=1}^{N} \alpha_n e^{in(\omega_R t+\theta_o)}\right] \tag{6.20}$$

by X(t). (6.15) then yields

$$\nu_o^Y(t\,|\,\theta=\theta_o) = 2\pi\nu_o\,\phi(\gamma/\sigma_x)\Psi(\dot{\gamma}/(2\pi\nu_o\sigma_x)) \tag{6.21}$$

and the unconditional mean crossing frequency of Y(t) then becomes

$$\nu_o^Y = \frac{1}{2\pi}\int_o^{2\pi} \nu_o(o,\theta_o)d\theta_o$$

$$= \nu_o \int_o^{2\pi} \phi(\mathrm{Re}[\sum_{n=1}^{N} \frac{\alpha_n}{\sigma_x} e^{in\theta_o}])\Psi(\mathrm{Re}[\sum_{n=1}^{N} \frac{-in\omega_R\alpha_n}{\sigma_x^*} e^{in\theta_o}])d\theta_o \qquad (6.22)$$

Note that in the integration over a full period of Z(t), the value of t is without influence and has been set to zero.

Likewise, the unconditional frequency of upcrossings of the level ξ by Y(t) can be written as

$$\nu_Y(\xi) = \nu_o \int_o^{2\pi} \phi(\mathrm{Re}[\frac{\xi - \sum_{n=0}^{N} \alpha_n e^{in\theta_o}}{\sigma_x}])$$

$$\Psi(\mathrm{Re}[\sum_{n=1}^{N} \frac{-in\omega_R\alpha_n}{\sigma_x^*} e^{in\theta_o}])d\theta_o \qquad (6.23)$$

The frequency of peaks of Y(t) can be found in a similar way. Note that the frequencies ν_o^Y, $\nu^Y(\xi)$ and ν_m^Y must be calculated numerically.

A bandwidth parameter for the combined signal can thus be defined in a similar way as for the pure random signal as the ratio of the mean crossing frequency ν_o and the frequency of peaks ν_m. The necessary calculations, however, are rather complicated which favours use of the spectral moments of the combined signal for characterizing the bandwidth.

Using the definition of spectral moments in (2.75) the results for the combined process become

$$\lambda_k = z \int_o^{\infty} \omega^k S_x(\omega)d\omega$$

$$+ \frac{1}{2}\sum_{n=1}^{N} (n\omega_R)^k |\alpha 4|^2 \qquad (6.24)$$

The bandwidth can then be characterized by the δ-parameter as given in (6.14).

The parameters that were derived here will be used in the following section to calculate extreme values of the response process Y(t) and will in addition provide the basis for the fatigue evaluation in Chapter 7.

6.2. Extreme Responses

An important point to the analysis of a structural design it is to determine whether or not the short-term strength will be exceeded causing failure during the planned lifetime. Due to the uncertainty of the loading and the structural strength the analysis in principle aims at securing that the probability of failure is below some acceptable level. The usual approach is to compare a characteristic maximum acceptable stress with a characteristic ultimate stress of the material, both of which may have been multiplied by partial factors. For a stochastic response the problem how to define and determine how a characteristic maximum response arises. A successful approach for wind-induced vibrations of building structures has been to use the expected value of the maximum response during a time period with an extreme mean wind speed. The calculations are based on an approximated distribution of the largest extreme (Davenport [2]) and the extreme mean wind speed typically corresponds to a return period of 50 years and the time period to 10 minutes (DS 409 [7]). Since the structural properties are constant, and the aerodynamic properties can be assumed to be independent of the wind speed, this extreme response is a good approximation to the extreme response when all wind conditions during a 50-year lifetime are considered.

For a wind turbine this simple approach is insufficient, as the extreme response may occur during operation at lower mean wind speed, and not only at the extreme mean wind speed, where the turbine often is shut down. In operation, the gust loading is added to a significant dynamic periodic response, and the struc-

tural and aerodynamic properties will depend on the wind speed. Thus, a service condition in which the turbine operates for a significant fraction of its lifetime may be responsible for the extreme responses. Consequently, a number of loadcases, characterized by mean wind speed and operational mode, should be analyzed with respect to extreme responses for time periods corresponding to the fraction of the planned lifetime spent in the loadcase. The determination of a characteristic extreme response in the form of expected values, however, will still be based on an idea similar to that of Davenport [2].

The evaluation of the distribution function of the largest extreme of a stochastic process during the time period of length T is closely connected to what is usually denoted the first-passage problem. Thus

$$P\{\max Y(t) < \xi,\ 0 \leq t \leq T\} \tag{6.25}$$

$$= P\{\text{no upcrossing of } \xi \text{ by } Y(t),\ 0 \leq t \leq T \mid Y(0) < \xi\} .$$

A simple approximation for the latter probability is obtained by assuming upcrossings to be events in a Poisson process, i.e. upcrossings are independent events. This is in fact the asymptotic solution for a normal process and increasing ξ (Cramer [1]) and and is quite accurate for a wideband process and high values of ξ. For large ξ, $P\{Y(0) < \xi\} \approx 1$ and

$$F^T_{max}(\xi) = P\{\max Y(t) < \xi,\ 0 \leq t < T\}$$

$$\cong \exp\{ - \nu_Y(\xi)T\} \tag{6.26}$$

using the expressions (6.17) and (6.23) for $\nu_Y(\xi)$ for a purely stochastic response and the combined response, respectively. The density function follows from differentiation

$$f^T_{max}(\xi) = \frac{d}{d\xi}[F^T_{max}(\xi)]$$

$$= - \nu'_Y(\xi)T\exp\{ - \nu_Y(\xi)T\} \tag{6.27}$$

In the case of several distinct operation conditions each with a time period of T_i

$$f^{o}_{max}(\xi, \sum_i T_i) = - \sum_i [- \nu^{i}_{Y}(\xi) T_i \exp\{- \sum_j \nu^{j}(\xi) T_j\}] \qquad (6.28)$$

From the probability density functions f^{o}_{max} the mean and the variance of the extreme response associated with a specific service condition (6.27) or with all possible load conditions (6.28) can be calculated using

$$\mu_{Ymax} = \int_{-\infty}^{\infty} x f_{max}(x,T) dx \qquad (6.29)$$

$$\sigma_{Ymax}^{2} = \int_{-\infty}^{\infty} (x-\mu^{Ymax})^2 f_{max}(x,T) dx \qquad (6.30)$$

Although this approach to determine the mean and variance is quite general and straightforward, the numerical work is extensive because f_{max} is a very narrow density function. Instead, the asymptotic extreme value distribution will be pursued. For that purpose the asymptotic distribution of the individual local maximas is needed.

Expressing that the number of upcrossings of a barrier ξ must be equal to the number of maxima greater than ξ minus the number of minima greater than ξ the following expression is obtained

$$\nu_Y(\xi) = \nu_m [F_{min}(\xi) - F_{max}(\xi)] \qquad (6.31)$$

in which F_{min} and F_{max} are the distribution functions of local minima and maxima, and ν_Y and ν_m are given in (6.22) and (6.24), respectively. For high barriers, $\xi \to \infty$

$$F_{min}(\xi) \sim 1 \qquad (6.32)$$

Hence, the asymptotic distribution of maxima is

$$1 - F_{max}(\xi) \simeq \nu_Y(\xi)/\nu_m \quad ; \quad \xi \to \infty \qquad (6.33)$$

During a period T the expected number of maxima is $\nu_m T$. The distribution of the maximal extreme during T can then be viewed as the extreme out of $N = \nu_m T$ extremes.

Since from (6.23)

$$\nu_Y(\xi) \to k \exp\{-\xi^2/\sigma_X^2\} \quad \text{for } \xi \to \infty \tag{6.34}$$

$F_{max}(\xi)$ is of the exponential type, Gumbel [3], and thus the asymptotic distribution of extremes is the extreme-1 distribution

$$\begin{aligned} P\{\max Y < y\} &= F_{max}^T(y) \\ &= \exp\{-\exp[-(y-\alpha_N)/\beta_N]\} \end{aligned} \tag{6.35}$$

The parameters α_N, β_N are determined from, Gumbel [3],

$$F_{max}(\alpha_N) = 1 - \frac{1}{N} \tag{6.36}$$

$$\beta_N = \frac{1}{N\, F'_{max}(\alpha_N)} \tag{6.37}$$

which in the present context implies that α_N, β_N are determined from

$$\nu_Y(\alpha_N) = 1/T \tag{6.38}$$

$$\beta_N = -1/\nu'_Y(\alpha_N)T) \tag{6.39}$$

The mean and the standard deviation for an Extreme-1 distribution are given in terms of α_N, β_N as

$$\mu_N = \alpha_N + \gamma\beta_N \quad ; \quad \gamma = 0.5772 \text{ (Euler's constant)} \tag{6.40}$$

$$\sigma_N = \frac{\pi}{\sqrt{6}}\beta_N \tag{6.41}$$

For a purely stochastic signal, i.e. $Z(t) = Z_o$, the familiar results from Davenport [2] are obtained. In this case the up-crossing intensity is given by (6.16) which leads to

$$\alpha_N = Z_o + \sigma_X\sqrt{2\log(\nu_o T)} \tag{6.42}$$

$$\beta_N = \sigma_X/\sqrt{2\log(\nu_o T)} \tag{6.43}$$

and

$$\frac{\mu_N - z_o}{\sigma_X} = \sqrt{2\log(\nu_o T)} + \frac{\gamma}{\sqrt{2\log(\nu_o T)}} \tag{6.44}$$

$$\sigma_N/\sigma_X = \frac{\pi}{\sqrt{6}}\frac{1}{\sqrt{2\log(\nu_o T)}} \tag{6.45}$$

The close agreement between the asymptotic maximum distribution and the distribution (6.27) based on the Poisson approximation is illustrated in Figs. 6.2 and 6.3 for various time periods. The periodic part of the signal is

$$Z(t) = \cos 2\pi t \tag{6.46}$$

while the stochastic part has a center frequency $\omega_o = 2\pi$ rad/s. A comparison of mean and standard deviation from (6.29), (6.30) and (6.40), (6.41) is shown in Table 6.1.

The main advantage of using the asymptotic extreme-1 distribution is that an expensive numerical integration is replaced by a usually fast-converging root-finding procedure.

The numerical work in connection with the evaluation of the characteristic extreme response being the evaluation of $\nu_Y(\xi)$ in (6.23) for a number of levels ξ, makes a simpler approximation of $\nu_Y(\xi)$ desirable. A simple approach is to define a periodic signal equivalent to Z(t) for which the upcrossing intensity $\nu_Y(\xi)$ can be determined in closed form.

When the variation in Z(t) is comparable to or larger than σ_X, extremes of the combined signal can be assumed to occur near the maximum of the periodic signal. Thus, consider a periodic step function process illustrated in Fig. 6.4 for which the mean -

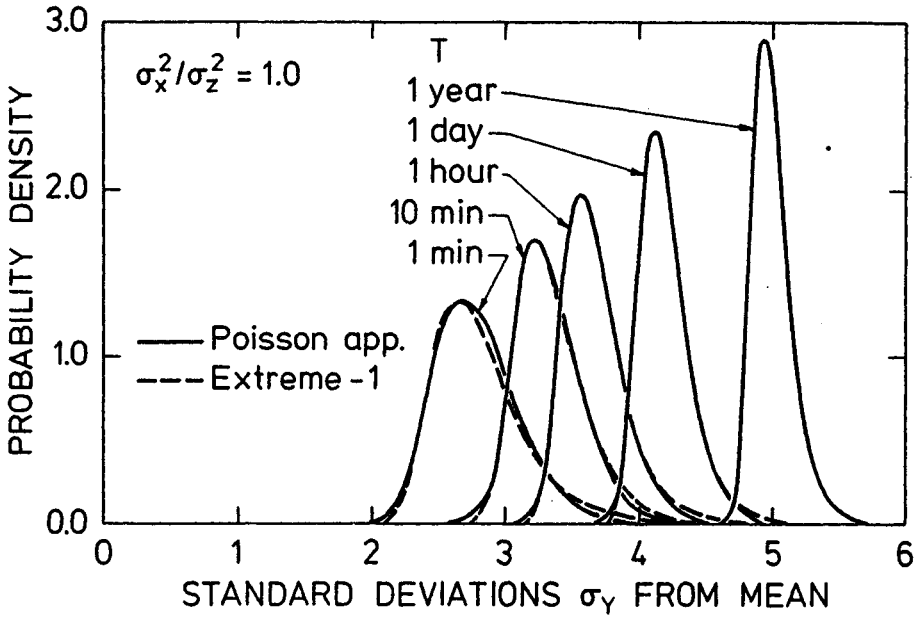

Fig. 6.2. Probability density functions of extremes, $(\sigma_x/\sigma_z)^2=1.0$.

μ_z, the variance σ_z^2, and the extremes z_{min}, z_{max} coincide with the corresponding values for Z(t). The times spent in the various levels become

$$\varepsilon_1 = t_1/T_o = \frac{\sigma_z^2}{(z_{max}-\mu_z)(z_{max}-z_{min})} \tag{6.47}$$

$$\varepsilon_2 = t_2/T_o = 1 - \frac{\sigma_z^2}{(z_{max}-\mu)(\mu-z_{min})} \tag{6.48}$$

$$\varepsilon_3 = t_3/T_o = \frac{\sigma_z^2}{(\mu-z_{min})(z_{max}-z_{min})} \tag{6.49}$$

(T_o is the period (6.2)). Note that ε_1 is an upper limit of the fraction of time the periodic signal spends at its maximum. With this representation of Z(t) the crossing intensity ν_Y becomes

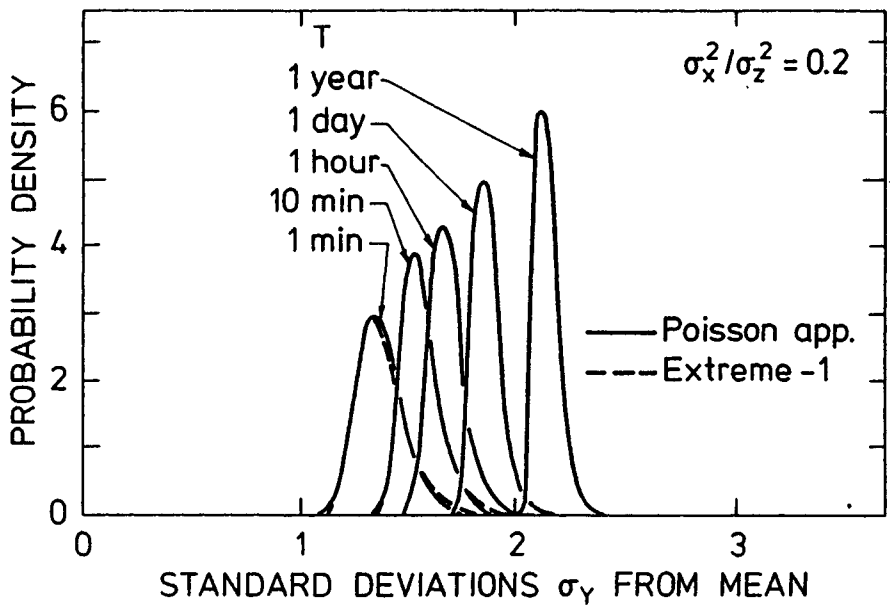

Fig. 6.3. Probability density functions of extremes, $(\sigma_x/\sigma_z)^2 = 0.2$.

$$\nu_Y(\xi) = \nu_X(\xi, z_{max})\ G(\xi, z_{max}, z_{min}, \mu_z, \sigma_z) \tag{6.50}$$

in which

$$G = [\varepsilon_1 + \varepsilon_2 \exp\{ \frac{-1}{2\sigma_x^2} (z_{max}-\mu_z)(2\xi-z_{max}-\mu_z)\}$$

$$+ \varepsilon_3 \exp\{ \frac{-1}{2\sigma_x^2} (z_{max}-z_{min})(2\xi-z_{max}-z_{min})\} \tag{6.51}$$

$$+ [\Phi((\xi-z_{min})/\sigma_X) - \Phi((\xi-z_{max})/\sigma_X)]/(T_O \nu_X(\xi-z_{max}))]$$

and ν_X are given in (6.17). The asymptotic behaviour of ν_y for large ξ is

$$\nu_Y(\xi) \underset{\xi\to\infty}{=} \varepsilon_1\ \nu_X(\xi-z_{max}) \tag{6.52}$$

Using this asymptotic expression in connection with (6.44) and (6.45) yields

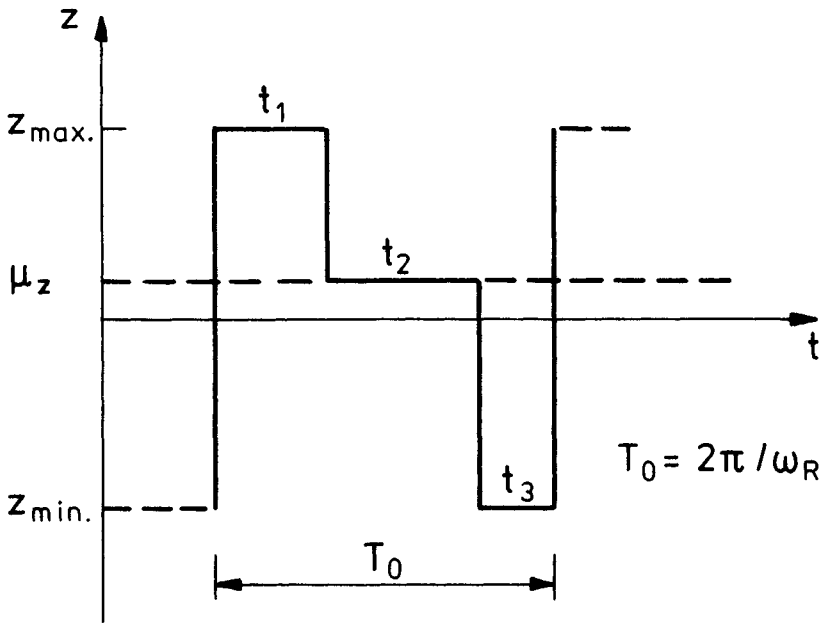

Fig. 6.4. An equivalent periodic signal.

$$\frac{\mu_N - z_{max}}{\sigma_x} = \sqrt{z \log(\varepsilon_1 \nu_o T)} + \frac{\gamma}{\sqrt{z \log(\varepsilon_1 \nu_o T)}} \tag{6.53}$$

$$\frac{\sigma_N}{\sigma_x} = \frac{\pi}{\sqrt{6}} \frac{1}{\sqrt{z \log(\varepsilon_1 \nu_o T)}} \tag{6.54}$$

in terms of the zero crossing frequency ν_o of X(t) (6.9). Due to the symmetry of the stochastic part of the signal the mean μ_N and the standard deviation σ_N of the minimum extreme is given similarly by

$$\frac{z_{min} - \mu_N}{\sigma_x} = \sqrt{2 \log(\varepsilon_3 \nu_o T)} + \frac{\gamma}{\sqrt{2 \log(\varepsilon_3 \nu_o T)}} \tag{6.55}$$

$$\frac{\sigma_N}{\sigma_x} = \frac{\pi}{\sqrt{6}} \frac{1}{\sqrt{2 \log(\varepsilon_3 \nu_o T)}} \tag{6.56}$$

Results for the maximum extreme mean and standard deviations for different time periods and periodic signals are shown in Table 6.1. The considered periodic signals are

1. $z(t) = \cos(2\pi t)$

2. $z(t) = 0.8 \cos(2\pi t) + 0.2 \cos(u\pi t)$

3. $z(t) = 0.556 \cos(2\pi t) + 0.167 \cos(4\pi t) + 0.278 \cos(8\pi t)$

and the ratios of standard deviations of Z(t) and X(t) are $(\sigma_x/\sigma_z)^2 = 0.2, 1.0$. A zero crossing frequency $\nu_o = 1$ Hz was chosen, and it is felt that the parameters are fairly representative for wind turbine responses. The columns marked (1) show results based on (6.29) and (6.30), (2) shows results from the extreme-1 distribution based on the exact ν_Y and (3) shows results based on (6.53) and (6.54). It is noted that the ratio of variances has only an insignificant effect and that the simple approximation based on a scaling of time yield very accurate results. The excellent agreement is furthermore shown in Fig. 6.5, which also contains results for Z(t) simply replaced by Z_{max}. It is concluded that (6.53) and (6.54) yield very good results, and this approach has thus been adopted in the computer program ROTORDYN.

As mentioned earlier a period T of operation is composed of several periods with different operation condition, each associated with a time period T_i such that $T = \Sigma T_i$. The distribution of the extreme during T is

$$F^o_{max}(x) = \pi_i F^{T_i}_{max}(x) \tag{6.57}$$

in terms of the distributions for each operation condition $F^{T_i}_{max}(x)$ which are assumed Extreme-1 distributed with mean and standard deviation from (6.53) and (6.54).

The mean overall extreme should be calculated from $F^o_{max}(x)$. A quick estimate, however, can be found noting that the probability

Table 6.1. Normalized mean μ_z $\frac{\mu_N - z_{max}}{\sigma_x}$ and variance $\sigma^2 = \sigma_x^2$ of the maximum extreme.

T (sec)	$\frac{\sigma_x^2}{\sigma_z^2} = 1$	Signal 1						Signal 2						Signal 3					
		(1)		(2)		(3)		(1)		(2)		(3)		(1)		(2)		(3)	
		μ	σ	μ	σ	μ	σ	μ	σ	μ	σ	μ	σ	μ	σ	μ	σ	μ	σ
60		2.53	0.44	2.57	0.50	2.58	0.55	2.47	0.45	2.52	0.50	2.42	0.55	2.39	0.45	2.45	0.50	2.13	0.63
600		3.28	0.36	3.50	0.59	3.35	0.41	3.23	0.36	3.26	0.39	3.23	0.41	3.15	0.36	3.17	0.40	3.02	0.43
3600		3.77	0.32	3.78	0.34	3.84	0.35	3.73	0.32	3.74	0.34	3.75	0.35	3.65	0.32	3.67	0.34	3.57	0.37
86400		4.51	0.27	4.52	0.28	4.60	0.29	4.48	0.27	4.49	0.29	4.51	0.29	4.40	0.27	4.42	0.29	4.37	0.30
31536000		5.65	0.22	5.65	0.23	5.74	0.23	5.62	0.22	5.63	0.23	5.67	0.23	5.56	0.22	5.56	0.23	5.56	0.23

T (sec)	$\frac{\sigma_x^2}{\sigma_z^2} = 0.2$	Signal 1						Signal 2						Signal 3					
		(1)		(2)		(3)		(1)		(2)		(3)		(1)		(2)		(3)	
		μ	σ	μ	σ	μ	σ	μ	σ	μ	σ	μ	σ	μ	σ	μ	σ	μ	σ
60		2.43	0.45	2.48	0.51	2.58	0.55	2.40	0.46	2.44	0.51	2.42	0.55	2.34	0.46	2.39	0.52	2.13	0.63
600		3.20	0.36	3.22	0.39	3.35	0.41	3.17	0.36	3.19	0.40	3.23	0.41	3.12	0.37	3.14	0.40	3.02	0.43
3600		3.70	0.32	3.71	0.34	3.84	0.35	3.67	0.32	3.68	0.34	3.75	0.35	3.62	0.32	3.64	0.35	3.57	0.37
86400		4.45	0.27	4.46	0.29	4.60	0.29	4.42	0.27	4.43	0.29	4.51	0.29	4.38	0.27	4.39	0.29	4.37	0.30
31536000		5.60	0.22	5.60	0.23	5.74	0.23	5.57	0.22	5.58	0.23	5.67	0.23	5.53	0.22	5.54	0.23	5.56	0.23

density functions are very narrow. The distribution functions of the individual load cases can be approximated by

$$F_{max}^{T_i}(x) \simeq H(x-\mu_{N_i}) \tag{6.58}$$

where H( ) is the Heaviside step function and μ_{Ni} the extreme mean. Thus, when the separation of the extreme means is large compared to the width of the density functions

$$F_{max}^{0}(x) = \exp(-\exp(-(x-\alpha_o)\beta_o)) \tag{6.59}$$

in which α_o, β_o are the parameters in the extreme distribution of the load case with the largest response extreme mean. Hence the characteristic extreme becomes

$$\mu^T = \max_i \mu_{N_i} \tag{6.60}$$

The characteristic value of the minimum response is defined similarly.

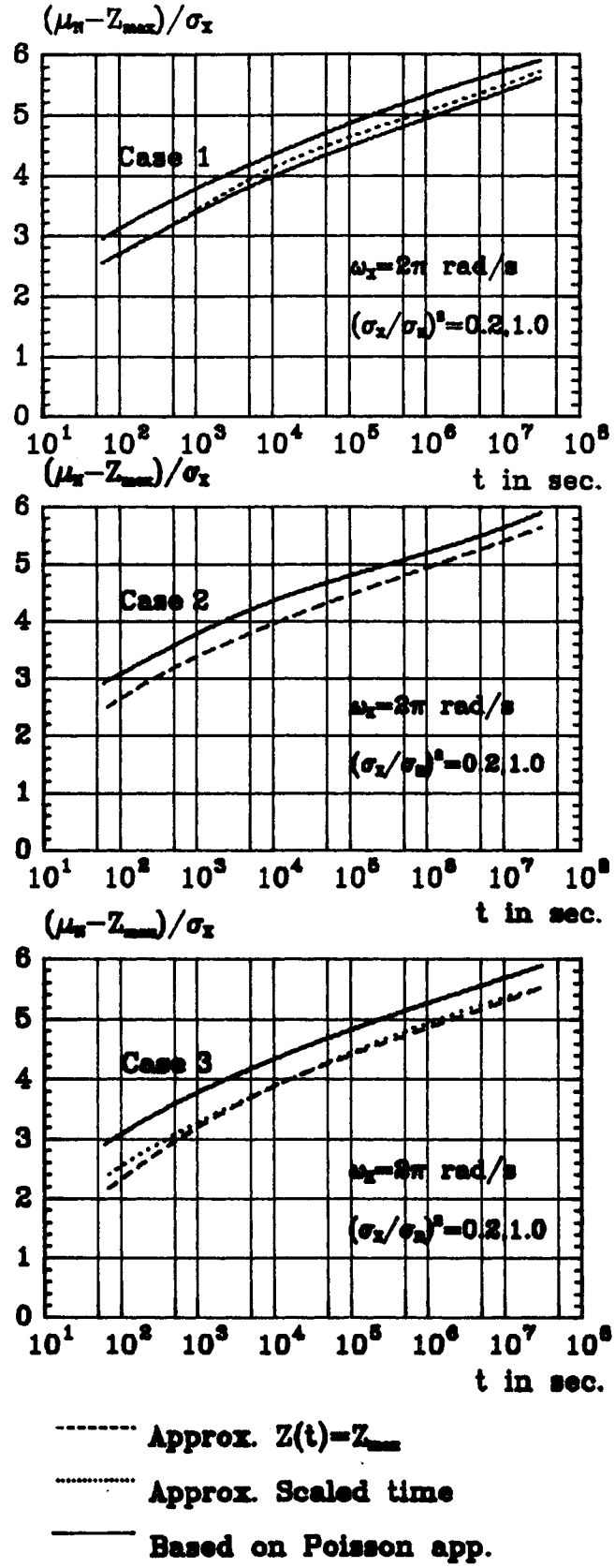

Fig. 6.5. Comparison of response extremes.

REFERENCES

[1] CRAMÉR, H. (1966). On the Intersections between the Trajectories of a Normal Stationary Stochastic Process and a High Level. Ark. Mat., 6, 337-349.

[2] DAVENPORT, A.G. (1964). Note on the Distribution of the Largest Value of a Random Function with Application to Gust Loading. Proc. Inst. Civ. Eng., London, 28, pp. 187+196.

[3] GUMBEL, E.J. (1958). Statistics of Extremes. (Columbia University Press, New York), 375 pp.

[4] KRENK, S. and MADSEN, P.H. (1982). Stochastic Response Analysis, invited lecture at NATO Advanced Study Institute on Reliability Theory and its Application in Structural and Soil Mechanics. Bornholm, Denmark, August-September, 1982.

[5] PAPOULIS, A. (1965). Probability, Random Variables and Stochastic Processes (McGraw-Hill Kogakusha, Tokyo), 583 pp.

[6] RICE, S.O. (1959). Mathematical Analysis of Random Noise. In: Selected Papers on Noise and Stochastic Processes. Ed. by Wax, N. (Dover, New York), p. 79.

[7] Dansk Ingeniørforening (1982). Norm for Sikkerhedsbestemmelser for Konstruktioner. DS-409 (Teknisk Forlag, Copenhagen), 29 pp.

7. FATIGUE MODEL FOR COMBINED PERIODIC AND STOCHASTIC RESPONSE

In the previous chapters, discussion was made of the application of the principal of superposition for the various deterministic and stochastic loads. Because the system model is linear, many desired response quantities can be computed by summing the effects of the different loads. However, Raab [1] has drawn attention to the fundamentally nonlinear character of fatigue analysis. For a given local stress time history, fatigue damage accumulates as a nonlinear function of the previous stress history. Thus, for a given machine operating condition, it is necessary to determine the fatigue damage rate for the total stress response consisting of the combined effects of all of the deterministic and stochastic loads. Since by definition the wind turbine operates in only one condition at a time, the damage rate can then be integrated in time to give an estimate of the overall lifetime.

In this chapter, an analysis procedure is proposed which gives an estimate of the fatigue life of a wind turbine which is subjected to both periodic and stochastic fluctuating loads. In order to describe the proposed model, the chapter is subdivided into four parts: fatigue damage laws, stochastic loading, irregular periodic loading, and damage from combined loading.

In the first section, the principles of the Palmgren-Miner approach to fatigue analysis are discussed. These principles are then applied in the second section to the case of a Gaussian, stochastic stress response. The case of an irregular periodic response is discussed next. A model for the combined stochastic and periodic stress response is proposed in the last section.

7.1. Fatigue damage laws

Recent studies of the fatigue behaviour of materials [2] have identified three phases in the fatigue failure process. The first, called crack initiation, involves the process by which cracks of identifiable size appear in a material after it is subjected to

fluctuating loads. Following their initiation, the cracks are propagated through the material by the continued application of the fluctuating load. At some point, when a crack has grown to a critical length, the stress concentration at the end of the crack becomes too large for the material to resist and a rapid plastic failure occurs. Unfortunately, in spite of the intense research efforts to understand the details of these fatigue processes, no design model yet exists which incorporates all aspects of fatigue phenomena. Two design approaches have, however, emerged which can predict the fatigue life under certain assumptions. Depending upon which assumptions apply in a given case (or which philosophy you believe!), either method can be used for design.

The first method can be described as the fracture mechanics approach [3]. In this approach, the crack propagation phase of the fatigue process is assumed to be dominant. Proponents of this approach have suggested that the crack propagation phenomenon underlies all fatigue processes [4]. All engineering materials exhibit flaws or small cracks whose distribution and size reflect the material characteristics and the manufacturing process by which the material is formed (casting, forging, bending, welding, heat treatment, etc.). Once the initial crack sizes are known, then each strain cycle resulting from the fluctuating load does an increment of damage resulting in an elongation of the cracks. The damage results from plastic deformations that occur because of stress concentrations at the end of the crack. The amount of resulting crack elongation depends on the range (maximum less minimum) of the strain cycle and the length of the crack. Assuming an approximately linear relation between the stress and strain ranges, equations of the following form have been proposed [5]:

$$\frac{da}{dn} = C(\Delta\sqrt{\pi a})^{\frac{1}{m}} \qquad (7.1)$$

where: a = surface crack length

$\frac{da}{dn}$ = crack length increase per cycle

Δ = range of strain for a cycle

C,m = material constants.

Knowing the initial crack length, the material constants, and the resulting sequence of strain ranges due to the fluctuating load, Eq. (8.1) can be integrated to give an estimate of the extent of the propagation of cracks in the material. When a critical crack length is reached, failure occurs and the lifetime is thus determined.

Two difficulties arise when attempting to use the fracture mechanics approach for design purposes. First, the initial characteristics of the cracks or flaws must be known, and second, the ordering of the different cycles in the lifetime calculation must also be known. This information is often unvailable to the designer. Indeed, when the loads are stochastic, the ordering cannot be known in a deterministic sense. Thus, it is necessary to propagate the statistics of the crack lengths and the loading through the nonlinear differential equation (7.1.), a difficult simulation problem.

In order to overcome the difficulties of the fracture mechanics approach to fatigue analysis, the somewhat simpler Palmgren-Miner [6] approach has been extended to cover the case of irregular load histories [7]. Two basic assumptions lie at the heart of this approach. First, it is assumed that the damage increment for each load cycle is characterized by the corresponding closed hysteresis path in the local plastic stress-strain diagram (see Fig. 7.1). Thus, any given load cycle is equivalent to a sinusoidal cycle with the same stress or strain range. For our purposes, it will be assumed that the cycle can be characterized by either the stress or the strain range. The second main assumption neglects the effect of the sequencing of the hysteresis cycles. It is assumed that each hysteresis cycle does an increment of damage which depends on its stress range regardless of the previous load history. This assumption is, of course, not precisely correct. However, it has been argued heuristically [8] that in the case of stochastic loading, the random sequencing tends to reduce the effects of different load sequences. In this case, sequences causing increased damage in general as likely to occur as those

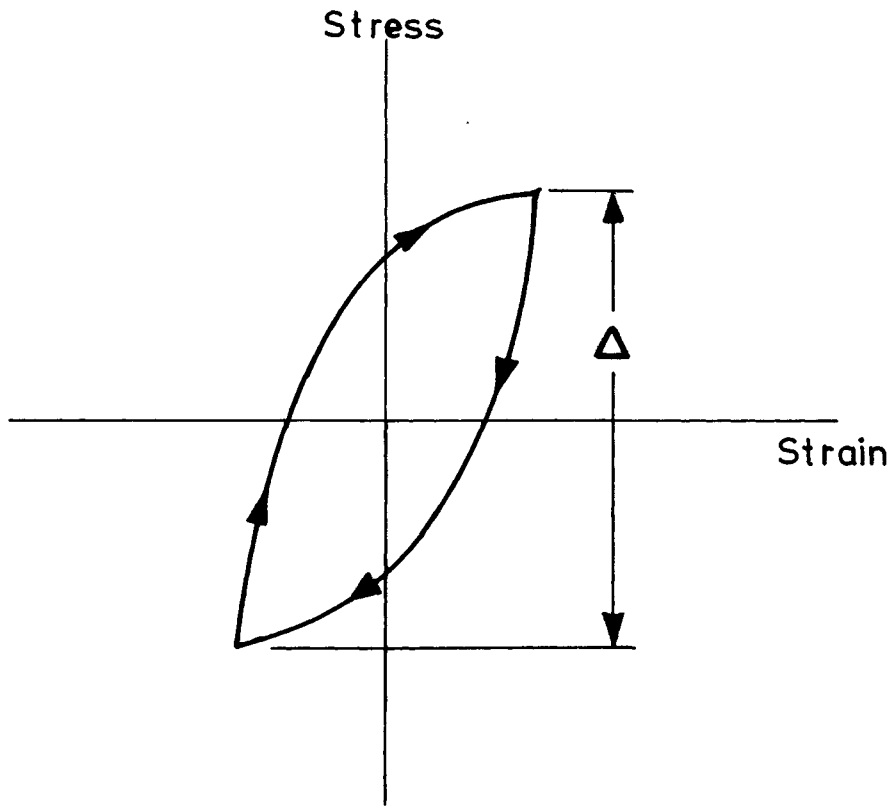

Fig. 7.1. The stress-strain hysteresis cycle.

causing decreased damage. Since the basic idea behind the Palmgren-Miner approach to fatigue analysis is to find a set of sinusoidal load cycles which does the same fatigue damage as the given load history, it is of fundamental interest to determine the damage characteristics for the given material under sinusoidal loading. This information is summarized in the S-N curve for the material. Figure 7.2 shows typical experimental results for the number of cycles to failure for a metallic material. The data typically can be arranged into three zones: The first is the upper barrier which represents the immediate-failure stress. The stress ranges associated with immediate failure are all those above twice the ultimate strength of the material (assuming zero mean stress). The second zone represents the so-called "fatigue limit". For sinusoidal stress ranges below the fatigue limit, essentially no fatigue damage results.

Not all materials exhibit a fatigue limit. Many non-ferrous alloys continue to exhibit some fatigue damage at small stress ranges [9]. The third zone is the power-law zone where the relation between stress range and cycles to failure can be represented by a straight line on a log-log plot.

Another important characteristic of the S-N relation is the scatter observed in the experimental data. Even among carefully controlled experiments, some variation is observed [10]. This scatter is attributed to variations from one test specimen to the next in the distribution of flaws, in the grain structure and even in the chemical composition. Efforts to control these variations in the test material can lead to better scientific insight into the phenomena of fatigue but can also be misleading to the designer. When a material is specified for a structural design, the designer is in reality specifying a more or less broad class of materials. In addition, fabrication techniques such as bending or welding can introduce flaws, residual stresses, hardened zones, etc. which considerably increase the variability in the fatigue strength observed. Thus, it is important for the designer to use

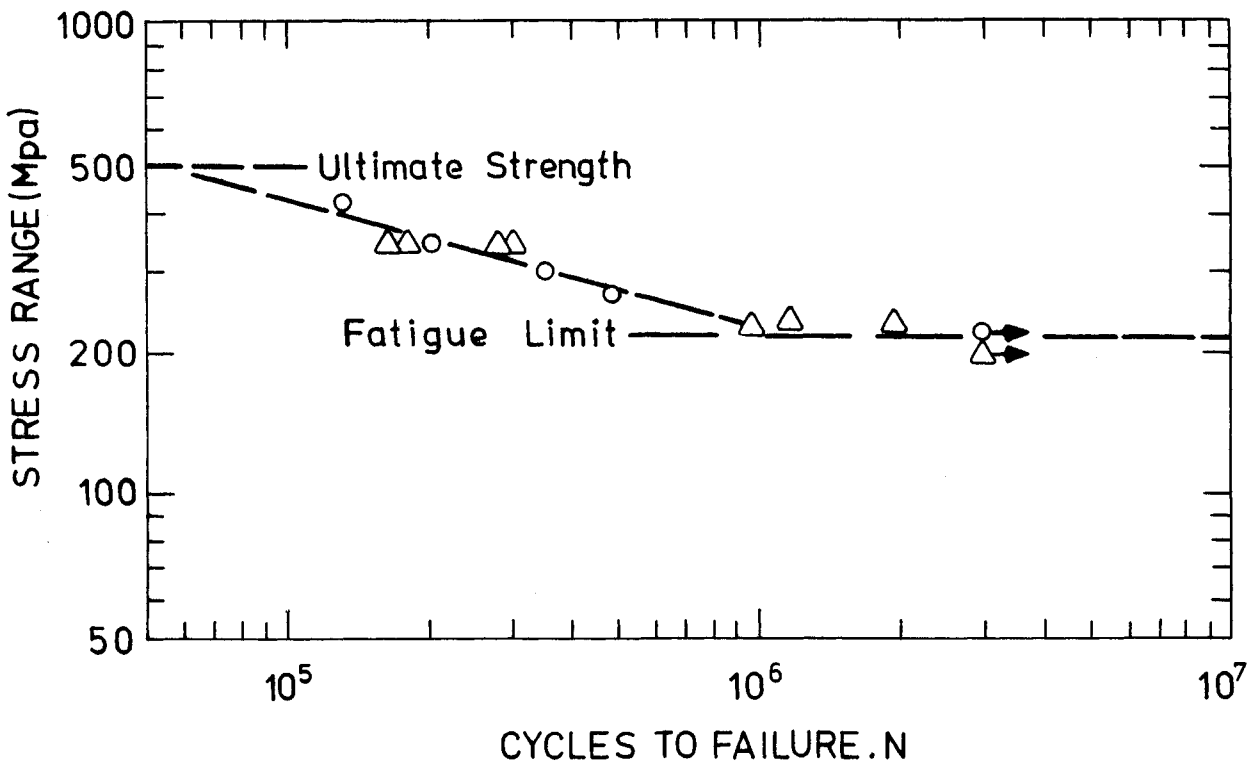

Fig. 7.2. Typical S-N curve for structural steel.

S-N data which reflects the full range of material variability actually expected to occur in the manufacturing process.

The variability in the S-N test data can be accounted for using a model of the following form:

$$T_L = \frac{D_f}{D_r} \tag{7.2}$$

where: T_L = fatigue lifetime
D_f = total damage at failure (a random variable)
D_r = damage rate from the average S-N curve.

For the power-law region of the S-N curve, the damage rate is given by the equation

$$D_r = \nu\left(\frac{\Delta}{S_1}\right)^m \tag{7.3}$$

where: Δ = local stress range due to sinusoidal loading
ν = frequency of sinusoidal loading
S_1, m = empirical material constants from the S-N curve.

The total damage at failure, D_f, is a random variable which accounts for the variability in the data. Several statistical models for D_f have been suggested [11], and a composite of several authors' data suggest the log-normal distribution with median 1.0 and coefficient of variation, $V_D = 0.65$ [12]. Using this model, the probability of failure in a given time interval, T, is given by:

$$P_f = \Phi\left(\frac{\log(TD_r)}{\sqrt{.434\log(1+V_D^2)}}\right) \tag{7.4}$$

where: $\Phi(\,.\,)$ = normal distribution function
$\log(\,.\,)$ = base 10 logarithm function
T = time interval
D_r = damage rate from Eq. 7.3
V_D = coefficient of variation.

The model for sinusoidal fatigue damage is thus given by Eqs. 7.3 and 7.4. It should be understood that Δ in Eq. 7.3 refers to local stress range. When local stress concentrations exist due to geometric effects, the elastic stress concentration factor can be conservatively used [13]. Also the effect of non-zero mean tensile stress leads to a reduction in fatigue life. The Goodman criterion [14] gives a modification of Eq. 7.3 which, including the stress concentration, becomes

$$D_r = \nu\left(\frac{K\Delta}{S_1}\right)^m \tag{7.5}$$

with

$$S_1 = \begin{cases} S_o\left(1 - \frac{K\mu}{S_u}\right) & \mu > 0 \\ S_o & \mu \leq 0 \end{cases} \tag{7.6}$$

where: S_o = empirical parameter from zero mean tests
S_u = ultimate strength
K = stress concentration factor
Δ = nominal cyclic stress range
μ = steady mean nominal stress.

In the case of welded structures, stress concentrations and residuals may be present due to the local weld geometry and flaws in workmanship. If it is assumed that, for a given detail, a tensile residual stress and a stress concentration occur simultaneously, then

$$S_1 = S_o\left(1 - \frac{S_R + K\mu}{S_u}\right) \tag{7.7}$$

where S_R is the residual tensile stress and μ is the nominal mean stress. Defining a modified stress concentration factor,

$$K^* \triangleq K\left(\frac{S_u}{S_u - S_R}\right) \tag{7.8}$$

gives

$$\frac{K\Delta}{S_1} = \frac{K^*\Delta}{S_o(1 - \frac{K^*\mu}{S_u})} \tag{7.9}$$

which is the same as if the residual stress were zero and the modified factor were used.

Now, if a static strength test were performed on the detail, an assumed elastic stress concentration factor gives

$$S_u = S_R + K\, S_N \tag{7.10}$$

where S_N is the nominal breaking stress. Defining an effective stress concentration factor so that

$$S_u = K^* S_N \tag{7.11}$$

Combining Eqs. 8.10 and 8.11 gives

$$K^* = K(\frac{S_u}{S_u - S_R}) \tag{7.12}$$

Notice that Eq. 7.12 is equivalent to Eq. 7.8. Thus, by performing several static tests, the average effective stress concentration factor can be determined, and it is also the appropriate stress concentration factor for fatigue design. The variability in the local factor K and residual stress S_R are then assumed to define a coefficient of variation for K* which then increases the variation observed in the damage at failure when fatigue tests are performed on the same specimens.

Assuming now that an appropriate sinusoidal fatigue damage model is defined, the question next arises as to how to use the Palmgren Miner approach to estimate the fatigue lifetime for irregular, fluctuating load histories. As mentioned before, the answer lies in the hysteresis paths traced by the given stress history in the local stress-strain diagram. The rainflow method originally proposed by Matsuishi and Endo [15] properly accounts for the hysteresis effects. In this method, one full cycle is counted for each

closed hysteresis path and half cycles are added for succeeding maxima and minima in the local stress which do not represent closed cycles. Several authors have corroborated the validity of this method for relating irregular load histories to equivalent sequences of sinusoidal load cycles [16,17,18]. With the rainflow method, it is then possible to estimate the fatigue lifetime if the sinusoidal-loading fatigue model is known and an appropriate load history to cover the machine lifetime is given. The major difficulty lies in determining the appropriate load history. In the case of random loading, extensive simulation is required to establish appropriate load histories.

Because the rain-flow procedure represents a complicated nonlinear operation applied to the stress history, analytical representations for the statistics of the rain-flow stress cycles are not known. However, the next sections present simplifications based on simulation data to approximate the damage rate in the case of irregular stationary stochastic and periodic load histories.

7.2 Stochastic loading

When the fluctuating stesses in the structure are random and described by stationary stochastic models, simplifications in the fatigue lifetime estimate are possible. The primary assumption is that the damage accumulation rate is stationary. Application of the rain-flow cycle counting procedure and the Palmgren-Miner damage summation law results in a total damage which is a random variable depending on the particular sample stress history used. Since the rain-flow procedure does not explicitly depend on time, the total damage predicted for a given time interval will be invariant under arbitrary time shifts. Thus, the damage rate is assumed to be a stationary random process, and the mean and variance will thus be constants depending on the statistics of the random fluctuating stress.

The simplest case is a zero-mean, narrow-band Gaussian stress process, where the rise and fall of the process is known to be Rayleigh distributed [19]. Since the height of a given stress peak

for a narrow-band process is highly correlated with the depth of the succeeding valley, it is assumed that the statistics of the rain-flow cycle ranges will be essentially equivalent to the statistics of the rise and fall between succeeding peaks and valleys. The probability density function for the cycle ranges is thus given by

$$f_{\Delta}(\xi) = \frac{\xi}{(2\sigma)^2} \exp\left(-\frac{1}{2}\left(\frac{\xi}{2\sigma}\right)^2\right) \tag{7.13}$$

where: σ^2 = variance of the stress process
ξ = given value of stress range

When the power law damage rate is assumed

$$D_r(\xi) = \nu_o\left(\frac{\xi}{S_1}\right)^m \tag{7.14}$$

The expected damage rate is

$$E\{D_r\} = \int_0^{\infty} D_r(\xi) f_{\Delta}(\xi) d\xi$$

$$= \nu_o\left(\frac{2\sqrt{2}\sigma}{S_1}\right)^m \Gamma\left(1 + \frac{m}{2}\right) \tag{7.15}$$

where $\Gamma(\cdot)$ = gamma function.

The coefficient of variation can also be computed and is given by

$$CV\{D_r\} = \sqrt{\frac{\Gamma(1+m)}{\Gamma(1 + \frac{m}{2})}} - 1 \tag{7.16}$$

where the coefficient of variation operator is defined by

$$CV\{\cdot\} = \sqrt{\frac{E\{(\cdot)^2\}}{(E\{\cdot\})^2}} - 1$$

Figure 7.3 shows the expected damage rate normalized by the

damage rate due to a sinusoidal stress with the same mean-square value. Note that both the mean damage rate and the coefficient of variation increase with increasing exponent, m. This behaviour is readily explained by the progressively greater more damage done by the large stress ranges in relation to the smaller ranges as m is increased.

The coefficient variation in the damage rate should be interpreted with caution. Since the machine operates in many different conditions in its lifetime, the total damage will be the sum of the damage due to many different finite samples from the distribution of the stochastic stress histories. For a single realization of a narrow-band stochastic process, the damage rate remains approximately constant for the time interval of operation. Thus, the total damage for the time interval T_1 is

$$D_1 = T_1 D_r \tag{7.17}$$

The mean and coefficient of variation for this damage increment are thus

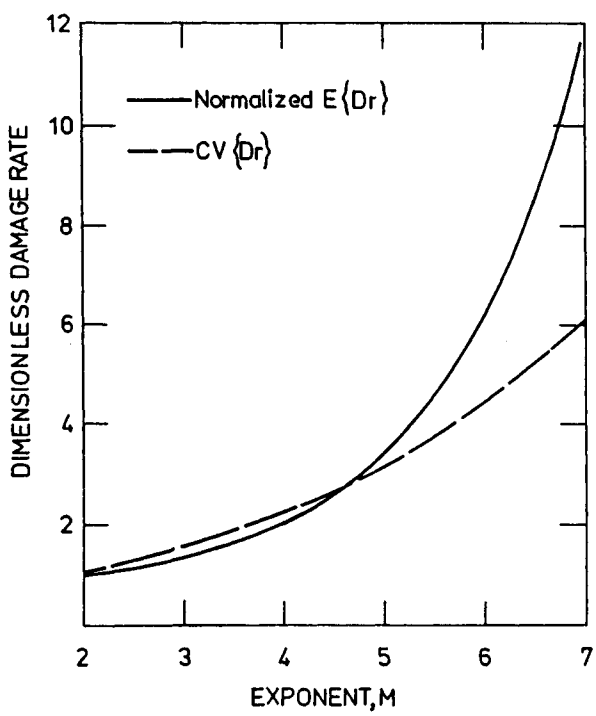

Fig. 7.3. Damage rate and coefficient of variation as a function of the power law exponent.

$$E\{D_1\} = T_1 E\{D_r\}$$
$$CV\{D_1\} = CV\{D_r\} \qquad (7.18)$$

Assuming that the machine lifetime consists of the sum of many independent samples with time intervals T_i, then the total damage is

$$D_{TOT} = \sum_{i=1}^{N} D_i \qquad (7.19)$$

The mean and coefficient of variation of the total damage are thus given by

$$E\{D_{TOT}\} = T_L E\{D_r\} \qquad (7.20)$$

$$CV\{D_{TOT}\} = \sqrt{\frac{T_o}{T_L}}\, CV\{D_r\} \qquad (7.21)$$

where $T_L = \Sigma T_i$ = total lifetime

$$T_o = \frac{\Sigma T_i^2}{\Sigma T_i} = \text{char. time interval}$$

Note that $T_o << T_L$ and that when all the time intervals are the same, $T_o = T_i$.

Similar results are obtained if the damage rate is assumed to be a slowly varying stochastic process with an expotential autocovariance function

$$\rho_{Dr}(\tau) = \exp(-\frac{\tau}{T_c}) \qquad (7.22)$$

In this case,

$$CV\{D_{TOT}\} = \sqrt{\frac{2T_c}{T_L}}\, CV\{D_r\} \qquad (7.23)$$

In the case of wind turbine structural vibrations, the stochastic fluctuations in the local stress are the result of the effects of atmospheric turbulence and machine structural resonances. Thus, it is expected that the damage rate would have a correlation time on the same order as the wind velocity fluctuations, so that

$$T_C \approx L/V \tag{7.24}$$

where L = turbulence integral scale
V = wind speed

Assuming L = 200 m, V = 10 m/S, and a lifetime of 10000 hr gives

$$CV\{D_{TOT}\} \approx 0.1\% \text{ to } 0.5\% \tag{7.25}$$

This variation is negligible compared to the variation inherent in the S-N curve fatigue data. Thus, it will be assumed for the remainder of this report that the variation in the total damage due to the stochastic nature of the loads will be negligible. Thus, the lifetime estimate will be computed from the mean damage rate and the variation will be modelled by the log-normal distribution as given in Eq. 7.4.

The application of the same procedure to wide-band stochastic processes is considerably more complicated. Figure 7.4 shows typical narrow-band and wide-band stress histories. Because of the irregularity of the wide-band processes, some peaks occur below the mean stress level so that the frequency of the peaks is somewhat higher than the frequency of the mean upcrossings. The times between successive peaks and between successive mean upcrossings are also random, varying from one time period to the next. Also due to the irregularity, the distribution of the peak levels, the distribution of the rise and fall, and the distribution of the rain-flow cycle ranges will all be somewhat different. The distribution of peaks is known analytically for Gaussian processes [20]. A numerical estimation of the rise and fall distribution is given by Rice and Beer [21]. However, no analytical results are available for the rain-flow cycle ranges.

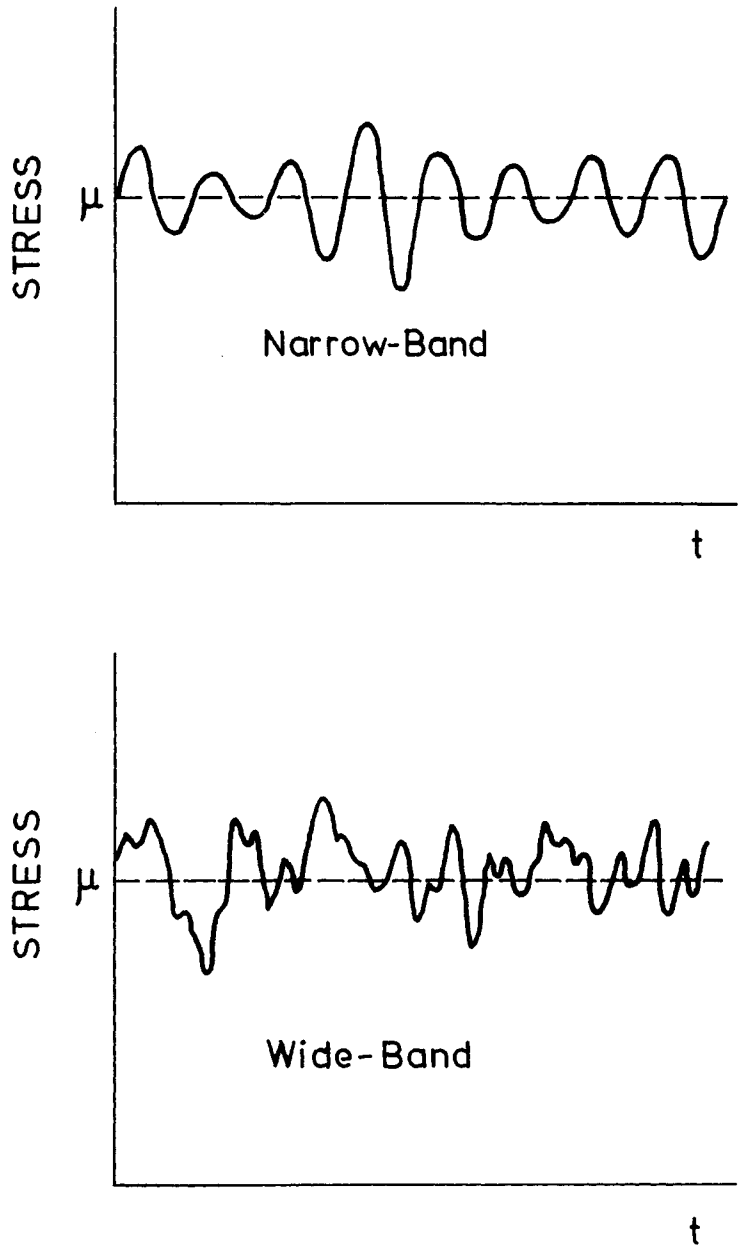

Fig. 7.4. Typical narrow- and wide-band time histories.

An early attempt to construct an analytically based theory for estimating fatigue damage for wide-band stochastic processes was proposed by Wirsching and Haugen [22]. The procedure was based on the distribution of stress peaks and assumed that each tensile peak does an increment of damage equivalent to a fully reversed sinusoid with zero steady mean and the same maximum value. For

a Gaussian stochastic process, the PDF of the peaks is given by [23]

$$f_m(\xi) = \frac{\sqrt{1-\alpha^2}}{\sigma}\phi\left(\frac{\xi-\mu}{\sigma\sqrt{1-\alpha^2}}\right) + \sqrt{2\pi}\,\frac{\alpha(\xi-\mu)}{\sigma^2}\,\phi\left(\frac{\xi-\mu}{\sigma}\right)\,\Phi\left(\frac{\alpha(\xi-\mu)}{\sigma\sqrt{1-\alpha^2}}\right) \tag{7.26}$$

where μ = the mean of the process
σ = the standard deviation of the process
α = the ratio of the mean upcrossings to peaks
$\phi(\cdot)$ = the normal density function
$\Phi(\cdot)$ = the normal distribution function.

As described in Chapter 6, the bandwidth parameter, α can be determined from the spectral moments of the process or equivalently by the variance of the process and its derivatives. It is given by

$$\alpha = \frac{\upsilon_o}{\upsilon_m} = \frac{\lambda_2}{\sqrt{\lambda_o\lambda_4}} \tag{7.27}$$

The fatigue damage rate is then estimated using the power-law portion of the S-N curve giving

$$E\{D_r\} \approx \int_{\mu}^{\infty} \upsilon_m \left(\frac{2(\xi-\mu)}{S_1}\right)^m f_m(\xi)\,d\xi \tag{7.28}$$

where S_1 is given by Eq. 7.6. This latter estimate of the damage rate (Eq. 7.28) can be shown to be conservative using the following arguments: First consider the random sequences of the values of the peaks and valleys of the process. The damage done by the actual process will be less than the damage done by a sequence of peaks and valleys where all peaks below the mean and all valleys above the mean are replaced by the mean value. These sequences are then reordered so that the peaks and valleys are paired according to the rain-flow procedure. Thus, the total damage is bounded by

$$D_{TOT} \leq \sum_{i=1}^{N} \left(\frac{x_p(i) + x_v(i)}{S_1} \right)^m \tag{7.29}$$

where $x_p(i)$ = the recorded sequence of peaks relative to the mean value with zero values for each peak below the mean

$x_v(i)$ = the magnitudes of the valleys relative to the mean value with zero values for each valley above the mean.

Thus, $x_p(i) > 0$ and $x_v(i) > 0$. Using the inequality

$$(A+B)^m \leq 1/2\left[(2A)^m + (2B)^m\right] \tag{7.30}$$

where $A, B > 0$ and $m \geq 1$ gives

$$D_{TOT} \leq 1/2 \sum_{i-1}^{N} \left(\frac{2x_p(i)^m}{S_1} \right) + \left(\frac{2x_v(i)^m}{S_1} \right) \tag{7.31}$$

Assuming x_p and x_v are identically distributed and stationary

$$E\{D_{TOT}\} \leq N\, E\left\{ \left(\frac{2x_p}{S_1} \right)^m \right\} \tag{7.32}$$

Dividing by the time interval T and assuming

$$\frac{N}{T} \to \nu_m \tag{7.33}$$

gives the desired relation for the damage rate

$$E\{D_r\} \leq \int_{\mu}^{\infty} \nu_m \left(\frac{2(\xi-\mu)}{S_1} \right)^m f_m(\xi)\, d\xi \tag{7.34}$$

In order to reduce the conservatism in using Eq. 7.34 with equality Wirshing and Light [24] developed an alternative approach. First, they observed that the damage rate, as computed using the peak distribution, depended on four statistical parameters of the stochastic process: μ, σ, ν_m, and α. The latter three parameters

are specified by the three spectral moments λ_o, λ_2, and λ_4 (see section 6.1). Second, earlier work [25] based on simulation indicated that the narrow-band equation

$$D_r = \upsilon_o \left(\frac{2\sqrt{2\sigma}}{S_1}\right)^m \Gamma\left(1+\frac{m}{2}\right) \tag{7.35}$$

where υ_o = mean upcrossing frequency for the wide-band process, provides an estimate of the damage rate which is usually conservative. Thus, it was postulated that

$$E\{D_r\} = C\, D_r \tag{7.36}$$

where D_r = damage rate computed from the narrow-band equation

C = a bandwidth "correction" term (<1).

It was further postulated that C depends only on the bandwidth parameter α and the exponent m. Wirshing and Light, then proceeded to correlate $C(\alpha, m)$ with simulation data for a wide range of spectral shapes.

In another paper, Sakai and Okamura [26] proceeded along similar lines and proposed an expression of the form

$$E\{D_r\} = \upsilon_m \left(\frac{f(\alpha,m)\sigma}{S_1}\right)^m \tag{7.37}$$

Equating 7.38 to Wirshing and Light's equation gives

$$f(\alpha,m) = 2\sqrt{2}\left[\alpha C(\alpha,m)\Gamma\left(1+\frac{m}{2}\right)\right]^{1/m}. \tag{7.38}$$

The regression equations for f and C given in the two papers, however, are in significant disagreement. This disagreement is partly due to the result quoted in Sakai and Okamura [27] that

$$\lim_{\alpha \to o} f(\alpha,m) = 2\left[\frac{1}{\sqrt{\pi}}\Gamma\left(\frac{1}{2} + \frac{m}{2}\right)\right]^{1/m} \tag{7.39}$$

which gives for $\alpha \to o$ (infinite bandwidth)

$$E\{D_r\} \to \frac{\nu_o}{\alpha}\,\frac{2}{\sqrt{\pi}}\left(\frac{\sigma}{S_1}\right)^m \to \infty \tag{7.40}$$

This result is contrary to intuition since it is difficult to conceive of a process where the spectral moment λ_o and λ_2 remain finite with $\lambda_4 \to \infty$ (required for $\alpha \to o$) while the high-frequency peaks remain large enough to do any damage. In fact, it is well known [28] that the expected rise and fall for a wide-band Gaussian process is given by

$$E\{\Delta\} = \sqrt{2\pi}\,\alpha\sigma. \tag{7.41}$$

where Δ = the rise or fall. Since Δ is always positive and $E\{\Delta\} \to o$ as $\alpha \to o$, the higher moments must also go to zero. It is again difficult to see how the damage can become infinite when the rise and fall of the process is going to zero.

With these results in mind, it was found that Wirshing and Light's expression could be rearranged into the form

$$E[D_r\} = \nu_o\left(\frac{g(\alpha,m)\,2\sqrt{2\sigma}}{S_1}\right)^m \Gamma\left(1 + \frac{m}{2}\right) \tag{7.42}$$

where $g(\alpha,m) = [C(\alpha,m)]^{1/m}$.

Plotting $g(\alpha,m)$ from the simulation results of Wirshing and Light and Sakai and Okamura gives the data shown in Fig. 7.5. Here it is seen that the systematic dependence on m is obscured by the variations in the data.

It was observed, however, that the spectral forms used by Wirshing & Light and Sakai & Okamura were not particularly characteristic of load power spectral densities observed for structures excited by atmospheric turbulence. Thus, in our research, we undertook a simulation study which included rational

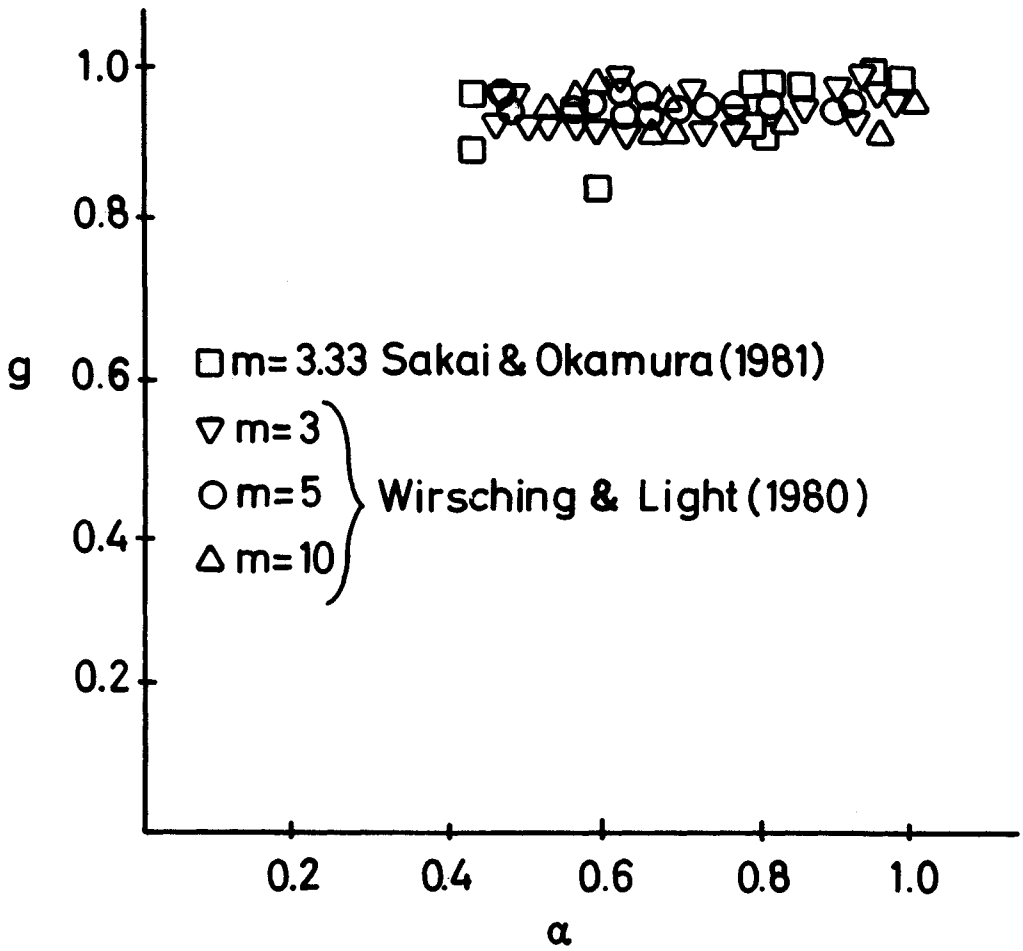

Fig. 7.5. Effective stress range factor from literature.

power spectral densities of the form:

$$S(\omega) \frac{S_o}{(\omega_o^2+\omega^2)(\omega_1^2-\omega^2)^2+r\zeta^2\omega_1^2\omega^2} \qquad (7.43)$$

This spectral form represents the physical case of low-pass filtered white noise with cut-off frequency ω_o, forcing a single degree of freedom structure with natural frequency ω_1, and damping ratio ζ. Figure 7.6 shows a typical spectral density of this form. Also shown are the single and double "box" spectral forms used here for comparison purposes. A general conclusion reached by examining the simulation results indicates that significantly less damage occurs when the rational and double-

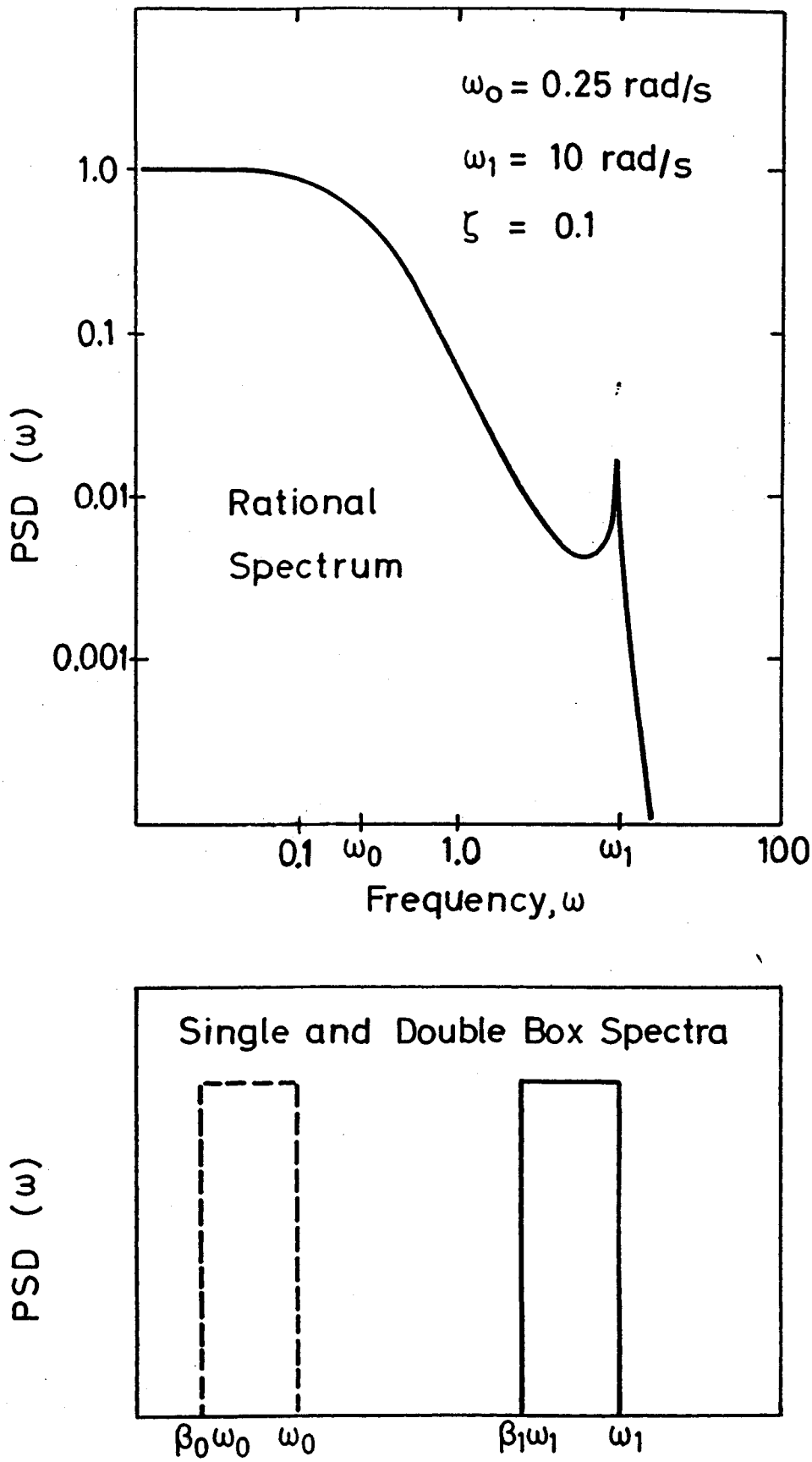

Fig. 7.6. Spectral forms used in simulation.

box spectral forms are utilized in comparison to the usual single-box spectral form. This result can be partially explained by the observation that for wide-band processes, characterized by high-frequency fluctuations superimposed on slower random variations (see Fig. 7.7.), the hysteresis cycle ranges have a distribution which appears more exponential than Rayleigh (see Fig. 7.8).

After examining our simulation results, it was found that less scatter in the data occurred when the bandwidth was characterized by a different parameter defined by

$$\delta = \frac{\lambda_1}{\sqrt{\lambda_0 \lambda_2}} \tag{7.44}$$

The simulation results are summarized in Figs. 7.9, 7.10 and 7.11. Also shown are linear approximations determined by standard regression analysis of the data. The resulting relation is given by:

$$g = 1 - (0.66 - 0.45\ m)\ (1-\delta) \tag{7.45}$$

where: g = "correction" term in Eq. 10

δ = bandwidth parameter from Eq. 12

m = material exponent in Eq. 4.

The parameters were varied to give the following ranges

$$0.3 < \delta < 1.0$$

and

$$3 < m < 7$$

The deviations in the simulation data were observed to be somewhat larger for higher material exponents. Considering the log damage ratio;

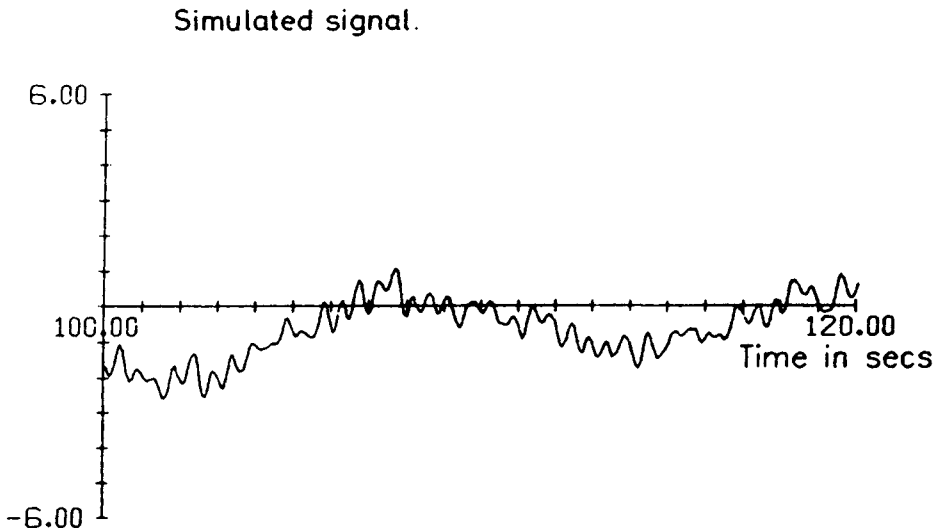

Fig. 7.7. Part of the simulated load history generated from the rational spectral form.

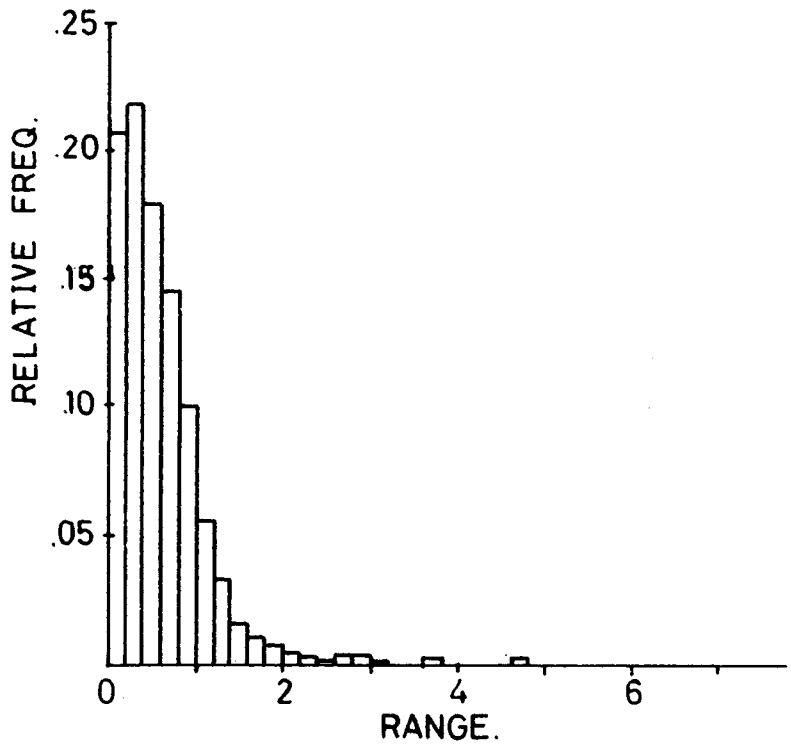

Fig. 7.8. Cyclic range relative frequency from simulated stochastic load history.

$$y = \log \left(\frac{D_S}{D_C}\right) \tag{7.46}$$

where: D_S = the value from simulation

D_C = the value computed using Eq. 13, the results given in Table 7.1 were computed.

Table 7.1. Mean and standard deviation of the log damage ratios for wide-band stochastic loading.

$$y = \log \left(\frac{D_S}{D_C}\right)$$

m	Mean	Std. Dev.
3	2.2×10^{-4}	0.045
5	-0.002	0.100
7	-0.014	0.154

The values from Table 1 are considerably smaller than the inherent fatigue life log-ratio standard deviation discussed in Section 7.1. Thus, the stochastic uncertainty increases the overall uncertainty only slightly in the fatigue lifetime estimate. It should also be remarked that the simulations were carried out using a procedure described by Yang [29], where the time series consists of a superposition of many sinewaves with amplitudes proportional to the square root of the power spectral density function and with uniformly distributed random phases. The superposition was carried out by generating a complex array of length 4096 with real and imaginary parts giving the desired magnitudes and phases. Two time series realizations were then formed as the real and imaginary parts, respectively, of the fast Fourier transform of the original complex array. This relatively large number of data points was necessary to fully characterize the wide bandwidths and to give sufficient frequency resolution for the cases studied in these simulations.

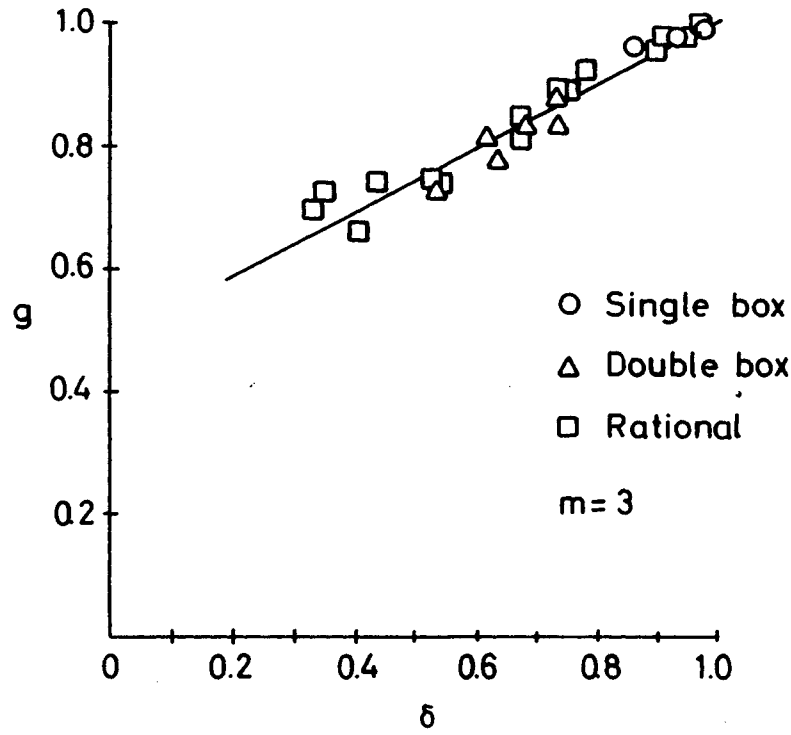

Fig. 7.9. Effective range correction factor for simulated wide-band loading with material exponent, m = 3.

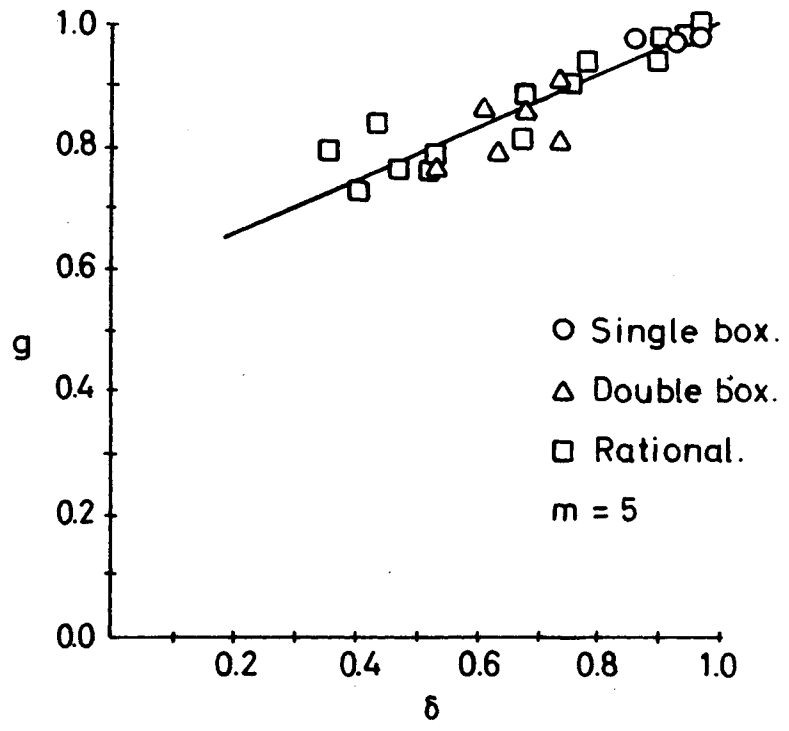

Fig. 7.10. Effective range correction factor for simulated wide band loading with amterial exponent, m = 5.

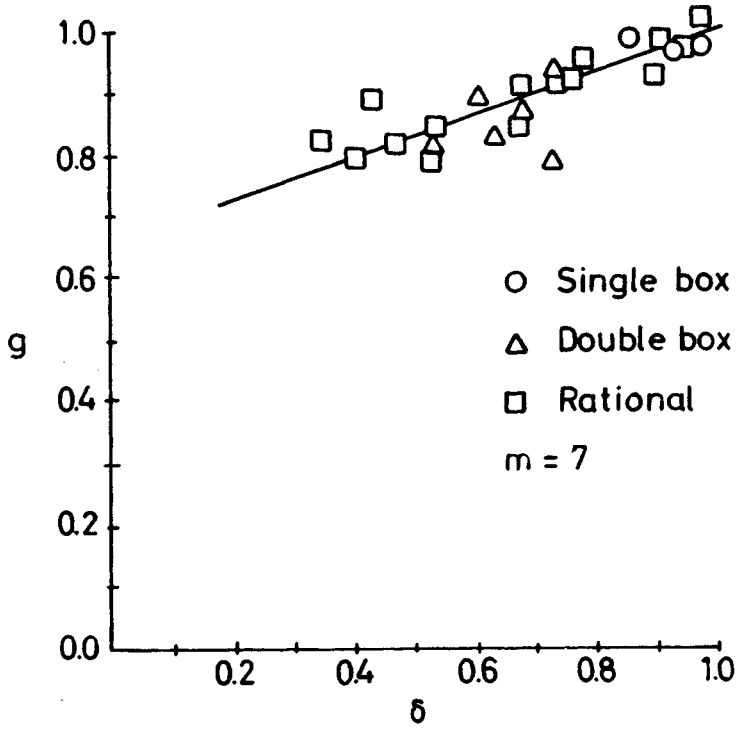

Fig. 7.11. Effective range correction factor for simulated wide-band loading with material exponent, m = 7.

The idea of correlating random fatigue data with the spectral moment parameters for wide-band stochastic processes is not entirely new. Talreja [30] proposed such a concept in 1973, and it has become common to plot the rms stress vs. cycles-to-failure in a log-log plot similar to the S-N curve. Eq. 7.42 predicts that such a plot will be a straight line for given mean stress μ and bandwidth parameter α. Figure 7.6 shows several authors' [31, 32, 33] test data. Figure 7.7 shows the experimentally derived correction factor g as given by the data in Fig. 7.6. The test data indicates that Eq. 7.43 may slightly underestimate the fatigue damage. However, too little test data are available to draw any definite conclusions and Eq. 7.43 will be used.

In summary, the following equation is proposed for wide-band Gaussian stochastic stress histories:

$$E\{D_r\} = \nu_o \left(\frac{Kg2\sqrt{2\sigma}}{S_1}\right)^m \Gamma\left(1+\frac{m}{2}\right) \qquad (7.47)$$

where:

$$g = 1 - (0.66 - 0.45\ m)\ (1-\delta)$$

$$S_1 = S_o\left(1+\frac{K\mu}{S_u}\right)$$

$$\sigma = \sqrt{\lambda_o}$$

$$\nu_o = \frac{1}{2\pi}\sqrt{\frac{\lambda_2}{\lambda_o}}$$

$$\delta = \frac{\lambda_1}{\sqrt{\lambda_o \lambda_2}}$$

μ = mean value

λ_o, λ_1, λ_2 = spectral moments

m, S_o, S_u = material constants

K = stress concentration factor

7.3 Irregular periodic loading

When the local stress history is given by a periodic deterministic time function, it is possible to determine the damage for one period using the rain-flow cycle counting procedure. Assuming that the lifetime consists of many periods, it can be estimated from the average damage rate defined by dividing the single period damage by the appropriate period.

Some care must be taken, however, when computing the rain-flow damage for a single period. Because the rain-flow procedure has memory from the previous time period, it is necessary to be sure that the cycle counts begin with the largest peak (or smallest valley) in the time period. Thus, it is convenient to define the time origin to be at the largest deterministic peak. With this definition, the computation of the average damage rate is straightforward, but perhaps somewhat tedious.

For periodic functions, it is possible to represent the function by its Fourier coefficient. Thus

$$Z(t) = R_e \left[\sum_{n=0}^{N} \alpha_n e^{in(\omega_R t+\theta]} \right] \tag{7.48}$$

where θ is an arbitrary phase angle. If the time origin is arbitrary then θ can have any value $0 \leq \theta \leq 2\pi$. As described in Chapter 6, $Z(t)$ can be regarded as a stochastic process if θ is random. When the phase angle θ is uniformly distributed, the autocovariance function is given by

$$E\{Z(t+\tau)Z(t)\} = \frac{1}{2} \text{Re} \sum_{n=1}^{N} |\alpha_n|^2 e^{in\omega_R \tau} \tag{7.49}$$

and the power spectral density by

$$S_Z(\omega) = \frac{1}{4} \sum_{k=-N}^{N} |\alpha_n|^2 \, \delta(\omega - k\omega_R) \tag{7.50}$$

where $\delta(\cdot)$ = Dirac impulse function, and $\alpha_0 = 0$.

Thus, it is seen that the information on the relative phase between the Fourier components is absent in the spectral representation of the process.

In the previous section on fatigue damage for Gaussian stochastic processes, the damage rate was found to correlate with the spectral moments of the process. The question now arises as to how important the relative phase between Fourier components is for determining the fatigue damage for periodic time histories.

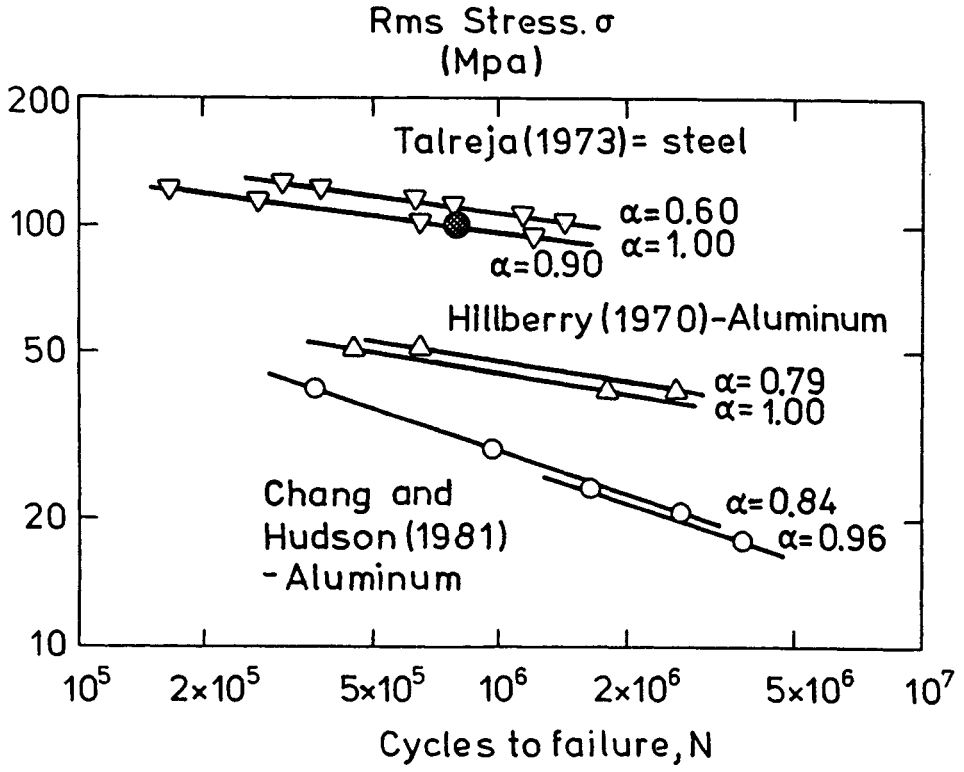

Fig. 7.12. Experimental data for cycles-to-failure vs. rms stress for wide band stochastic loading.

In other words, is it possible to use an approach similar to Section 7.2 to determine the fatigue damage rate?

In order to answer this question, a study was made of the rain-flow cycle ranges for a signal consisting of two sinusoids. Thus,

$$Z(t) = A\sin t + B\sin(Ct+\theta) \tag{7.51}$$

with $A^2+B^2 = 1$, $0<\theta<2\pi$ and C = positive integer. The effective rain-flow range, defined by

$$\Delta_e \triangleq \left(\frac{1}{N}\sum_{i=1}^{N} \Delta_i^m\right)^{1/m} \tag{7.52}$$

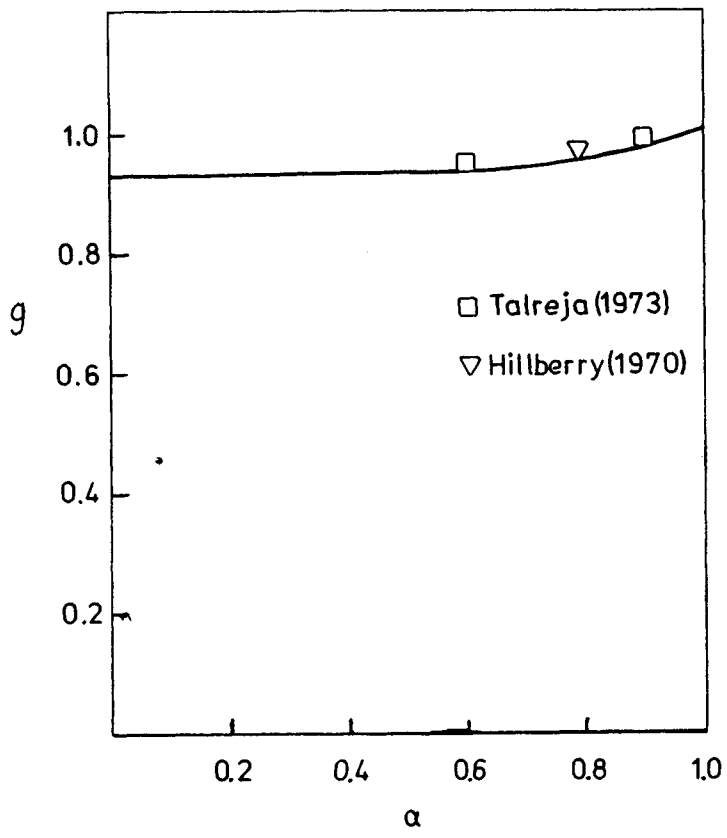

Fig. 7.13. Effective stress range factor compared to experimental data.

where N = the number of peaks in one period
Δ_i = the rain-flow cycle range associated with each peak
m = the power law exponent

was computed and the variation due to phase angle was observed. Tables 7.1 to 7.7 show the result for the case when m = 5. The average and standard deviation were computed assuming that θ was uniformly distributed. Notice that the coefficient of variation is less than 10% except when the B coefficient is small enough so that the number of peaks per period is reduced for certain relative phase angles and not others. Because both the number of mean upcrossings and the number of peaks per period can change abruptly with the variation in phase angle, it is expected that a perfect correlation of damage with the spectral moments or bandwidth parameter will not be possible.

Table 7.2. Effective stress range, C= 2.

C = 2.000 M = 5

A	B	AVERAGE	ST. DEV.	COEF. VAR.
0.2236	0.9747	2.0334	0.0141	0.0070
0.3162	0.9487	2.0592	0.0257	0.0125
0.3873	0.9220	2.0785	0.0353	0.0170
0.4472	0.8944	2.0924	0.0436	0.0208
0.5000	0.8660	2.1013	0.0506	0.0241
0.5477	0.8367	2.1058	0.0568	0.0270
0.5916	0.8062	2.1062	0.0622	0.0295
0.6325	0.7746	2.1027	0.0669	0.0318
0.6708	0.7416	2.0953	0.0711	0.0339
0.7071	0.7071	2.0842	0.0747	0.0359
0.7416	0.6708	2.0692	0.0779	0.0376
0.7746	0.6325	2.0504	0.0805	0.0393
0.8062	0.5916	2.0274	0.0826	0.0407
0.8367	0.5477	2.0000	0.0840	0.0420
0.8660	0.5000	1.9679	0.0846	0.0430
0.8944	0.4472	1.9804	0.1672	0.0844
0.9220	0.3873	2.0561	0.2169	0.1055
0.9487	0.3162	2.0908	0.1378	0.0659
0.9747	0.2236	2.0531	0.0558	0.0272
TOTAL		2.0608	0.1005	0.0488

Table 7.3. Effective stress range, C= 3.

C = 3.000 M = 5

A	B	AVERAGE	ST. DEV.	COEF. VAR.
0.2236	0.9747	2.0259	0.0242	0.0120
0.3162	0.9487	2.0492	0.0462	0.0225
0.3873	0.9220	2.0687	0.0657	0.0318
0.4472	0.8944	2.0841	0.0830	0.0398
0.5000	0.8660	2.0956	0.0984	0.0470
0.5477	0.8367	2.1033	0.1121	0.0533
0.5916	0.8062	2.1072	0.1244	0.0590
0.6325	0.7746	2.1073	0.1354	0.0642
0.6708	0.7416	2.1036	0.1452	0.0690
0.7071	0.7071	2.0959	0.1539	0.0734
0.7416	0.6708	2.0842	0.1616	0.0775
0.7746	0.6325	2.0679	0.1683	0.0814
0.8062	0.5916	2.0468	0.1741	0.0851
0.8367	0.5477	2.0201	0.1788	0.0885
0.8660	0.5000	1.9869	0.1824	0.0918
0.8944	0.4472	1.9457	0.1844	0.0948
0.9220	0.3873	1.8940	0.1843	0.0973
0.9487	0.3162	1.8692	0.2605	0.1394
0.9747	0.2236	2.0555	0.3610	0.1756
TOTAL		2.0427	0.1810	0.0886

Table 7.4. Effective stress range, C= 4.

C = 4.000 M = 5

A	B	AVERAGE	ST. DEV.	COEF. VAR.
0.2236	0.9747	2.0113	0.0026	0.0013
0.3162	0.9487	2.0241	0.0053	0.0026
0.3873	0.9220	2.0360	0.0079	0.0039
0.4472	0.8944	2.0462	0.0102	0.0050
0.5000	0.8660	2.0542	0.0124	0.0060
0.5477	0.8367	2.0597	0.0144	0.0070
0.5916	0.8062	2.0625	0.0163	0.0079
0.6325	0.7746	2.0624	0.0179	0.0087
0.6708	0.7416	2.0591	0.0195	0.0095
0.7071	0.7071	2.0523	0.0209	0.0102
0.7416	0.6708	2.0418	0.0222	0.0109
0.7746	0.6325	2.0272	0.0233	0.0115
0.8062	0.5916	2.0079	0.0244	0.0121
0.8367	0.5477	1.9831	0.0253	0.0128
0.8660	0.5000	1.9518	0.0261	0.0134
0.8944	0.4472	1.9123	0.0267	0.0140
0.9220	0.3873	1.8617	0.0271	0.0146
0.9487	0.3162	1.7949	0.0271	0.0151
0.9747	0.2236	1.8117	0.0311	0.0171
TOTAL		1.9926	0.0862	0.0433

Table 7.5. Effective stress range, C = 5.

C = 5.000 M = 5

A	B	AVERAGE	ST. DEV.	COEF. VAR.
0.2236	0.9747	2.0012	0.0058	0.0029
0.3162	0.9487	2.0053	0.0119	0.0060
0.3873	0.9220	2.0099	0.0181	0.0090
0.4472	0.8944	2.0141	0.0240	0.0119
0.5000	0.8660	2.0173	0.0296	0.0147
0.5477	0.8367	2.0190	0.0348	0.0173
0.5916	0.8062	2.0188	0.0397	0.0197
0.6325	0.7746	2.0164	0.0443	0.0220
0.6708	0.7416	2.0115	0.0485	0.0241
0.7071	0.7071	2.0038	0.0524	0.0262
0.7416	0.6708	1.9929	0.0560	0.0281
0.7746	0.6325	1.9783	0.0593	0.0300
0.8062	0.5916	1.9595	0.0622	0.0318
0.8367	0.5477	1.9356	0.0649	0.0335
0.8660	0.5000	1.9055	0.0672	0.0353
0.8944	0.4472	1.8675	0.0692	0.0370
0.9220	0.3873	1.8188	0.0706	0.0388
0.9487	0.3162	1.7537	0.0713	0.0406
0.9747	0.2236	1.6586	0.0700	0.0422
TOTAL		1.9467	0.1127	0.0579

Table 7.6. Effective stress range, C = 7.

C = 7.000	M = 5			
A	B	AVERAGE	ST. DEV.	COEF. VAR.
0.2236	0.9747	1.9873	0.0022	0.0011
0.3162	0.9487	1.9784	0.0048	0.0024
0.3873	0.9220	1.9712	0.0074	0.0038
0.4472	0.8944	1.9650	0.0101	0.0052
0.5000	0.8660	1.9590	0.0128	0.0065
0.5477	0.8367	1.9529	0.0154	0.0079
0.5916	0.8062	1.9462	0.0179	0.0092
0.6325	0.7746	1.9385	0.0203	0.0105
0.6708	0.7416	1.9293	0.0226	0.0117
0.7071	0.7071	1.9184	0.0247	0.0129
0.7416	0.6708	1.9052	0.0267	0.0140
0.7746	0.6325	1.8893	0.0285	0.0151
0.8062	0.5916	1.8699	0.0302	0.0161
0.8367	0.5477	1.8464	0.0317	0.0172
0.8660	0.5000	1.8174	0.0331	0.0182
0.8944	0.4472	1.7814	0.0344	0.0193
0.9220	0.3873	1.7354	0.0354	0.0204
0.9487	0.3162	1.6740	0.0361	0.0216
0.9747	0.2236	1.5834	0.0363	0.0229
TOTAL		1.8762	0.1121	0.0597

Table 7.7. Effective stress range, C = 10.

C = 10.00	M = 5			
A	B	AVERAGE	ST. DEV.	COEF. VAR.
0.2236	0.9747	1.9761	0.0002	0.0001
0.3162	0.9487	1.9556	0.0004	0.0002
0.3873	0.9220	1.9370	0.0007	0.0004
0.4472	0.8944	1.9199	0.0010	0.0005
0.5000	0.8660	1.9038	0.0013	0.0007
0.5477	0.8367	1.8884	0.0016	0.0008
0.5916	0.8062	1.8733	0.0019	0.0010
0.6325	0.7746	1.8583	0.0022	0.0012
0.6708	0.7416	1.8428	0.0025	0.0013
0.7071	0.7071	1.8266	0.0027	0.0015
0.7416	0.6708	1.8091	0.0030	0.0017
0.7746	0.6325	1.7899	0.0033	0.0018
0.8062	0.5916	1.7683	0.0035	0.0020
0.8367	0.5477	1.7435	0.0037	0.0021
0.8660	0.5000	1.7144	0.0039	0.0023
0.8944	0.4472	1.6793	0.0041	0.0024
0.9220	0.3873	1.6355	0.0042	0.0026
0.9487	0.3162	1.5777	0.0043	0.0028
0.9747	0.2236	1.4928	0.0044	0.0030
TOTAL		1.7996	0.1289	0.0716

Table 7.8. Effective stress range, C = 20.

C = 20.00 M = 5

A	B	AVERAGE	ST. DEV.	COEF. VAR.
0.2236	0.9747	1.9626	0.0000	0.0000
0.3162	0.9487	1.9269	0.0001	0.0000
0.3873	0.9220	1.8923	0.0001	0.0001
0.4472	0.8944	1.8586	0.0001	0.0001
0.5000	0.8660	1.8258	0.0002	0.0001
0.5477	0.8367	1.7938	0.0003	0.0001
0.5916	0.8062	1.7627	0.0003	0.0002
0.6325	0.7746	1.7322	0.0004	0.0002
0.6708	0.7416	1.7023	0.0004	0.0003
0.7071	0.7071	1.6728	0.0005	0.0003
0.7416	0.6708	1.6436	0.0006	0.0003
0.7746	0.6325	1.6143	0.0006	0.0004
0.8062	0.5916	1.5844	0.0007	0.0004
0.8367	0.5477	1.5534	0.0008	0.0005
0.8660	0.5000	1.5202	0.0008	0.0005
0.8944	0.4472	1.4835	0.0009	0.0006
0.9220	0.3873	1.4409	0.0009	0.0006
0.9487	0.3162	1.3877	0.0010	0.0007
0.9747	0.2236	1.3124	0.0010	0.0008
TOTAL		1.6669	0.1823	0.1094

In order to simplify these results, the following approximation is made. The largest range in one period will be most important in estimating the fatigue damage. The smaller ranges will cause damage in relation to the largest range in a similar way as the the smaller ranges in the stochastic case. Thus, a similar band-width correction is utilized. The average damage rate is thus approximated by the equation

$$E\{D_r\} = \nu_o \left(\frac{Kg\,\Delta_{max}}{S_1}\right)^m \qquad (7.53)$$

where:

$$g = 1-(0.66 - 0.45\ m)\ (1-\delta)$$

$$\nu_o = \frac{1}{2\pi}\sqrt{\frac{\lambda_2}{\lambda_o}}$$

$$\delta = \frac{\lambda_1}{\sqrt{\lambda_o \lambda_2}}$$

Δ_{max} = maximum stress range in one period

$$\lambda_n = -\frac{1}{2}\sum_{k=1}^{\infty}(k\omega_o)^n|\alpha_k|^2 \qquad n = 0,1,2$$

K = stress concentration factor

S_1,m = material parameters.

Applying the approximate model to compare computed damage with simulated damage gives the results in Table 7.9.

Table 7.9. Log damage ratios for irregular periodic loading consisting of two sinewaves.

$$y = \log\left(\frac{D_S}{D_C}\right)$$

m	Mean	Std. Div.
3	-0.28	0.13
5	-0.31	0.22
7	-0.32	0.26

The rather low values of the mean attest to the conservatism of the model. The large values of standard deviation indicate that the smaller ranges not considerred explicitly in the model have a somewhat variable effect on the damage rate. It was observed in these results that combinations having the same relative amplitudes (i.e. identical spectral moment parameters) but different phases had different damage rates. Thus, it must be concluded that in the case of irregular periodic loading, the relative phases of the Fourier components have a marked effect on the damage rate. This result is partially accounted for in the simple model given by Eq. 7.54 by using the maximum stress range in the periodic loading. This quantity is found to depend significantly on the phase information in the Fourier coefficients.

This resulting phase dependency is in sharp contrast to the case of purely stochastic loading discussed in the previous section. In this latter case, the phase spectrum is purely random, resulting in the local phase characteristics of a specific realization being averaged out.

7.4 Damage from combined loading

In the previous sections two types of irregular loading were studied. Section 7.2 considered the case of a Gaussian stochastic process while Section 7.3 presented results for a periodic time history with a random phase. In this section, we wish to consider the case of combined loading consisting of the sum of the two previous cases. Thus, we want to establish an estimate of the damage rate for a stress response history given by

$$Y(t) = Z(t) + X(t) \tag{7.54}$$

where $Z(t)$ = a periodic time function
$X(t)$ = a zero-mean Gaussian stochastic process

Unfortunately, no analytical expression exists for the distribution of rise and fall or the rain-flow cycle ranges for the general case. However, Rice [33] has determined the rise and fall statistics for the special case of a sinusoid plus a narrow-band stochastic process.

In this case, the combined response is given by

$$Y(t) = A\cos\omega_o t + R\cos(\omega_o t+\theta) \tag{7.55}$$

where A = amplitude of sinusoid
R = Rayleigh-distributed random amplitude
θ = uniformly distributed random phase

The combined amplitude density function is the same as the peak density function and is given by

$$f_m(\xi) = \int_0^{2\pi} \frac{\xi}{2\pi\sigma_x^2} \exp\left(-\frac{\xi^2+A^2-2A\xi\cos\theta}{2\sigma_x^2}\right)d\theta$$

$$= \frac{\xi}{\sigma_x^2} \exp\left(-\frac{\xi^2+A^2}{2\sigma_x^2}\right) I_o\left(\frac{\xi A}{\sigma^2}\right) \qquad (7.56)$$

where ξ = combined amplitude value
σ_x = rms of X(t)
$I_o(\cdot)$ = modified Bessel function

Fig. 7.9 shows sketches of the density function for two cases: one where A >> σ and the other where A << σ.

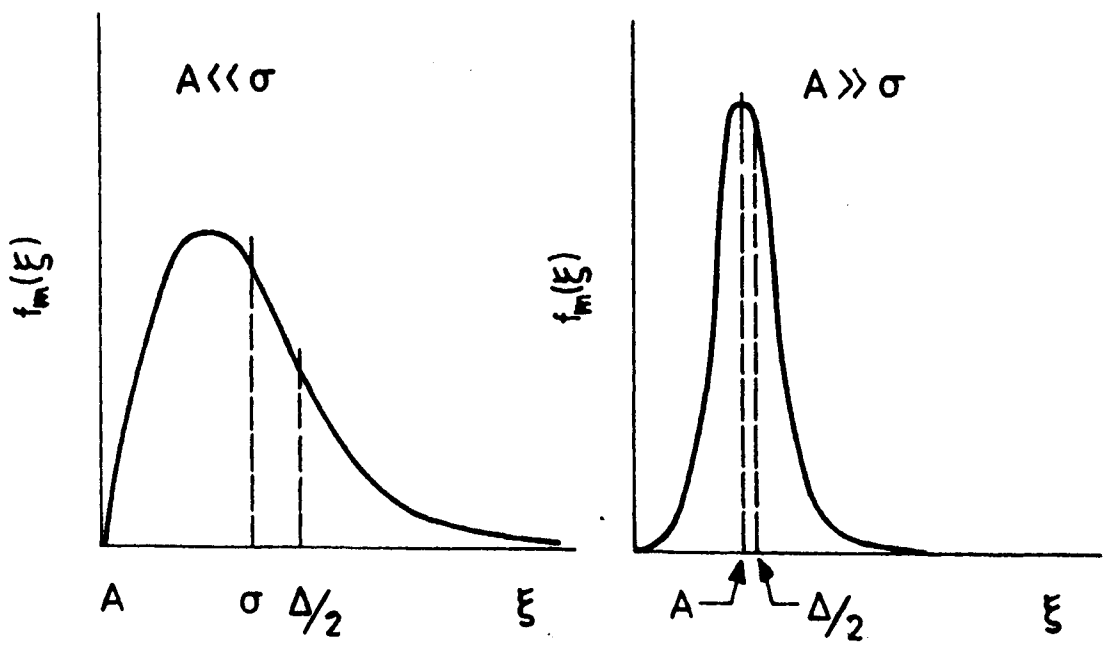

Fig. 7.14. Peak density function for combined sinusoid and narrow-band process.

When this density function is used with the power-law damage rate, the expected damage rate can be computed by integration so that

$$E\{D_r\} = \int_0^\infty \nu_o \left(\frac{2\zeta}{S_1}\right)^m f_m(\zeta)\,d\zeta \tag{7.57}$$

where $\nu_o = \dfrac{\omega_o}{2\pi}$

S_1, m = constants as in section 7.2.

Carrying out the integration gives

$$E\{D_r\} = \nu_o \left(\frac{2\sqrt{2}\,\sigma_x}{S_1}\right)^m \Gamma\left(1+\frac{m}{2}\right) M\left(-\frac{m}{2},1,-\left(\frac{\sigma_z}{\sigma_x}\right)^2\right) \tag{7.58}$$

where σ_z = rms of $Z(t) = \dfrac{A}{\sqrt{2}}$

$\Gamma(\cdot)$ = gamma funcion

$M(\cdot,\cdot,\cdot)$ = confluent hypergeometric function

Notice when $\dfrac{\sigma_z}{\sigma_x} \to 0$ (i.e. no deterministic sinusoid)

$$M\left(-\frac{m}{2},1,0\right) = 1 \tag{7.59}$$

resulting in the expression given by Eq. 7.15. When $\sigma_z/\sigma_x \to \infty$, it is easily shown using the asymptotic expansion for $M(\cdot,\cdot,-\infty)$ that

$$E\{D_r\} \to \nu_o \left(\frac{2\sqrt{2}\,\sigma_z}{S_1}\right)^m \tag{7.60}$$

which is the result for a deterministic sinusoid. Thus, it is seen that the effect of adding a stochastic term to a sinusoidal stress function is to increase the damage rate. This results

from two effects: First, the combined rms level is increased, and second when m > 2 there is an additional increase due to the spreading of the density function. The spreading of the density function in the latter case causes the larger range values, which are raised to the mth power to count more heavily in the averaging process.

As mentioned before, analytic results are unavailable for the general irregular ease of the sum of periodic and stochastic terms. It is possible, however, to formulate the density function for peak values of the combined signal. As described in Section 7.2 this density function gives only a very conservative estimate of the damage rate. To circumvent this problem, it is proposed to view the confluent hypergeometric function in Eq. 7.59 as an approximate interpolating function between the purely periodic signal and the Gaussian stochastic signal even in the irregular, wideband case. Thus, a model of the following form is proposed:

$$E\{D_r\} = \nu_o \left(\frac{\Delta_e}{S_1}\right)^m \tag{7.61}$$

where $\Delta_e = 2\sqrt{2}Kg\,\sigma_x \left[\Gamma\left(1+\frac{m}{2}\right) M\left(-\frac{m}{2}, 1, -\beta^2\right)\right]^{1/m}$

$$\beta = \frac{\Delta_{max}}{2\sqrt{2}\,\sigma_x}$$

$$g = 1 - (0.66 - 0.45\ m)\ (1-\delta)$$

σ_x = stochastic rms

$$\delta = \frac{\lambda_1}{\sqrt{\lambda_o \lambda_2}}$$

$$\nu_o = \frac{1}{2\pi}\sqrt{\frac{\lambda_2}{\lambda_o}}$$

S_1, m, K as defined previously

and λ_0, λ_1, λ_2, are the spectral moments of the combined process.

The term Δ_e can be regarded as the effective sinusoidal stress range for the combined stress time history. In the case when a pure sinusoidal stress occurs, Δ_e = 2 × amplitude. This model also includes all the resulting models of the previous sections as special cases. Thus, assuming K = 1, the following cases result:

1. Sinusoid: $\Delta_e = 2A$

1. Narrow-band stochastic: $\Delta_e = 2\sqrt{\sigma_x}\left(\Gamma\left(1+\frac{m}{2}\right)\right)^{1/m}$

2. Wide-band stochastic: $\Delta_e = 2\sqrt{2g}\,\sigma_x\left(\Gamma\left(1+\frac{m}{2}\right)\right)^{1/m}$

3. Irregular periodic: $\Delta_e = -g\,\Delta_{max}$

4. Sinusoid + narrow-band: $\Delta_e = 2\sqrt{2}\sigma_x\left[\Gamma\left(1+\frac{m}{2}\right)\right)M\left(-\frac{m}{2}, 1, -\left(\frac{A}{\sqrt{2}\sigma_x}\right)^2\right)\Big]^{1/m}$

It was felt that the correction for irregularity should be applied using the bandwidth parameter, δ, defined for the combined signal. Thus, in the case of a pure sinusoid plus a small wide-band stochastic process the correction would be similar to the case of an irregular periodic signal.

In order to test this latter hypothesis, 24 simulation cases were run using the rational spectral form given in Eq. 7.44 combined with a pure sinusoid. Two cases each involving combinations of four damping ratios and three ratios of mean-square stochastic-to-deterministic parts were tried. The results showing the log damage ratios for the simulation and for the computations are summarized in Table 7.10.

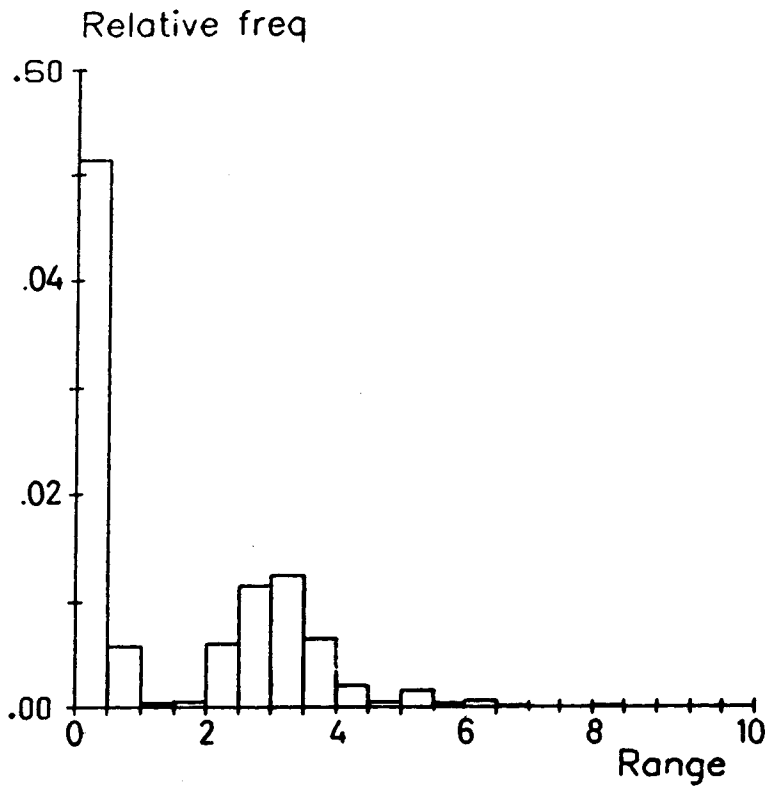

Fig. 7.15. Relative frequency of cyclic ranges for combined periodic and stochastic load history.

Table 7.10. Mean and standard deviation of log damage ratios for combined sinusoids and wide-band stochatic loading.

$$y = \log \left(\frac{D_S}{D_C}\right)$$

m	Mean	Std. Dev.
3	0.015	0.030
5	-0.023	0.078
7	-0.062	0.117

The results given in Table 7.10 show similar variability as compared to Table 7.1 and again it is considerably smaller than the inherent variability in estimating fatigue lifetimes.

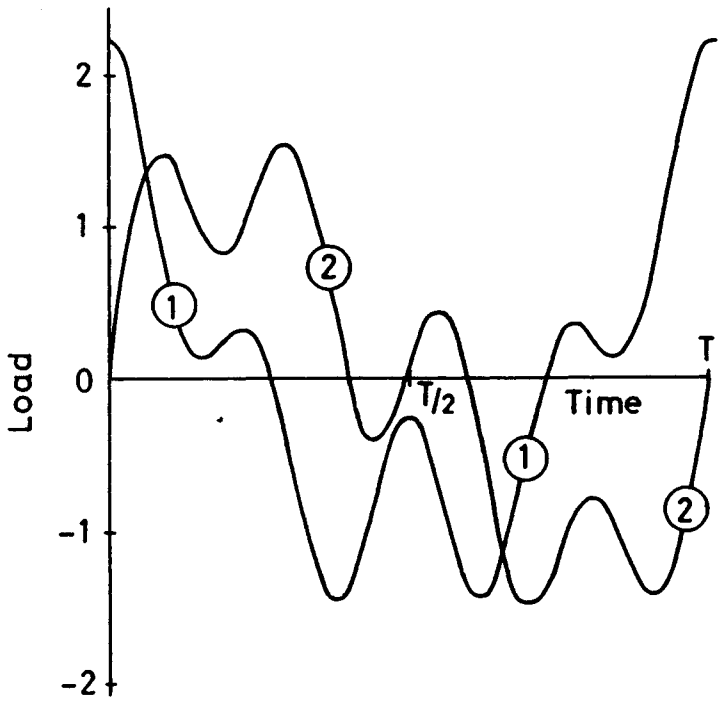

Fig. 7.16. Two irregular periodic functions used for combined loading simulations.

The case when the periodic part of the loading is also highly irregular presents additional challenges. In general, the periodic loading will have two or more stress ranges associated with each fundamental period. In the case when the stochastic part is small, the resulting distribution of hysteresis cycle ranges will be multimodal with the several cycle ranges associated with the periodic part appearing as peaks in the range density function, as shown in Fig. 7.15. As the stochastic part becomes large, the Rayleigh or more exponential form of the density function will be dominant, eliminating the multimodal character of the resulting density function.

In order to test the approximate model in this case several simulations were run using the following two irregular periodic functions:

$$Z_1(t) = 1.2216 \cos \omega_o t + 0.3669 \cos 2\omega_o t + 0.6108 \cos 4\omega_o t \quad (7.62)$$

$$Z_2(t) = 1.2216 \sin \omega_o t + 0.3669 \sin 2\omega_o t + 0.6108 \sin 4\omega_o t \quad (7.63)$$

These two functions are plotted in Fig. 7.16. Note that even though these two functions have identical magnitude spectra, the shift in the phases causes significantly different cyclic stress ranges. The ratio of the damage for loading using the first function to the damage due to loading by the second is given approximately by

$$\frac{D_1}{D_2} = (1.2)^m \quad (7.64)$$

In this case, the ratio is very nearly the same as

$$\frac{D_1}{D_2} = \left(\frac{\Delta_{max1}}{\Delta_{max2}}\right)^m \quad (7.65)$$

which is predicted using the model given by Eq. 7.54. For the following simulation results, a stochastic part with a rational spectrum of the form given by Eq. 7.44 was used. The same 12 combinations of parameters were used as in the previous results for the combined sinusoidal and stochastic results. Considering the two periodic functional forms, 24 total cases were simulated. The resulting ratios are summarized in Table 7.11.

Table 7.11. Log damage ratios for irregular periodic plus stochastic loading.

$$y = \log \left(\frac{D_S}{D_C}\right)$$

m	Mean	Std. Dev.
3	-.0.96	.032
5	-.127	.060
7	-.166	.060

Comparing the results from Table 7.11 with those from Table 7.10 clearly shows the conservatism in using the maximum cyclic range to characterize the periodic part of the loading. The small size of the standard deviation in Table 7.11 suggests that if a less conservative model for the irregular periodic part of the loading were developed, an improvement in the predictive capability of the combined model could be achieved.

REFERENCES

[1] RAAB, A. (1980). Combined Effects of Deterministic and Random Loads in Wind Turbine Design. In: Papers presented at the 3rd International Symposium on Wind Energy Systems held in Copenhagen, August 26-29, 1980. (BHRA Fluid Engineering, Cranfield, Bedford), Paper D1, 169-182.

[2] COLLINS, J.A., Failure of Materials in Mechanical Design. (Wiley, New York), p. 275.

[3] ASCE Committee on Fatigue and Fracture Reliability (1982). Fatigue Reliability. J. Struct. Div. Proc. Am. Soc. Civ. Eng., 108, p. 10.

[4] Ibid., 26-29.

[5] PARIS, P. and ERDOGAN, F. (1963). A Critical Analysis of Crack Propagation Laws, J. Basic Eng., Trans. ASME, 85, 528-534.

[6] MINER, M.A. (1945). Cumulative Damage in Fatigue. J. Appl. Mech., 12, 1945, A 159 - A 164.

[7] DOWLING, N.E. (1972). Fatigue Failure Predictions for Complicated Stress-Strain Histories. J. Mater., 7, 71-87.

[8] TALREJA, R., Technical University of Denmark, Lyngby, Denmark, private communication.

[9] COLLINS, op. cit. (1981), 183-4.

[10] Ibid., 180-183.

[11] ASCE, op. cit. (1982), 76-77.

[12] Ibid., p. 54.

[13] Ibid., p. 9.

[14] Ibid., p. 58.

[15] MATSUISHI, M. and ENDO, T. (1968). Fatigue of Metals Subjected to Varying Stress. Proc. J. Soc. Mech. Eng. Engineers, (in Japanese) n. 68-2, 37-40.

[16] DOWLING, op. cit. (1972), p. 74

[17] WIRSCHING, P.H. and SHEHATA, A.M. (1977). Fatigue Under Wide Band Random Stresses Using the Rain-Flow Method. J. Eng. Mater. Technol., Trans. ASME Ser. H, 99, p. 207.

[18] ASCE, op. cit. (1982), p. 59.

[19] YANG, J.-N. Statistics of Random Loading Relevant to Fatigue. J. Eng. Mech. Div., Proc. Am. Soc. Civ. Eng., 100, 469-475.

[20] RICE, S.O. (1959). Mathematical Analysis of Random Noise. In: Selected Papers on Noise and Stochastic Processes. Ed. by Wax, N. (Dover, New York), p. 79.

[21] RICE, J.R. and BEER, F.P. (1965). On the Distribution of Rises and Falls in a Continuous Random Process. J. of Basic_ Eng., Trans. ASME., 87, 398-404.

[22] WIRSCHING, P.H. and HAUGEN, E.B. (1974). A General Statistical Model for Random Fatigue. J. Eng. Mater. Tech., Trans, ASME Ser. H, 96, 34-40.

[23] CARTWRIGHT, D.E. and LONGUET-HIGGINS, M.S. (1956). The Statistical Distribution of the Maxima of Random Function. Proc. R. Soc., London, A 237, 212-232.

[24] WIRSCHING, P.H. and LIGHT, M.C. (1980). Fatigue Under Wide Band Random Stresses J. Struct. Div., Proc. Am. Soc. Civ. Eng., 106, 1593-1607.

[25] WIRSCHING and SHEHATA (1977), op. cit. p. 211.

[26] SAKAI, S. and OKAMURA, H. (1981). Evaluation of Cumulative Fatigue Damage Under Random Loads. In: Proceedings of ICOSSAR '81 International Conference on Structural Safety and Reliability held at Trondheim, Norway, June 23-25, 1981, 177-186.

[27] TAKEUCHI, S. and YAMAMOTO, Y., Approximate Distribution and Simulation of Successive Extremes for Gaussian Random Process. J. Soc. Nav. Archit. Jpn., 131, 97-113 (in Japanese) quoted by Sakai and Okamura (1981) op. cit., p. 183.

[28] KRENK, S. (1980). First-Passage Times and Extremes of Stochastic Processes. Lectures on Structural Reliability, held at Aalborg University Centre, May 1980. Ed. by Thoft-Christensen (Institute of Building Technology and Structural Engineering, Aalborg, Denmark), p. 80.

[29] YANG, J.-N. (1972). On the Normality and Accuracy of Simulated Random Processes. J. Sound Vib., 26, 417-428.

[30] TALREJA, R. (1973). On Fatigue Life Under Stationary Gaussian Random Loads. Eng. Fracture Mech., 5, 993-1007.

[31] Ibid., p. 1004.

[32] HILLBERRY, B.M. (1970). Fatigue Life of 2024-T3 Aluminum Alloy Under Narrow- and Broad-Band Random Loading. In: Effects of Environment and Complex Load History on Fatigue Life. Symposium held at Atlanta, Ga., 1968 (ASTM STP; 462) 167-183.

[33] RICE, op. cit. (1954), p. 239.

8. LIFETIME EVALUATION

Utilization of the model (computer code) for its prime purpose of predicting the lifetime of wind turbine structures has one major unavoidable difficulty, namely to describe and specify the input to the program. The form of this input is meant to ease the determination of responses once the structure itself has been modelled, the basic data for the materials used in the structure is specified, and the load cases, their frequencies, and, finally, the wind field have been described. This chapter gives the form such data must have in order to be acceptable for the model.

8.1. Material data, S-N curves

In the model for lifetime evaluation described in the previous chapters, some important material properties must be specified. The first step is to isolate those points on the structure where failure is likely to occur and to determine the local stress in terms of the geometry as described by the degrees of freedom in the structural model. With this stress response variable specified, it is next required to identify the material properties appropriate for the point in question. There are two different approaches available for accounting for the uncertainty in making the choice of material properties to be used for design. In the code approach, conservative fatigue data are combined with specified load safety factors and stress concentration factors to insure a reliable estimate of lifetime. In the statistical reliability approach, typical or average fatigue data and stress concentrations are used to give an estimate of the typical lifetime. The variability in the lifetime due to all sources of uncertainty is then estimated, and given an appropriate level of reliability a conservative lifetime estimate results. Either method can be used in conjunction with the computer model. If conservative fatigue data and appropriate factors of safety are used the resulting lifetime estimate is conservative. If, however, typical or average data are used with no safety factor, the resulting lifetime estimate will be an average valve.

Briefly, the required properties obtainable from typical design handbooks are the following:

1. Ultimate strength - the minimum tensile stress which results in immediate failure of the material when no fatigue cycling is present.
2. Stress concentration factor - the geometric factor which depends upon the structural details due to holes, weld geometry and precracks. This factor can be determined experimentally as the ratio of the nominal local stress when the actual detail fails to the corresponding failure stress for a smooth specimen subjected to pure tension. Any factors of safety as prescribed by code should multiply this factor.
3. S-N data - the two parameters describing the stress/cycle failure relation for constant amplitude or random amplitude cyclic fatigue tests for the given material. The mean stress is taken to be zero (non-zero mean stress is accounted for in the model using the Goodman correction), and the high cycle fatigue relation is assumed to be of the form:

$$N_f = \left(\frac{S_o}{\Delta}\right)^m$$

where N_f = number of cycles to failure
Δ = max-min stress range for each cycle
S_o,m = the material parameters in question.

These material parameters are obtained by plotting the number of cycles to failure vs. the stress range using log-log scales (the S-N curve) and fitting a straight line to the test data.

8.2. Pertinent load cases and their frequencies

While the material data are not specifically connected to wind turbines, the specification of load cases are closely connected to the operation strategy of the wind turbine and the terrain in which it is situated. The operation strategy will imply

numerous different operational cases, and often consecutive load cases will not be independent, i.e. the sequence of events may be of some significance. It seems relevant, as argued earlier, to subdivide the load/response history into periods in which the response process can be considered either stationary or a well defined, time-limited transient event.

The following main groups of load cases should be considered:

I. Stationary load cases: Defined as operational time periods where the response can be evaluated by means of stationary statistical methods employed on the frequency domain representation of the response. Such load cases split into two types:

I.1. Wind turbine in operation.
I.2. Wind turbine in stand still, i.e. the rotor is not rotating.

II. Transient load cases: Load cases, where a statistical evaluation is not possible. Time integration must be employed to get estimates of the response amplitudes.

These load cases are subdivided into a number of load cases, which are considered independent of each other. At this stage, the program is not prepared to include all such cases. In the following, the load cases found relevant by the authors are listed. The list is not complete for all wind turbine design possibilities and should be up-dated in accordance with information about different wind turbine designs and operational strategies.

I. Stationary load cases.

I.1. Wind turbine in operation.

I.1.1. Wind perpendicular to rotor.
I.1.2. Wind not perpendicular to rotor: a number of yaw angles should be selected representing the actual (expected) operational pattern.
I.1.3. Constant rate yawing.

1.2. Wind turbine in stand-still position.

I.2.1. Wind perpendicular to rotor, blade pitch angle $\phi = 0^{o}$.

I.2.2. Wind perpendicular to rotor, blade pitch angle selected as "critical".

II. Transient load cases.

II.1. Start of wind turbine, all possible modes.

II.2. Stop of wind turbine, all possible modes.

II.3. Idling (rotating without being grid connected).

II.4. Start/stop of yawing motor.

For each load case, the response characteristics should be determined for a pertinent number of windspeed intervals (bins). The input wind speed for the model is an average wind speed and should be chosen as $v_i = (v_i + v_{i+1})/2$, where v_i and v_{i+1} are respectively the upper and lower limits of the intervals. The interval length is determined so the mean value of responses do not vary significantly from one interval to neighbouring ones.

When the response statistics in each load case has been determined the frequencies of the load cases are evaluated. It is assumed that the 10-minutes average wind speeds are Weibull distributed so that the density function is given by

$$f(u) = \left(\frac{C}{A}\right)\left(\frac{u}{A}\right)^{C-1} e^{-\left(\frac{u}{A}\right)^{C}} \qquad (8.1)$$

where A and C are the socalled Weibull parameters, which are assumed to be known for a specific site. Given the distribution (8.1), the probability of having wind speeds in the interval $[v_i, v_{i+1}]$ is

$$F_i = e^{-\left(\frac{u_i}{A}\right)^{C}} - e^{-\left(\frac{u_{i+1}}{A}\right)^{C}} \qquad (8.2)$$

For each chosen wind speed interval, the relative appearances of yawing, skew wind relative to rotor, stand-still, etc. are estimated for the stationary load cases.

For the transient load cases, the number of events and the corresponding number of load cycles and amplitudes is estimated. The analysis of transient loadcases, however, has been considered to be outside the scope of this report. Given the responses and their relative frequencies the fatigue life and the extreme responses throughout the expected lifetime can be computed (Chs. 6 and 7).

9. SUMMARY AND CONCLUSIONS

A number of sub-models for use in the evaluation of the load-carrying capacity of a wind turbine rotor with respect to short-term strength and material fatigue are presented. The models constitute the theoretical basis of a computer code ROTORDYN which in conjunction with an initial finite element analysis and eigenvalue extraction performs a dynamic analysis of a wind turbine rotor for lifetime prediction.

The report begins with an introduction in Chapter 1, and describes the structural model in Chapter 2. The model is essentially linear and solves for periodic and stochastic loading in the frequency domain.

The aerodynamic model which is based on blade element theory is presented in Chapter 3.

The stationary deterministic loads arising from a spatially non-uniform wind field and gravity as well as loads caused by the rotation are treated in Chapter 4, while the turbulence loading is formulated in Chapter 5 in terms of a stochastic model. The turbulence is introduced in terms of power spectra as seen from a point in a rotating frame of reference.

Statistics of the combined deterministic periodic and stochastic response are presented in Chapter 6, and an asymptotic theory is derived for the extremes of the responses during typical operation of the wind turbine.

A fatigue model is presented in Chapter 7 which takes into account the special structure of the stress response. The model avoids computer simulation and succeeding rainflow counting and yields an analytic solution for the expected damage rate at a given mean wind speed.

Finally, the strategy for applying the model for evaluation of the total lifetime of the rotor is discussed in Chapter 8. At the present stage the project has resulted in a computer program

which can analyze a horizontal-axis propeller wind turbine during turbine during steady operation with respect to structural loads, stresses and displacements as well as the resulting fatigue damage and extreme loads. The program is flexible enough to cover most Danish wind turbine types, including turbines with fixed-pitch blades and with pitch control, but is restricted to a constant rotational speed, an active yaw mechanism and a relatively stiff tower.

From a comparison between measured data from the Nibe-B turbine and results from the program [1] it was concluded that for wind turbines of the assumed type in operation the computer program calculates reponses of the rotors, their extremes and the associated fatigue damage with satisfactory accuracy.

It is the author's opinion that the program constitutes a significant improvement in the available design tools for wind turbines.

REFERENCES:

[1] MADSEN, P.H. et al. (1984). Lifetime Analysis of the Nibe-B Wind Turbine using the Computer Code ROTORDYN. Risø Report M-2459.

ANNEX 1

FINITE-ELEMENT ANALYSIS OF WIND TURBINE ROTORS

BASIC CONCEPTS

The equation of motion of a linear discretized system with n degrees of freedom and with time invariant coefficient matrices reads

$$\underline{\underline{M}}\,\ddot{\underline{X}} + \underline{\underline{C}}\,\dot{\underline{X}} + \underline{\underline{K}}\,\underline{X} = \underline{P} \qquad (1)$$

in terms of the mass matrix $\underline{\underline{M}}$, the damping matrix $\underline{\underline{C}}$; the stiffness matrix $\underline{\underline{K}}$ and the external force vector $\underline{P}$. $\underline{X}$ denotes the vector containing the degrees of freedom, which usually consists of displacement quantities such as displacements and rotations of specific points of the structure, the nodes. Correspondingly, $\underline{P}$ consists of nodal loading contributions in terms of forces and moments.

This fundamental model is usually obtained using the finite-element technique such that $\underline{X}$ represents the degrees of freedom of selected points of the structure, the nodes. The mass matrix $\underline{\underline{M}}$, the stiffness matrix $\underline{\underline{K}}$ and possibly the damping matrix $\underline{\underline{C}}$ is automatically generated by the chosen finite-element program which also transforms the external distributed load and forces to the force vector $\underline{P}$.

The geometry of the wind turbine structure is expressed in rotating coordinates, in which case time-invariant coefficient matrices are obtained for the rotor system. However, the rotor system, consisting of the blades, stays, hub and a simplified main shaft, may in addition be extended to contain the actual drive train, i.e. shafts, gearbox and generator, whereas the influence of the tower can be included only in an idealized rotationally symmetric form.

In order to introduce the notation as well as certain concepts used in the following the basic theory of finite elements in its simplest form is briefly reviewed. A detailed discussion can be found in Zienkiewicz [1].

The displacement field in element I, $\underline{u}_I$, is uniquely determined by the element node displacement vector $\underline{V}_I$

$$\underline{u}_I = \underline{\underline{N}}_I \underline{V}_I \tag{2}$$

in terms of the displacement interpolation matrix $\underline{\underline{N}}_I$. Similarly the generalized strain field $\underline{\varepsilon}_I$ is obtained from $\underline{V}_I$

$$\underline{\varepsilon}_I = \underline{\underline{B}}_I \underline{V}_I \tag{3}$$

in which $\underline{\underline{B}}_I$ is the generalized strain distribution matrix such that the virtual internal work A^I is

$$A^I = \underline{\sigma}_I^T \underline{\varepsilon}_I \tag{4}$$

$\underline{\sigma}_I$ is related to the strain by the constitutive equation which is the case of a linear elastic material reads

$$\underline{\sigma}_I = \underline{\underline{D}}_I \underline{\varepsilon}_I = \underline{\underline{D}}_I \underline{\underline{B}}_I \underline{V}_I = \underline{\underline{S}}_I \underline{V}_I \tag{5}$$

in terms of the elasticity matrix $\underline{\underline{D}}_I$ or the stress displacement matrix $\underline{\underline{S}}_I$. The element stiffness matrix is defined

$$\underline{\underline{k}}_I = \int_{V_O} \underline{\underline{B}}_I^T \underline{\underline{D}} \, \underline{\underline{B}}_I \, dV \tag{6}$$

where V_O is volume spanned by the element.

Equating the work done by the distributed inertial forces through the element displacements $\underline{V}_I$ with the work done by nodal inertia forces the element mass matrix $\underline{\underline{M}}_I$ becomes

$$\underline{\underline{M}}_I = \int_{V_O} \rho \; \underline{\underline{N}}_I^T \underline{\underline{N}}_I \, dV \tag{7}$$

in which ρ is the mass density in V_O. Similarly, when a damping density μ can be defined in a meaningful way the element damping

matrix can be written

$$\underline{\underline{C}}_I = \int_{V_o} \mu \, \underline{\underline{N}}_I^T \, \underline{\underline{N}}_I \, dV \tag{8}$$

The element load vector $\underline{R}_I$ is viewed as the element nodal forces that perform the work $\underline{V}_I^T \, \underline{R}_I$ for the displacements $\underline{V}_I$. Thus in a work sense $\underline{R}_I$ must be equivalent to the distributed load $\underline{q}_I$ for possible element displacements $\underline{u}_I$, and

$$\underline{R}_I = \int_{V_o} \underline{\underline{N}}_I^T \, \underline{q}_I dV \tag{9}$$

The transformation of the element quantities described in Eqs. 2-8 into the system equation is usually performed in two steps. Firstly, the element quantities are transformed from local coordinates to global coordinates; secondly, the element matrices are inserted into system matrices M, K and C and the system load vector $\underline{P}$. The relation between the element node displacements in local coordinates $\underline{V}_I$ and the global displacements $\underline{X}$ is formally written

$$\underline{V}_I = \underline{\underline{T}}_I \, \underline{\underline{a}}_I \, \underline{X} = \underline{\underline{G}}_I \, \underline{X} \tag{10}$$

using the element coordinate transformation matrix T_I which consists of direction cosines, and the element connection matrix a_I, which usually consist of zeros and ones.

Note that all responses in the element: stress, strain or displacements are uniquely determined from $\underline{X}$; thus, for example, the stress response is

$$\underline{\sigma}_I = \underline{\underline{S}}_I \, \underline{\underline{G}}_I \, \underline{X} \tag{11}$$

Equating work in either system, the system matrices M, C, and K is given by the element matrices by

$$\underline{\underline{M}} = \sum_{\text{elements}} \underline{\underline{G}}_I^T \, \underline{\underline{M}}_I \, \underline{\underline{G}}_I \tag{12}$$

$$\underline{\underline{C}} = \sum_{\text{elements}} \underline{\underline{G}}_I^T \, \underline{\underline{C}}_I \, \underline{\underline{G}}_I \tag{13}$$

$$\underline{\underline{K}} = \sum_{\text{elements}} \underline{\underline{G}}_I^T \, \underline{\underline{K}}_I \, \underline{\underline{G}}_I \qquad (14)$$

while the global load vector is

$$\underline{P} = \sum_{\text{elements}} \underline{\underline{G}}_I^T \, \underline{R}_I \qquad (15)$$

All mass, damping, stiffness or load quantities do not necessarily have to be introduced at element level, but can equally well be inserted directly in the global quantities. Often the mass and especially the damping properties are supplemented if not solely specified by element-independent terms, concentrated masses, discrete dampers, etc.

THE FINITE-ELEMENT MODEL

The actual modelling procedure using a finite element computer program is considered to be beyond the scope of this report being strongly dependent on the program used. A few comments will be given, however.

As mentioned earlier, a linear structural model is assumed, a model which can be produced by most linear general-purpose finite-element codes with three-dimensional truss- and beam elements. So far the structural model has been formulated using SAP-IV [4] which is a relatively unsophisticated general-purpose linear finite-element code. Other linear codes equipped with a restart facility where the structural information is saved on files may be equally suited after a modification of the interface subprograms in ROTORDYN.

When the rotorblades are modelled by beam elements two problems should be considered. Firstly, as the blade geometry is rather complex geometry - often thin-walled and with several cells - the formulation of the geometric properties in terms of geometric moments is a difficult task which may require special computer programs. The task is further complicated by the frequent use of anisotropic materials like GRP or wood in the blades.

Secondly, the geometric properties thus obtained can be difficult to specify in connection with a general beam element. In the basic concept of beam theory a cross-section of a blade is characterized by the elastic axial, bending, shear and torsional stiffnesses as well as the mass density with respect to the corresponding centres and their location. In general, these centres do not coincide, which should be taken into account.

Systems of coordinates, axes and different centres in a cross-section are illustrated in Fig. 1. A local X_o, Y_o, Z_o coordinate system for each blade is defined with the Z_o-axis pointing along the geometric system line of the blade from the intersection of the blades to the tip and the X_o-axis in parallel to the rotor plane.

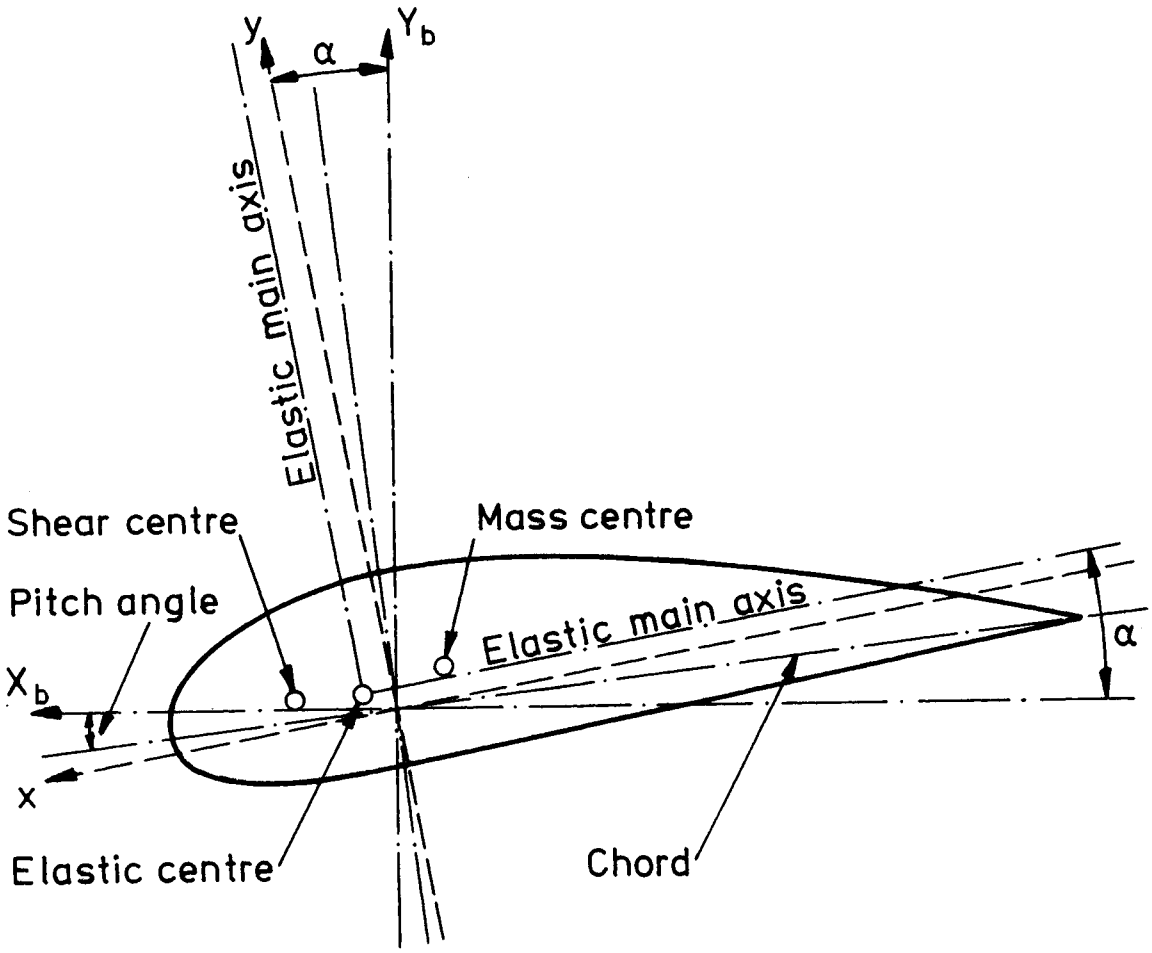

Fig. 1. Geometry definitions for blade cross-section.

A very simplified way of specifying the beam properties along the rotor blade is for any cross-section to ignore the different positions of the centres of mass, elasticity, shear and aerodynamic loads, i.e. to calculate all masses, loads and stiffnesses with respect to the corresponding centre and then treat geometrically all these centres as coinciding with the intersection point of the system line with the cross-section. The elastic main axes (X,Y,Z) of this double symmetric homogeneous beam element are chosen in parallel to the real elastic main axes at an angle β = α-pitch angle (see Fig. 1) with the chord, normally specifying the pitch angle. Several ad hoc modelling concepts introducing different levels of simplifications are possible. In Lundsager and Gunneskov [3], for example, it is proposed to model the eccentricity of the mass centre - leading to dynamic coupling of bending and torsion - by means of separate weightless stiff cantilever beam elements with a lumped mass at one end and fixed to a node in the chosen blade axis in the other.

It is seen that the use of the common prismatic beam element can be adapted to model rotorblades with various degrees of accuracy. A correct representation of the properties is naturally to be preferred.

Having specified the cross-section along the blade, the model is established by dividing the blade into a finite number of elements each of constant cross-section along the entire element length. The specifications of the elements - including the twist of the main axes - are fitted to the actual blade data at the middle of each element. The number of elements that are to be used along each blade depends on both the number of modes and the corresponding model shapes to be included in the dynamic analysis. The number of modes is typically of the order of two flapwise and two lead-lag modes for each blade.

In order to estimate an adequate number of elements, the eigenfrequences are plotted versus the number of elements in the blade model for the modes of interest. The analysis is carried out for different discretizations. As it is known that the solutions converge with a certain rate for the particular element type

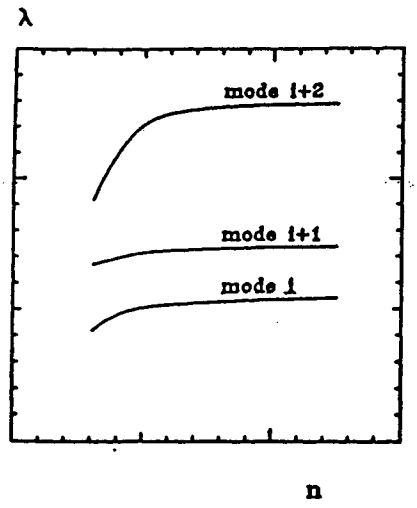

Fig. 2. Plot of eigenfrequencies, λ, versus the number, n, of elements in the finite-element model of each blade for estimating adequate discretization.

(Strong and Fix [2]) a choice of an adequate number of elements can be made. The approach is illustrated in Fig. 2.

The modelling of the rest of the structure should present no further problem for the experienced finite-element user.

INFORMATION FROM THE FINITE-ELEMENT ANALYSIS

In order to summarize, the following information must be extracted from the files that are generated by the initial finite element analysis:

- Node geometry
- Mass matrix $\underline{\underline{M}}$
- Stiffness matrix $\underline{\underline{K}}$
- Modal frequencies ω_i
- Mode shape vectors $\underline{v}_i$
- Connection information on elements, node, and global equation numbers
- Stress-displacement matrices $\underline{\underline{S}}_I$.

REFERENCES

[1] ZIENKIEWICS, O.C. (1971). The Finite Element Method in Engineering Science (McGraw-Hill, London) 535 pp.

[2] STRANG, G. and FIX, J. (1977). An Analysis of the Finite-Element Method (Prentice-Hall, Englewood Cliffs N.J) 320 pp.

[3] LUNDSAGER, P. and GUNNESKOV, O. (1980). Static Deflection and Eigenfrequency Analysis of the Nibe Wind Turbine Rotors. Theoretical Background. Risø-M-2199, 31 pp.

[4] BATHE, K.-J., WILSON, E.L. and PETERSON, F.E. (1973). SAP-IV, A Structural Analysis Program for Static and Dynamic Analysis of Linear Structural Systems. PB-221967/3, 182 pp.

Sales distributors:
G.E.C. Gad Strøget
Vimmelskaftet 32
DK-1161 Copenhagen K, Denmark

Available on exchange from:
Risø Library, Risø National Laboratory,
P.O.Box 49, DK-4000 Roskilde, Denmark

ISBN 87-550-1046-6
ISSN 0106-2840